



CONTENTS

Thermodynamics

- B. D. Djordjević, I. R. Radović, M. Lj. Kijevčanin, A. Ž. Tasić and S. P. Šerbanović: Molecular interaction studies of the volumetric behaviour of binary liquid mixtures containing alcohols (Authors' review) 477

Organic Chemistry and Biochemistry

- S. Manivarman, G. Rajarajan, G. Manikandan, M. Sekar, J. Jayabharathi and V. Thanika-chalam: A mechanistic investigation of the oxidation of *N*, α -diphenylnitrones by dichloramine-T in aqueous acetonitrile medium – a non-linear Hammett plot..... 493
- I. Stevanović, M. Jovanović, A. Jelenković, M. Čolić and M. Ninković: Effects of various nitric oxide synthase inhibitors on AlCl₃-induced neuronal injury in rats 503
- K. Milovanović, L. Burazer, O. Vučković, M. Atanasković-Marković, T. Čirković Veličković, R. M. Jankov and M. Gavrović-Jankulović: Isolation and characterization of the 68 kD allergen from house dust mite *Dermatophagoides pteronyssinus* 513

Inorganic Chemistry

- A. P. Mishra, R. K. Mishra and S. P. Shrivastava: Structural and antimicrobial studies of coordination compounds of VO(II), Co(II), Ni(II) and Cu(II) with some Schiff bases involving 2-amino-4-chlorophenol 523
- A. Tavman, S. İkiz, A. F. Bağcigil, N. Y. Özgür and S. Ak: Preparation, characterization and antibacterial effect of 2-methoxy-6-(5-H/Me/Cl/NO₂-1*H*-benzimidazol-2-yl)phenols and some transition metal complexes..... 537

Theoretical Chemistry

- J. Đurđević, I. Gutman and R. Ponec: Verifying the PCP-rule by five-center bond indices 549

Physical Chemistry

- K. Bahgat, N. A.-D. Jasem and T. El-Emary: Theoretical and experimental investigations on the structure and vibrational spectra of 6-amino-3-methyl-1-phenyl-1*H*-pyrazolo[3,4-*b*]pyridine-5-carboxylic acid and 6,7-dihydro-3-methyl-6-oxo-1-phenyl-1*H*-pyrazolo[3,4-*b*]pyridine-5-carbonitrile 555

Electrochemistry

- A. V. Tomašević, M. L. Avramov Ivić, S. D. Petrović, M. B. Jovanović and D. Ž. Mijin: A study of the electrochemical behaviour of methomyl on a gold electrode in a neutral electrolyte..... 573
- G. Karim-Nezhad, M. Hasanzadeh, L. Saghatforoush, N. Shadjou, B. Khalilzadeh and S. Ershad: Electro-oxidation of ascorbic acid catalyzed on cobalt hydroxide-modified glassy carbon electrode 581

Metallurgy

- V. Rajković, D. Božić and M. T. Jovanović: Characteristics of Cu–Al₂O₃ composites of various starting particle size obtained by high-energy milling..... 595

Published by the Serbian Chemical Society
Karnegijeva 4/III, 11000 Belgrade, Serbia
Printed by the Faculty of Technology and Metallurgy
Karnegijeva 4, P.O. Box 35-03, 11120 Belgrade, Serbia



J. Serb. Chem. Soc. 74 (5) 477–491 (2009)
JSCS–3848

AUTHORS' REVIEW

**Molecular interaction studies of the volumetric behaviour of
binary liquid mixtures containing alcohols**

BOJAN D. DJORDJEVIĆ*#, IVONA R. RADOVIĆ#, MIRJANA LJ. KIJEVČANIN#,
ALEKSANDAR Ž. TASIĆ and SLOBODAN P. ŠERBANOVIĆ#

*Faculty of Technology and Metallurgy, University of Belgrade, Karnegijeva 4,
P.O. Box 35-03, 11120 Belgrade, Serbia*

(Received 13 January 2009)

Abstract: An attempt has been made to relate the volumetric effects involved in the binary mixtures of normal and branched alcohols and various components (aromatics, halo and nitroaromatics and haloaliphatics) with the molecular interactions of unlike molecules. This review is a condensation of research activities developed in recent years as results of a better understanding of volumetric behaviour and a stronger insight into the complex structure of those mixtures. The influence of important contributions of a physical, chemical and geometrical nature that change excess molar volume, V^E (positive, sigmoidal, negative) is considered and explained in detail. It appears that the balance between these contributions is quite sensitive to the behaviour of the alcohol molecules in contact with the chosen compounds.

Keywords: molecular interactions; volumetric properties; excess volume; alcohols; binary liquid mixtures.

CONTENTS

1. INTRODUCTION
2. VOLUMETRIC PROPERTIES
3. ALCOHOL + AROMATIC SYSTEMS
 - 3.1. 1-Alcohols with aromatics
 - 3.2. Branched alcohols with aromatics
4. ALCOHOL + HALO-AROMATIC OR + NITROAROMATIC SYSTEMS
 - 4.1. 1-Alcohols with haloaromatics or nitroaromatics
 - 4.2. Branched alcohols with haloaromatics
5. ALCOHOL + HALOALIPHATIC SYSTEMS
6. CONCLUSIONS

* Corresponding author. E-mail: bojan@tmf.bg.ac.rs

Serbian Chemical Society member.

doi: 10.2298/JSC0905477D

1. INTRODUCTION

The knowledge of the structure and molecular interactions of liquid mixtures is very important from fundamental and engineering point of view.

Fundamental thermodynamic and thermophysical properties are essential sources of information necessary for a better understanding of the non-ideal behaviour of complex systems because of physical and chemical effects, which are caused by molecular interactions, intermolecular forces, *etc.*, of unlike molecules.

From a practical point of view, these properties are necessary for the development of thermodynamic models required in adequate and optimized processes of the chemical, petrochemical, pharmaceutical, and other industries. In addition, extensive information about structural phenomena of mixtures is of essential importance in the development of theories of the liquid state and predictive methods. This review is focused on the qualitative explanation of the influence of molecular structure on volumetric properties of different alcohols with some aromatics and halo-aromatics, nitro compounds or halo-aliphatics. In addition, this study also provides a better insight into the nature of the molecular interaction in the aforementioned systems. Besides their theoretical importance, these systems were chosen since they are very interesting from a practical point of view: (i) due to their diverse industrial applications, they are present as pollutants causing air, water and soil contamination, and some of them have cancerous features; (ii) alcohols and other organic compounds are employed in a variety of industrial and consumer applications, such as perfumes, cosmetics, paints, varnishes, drugs, fuels, explosives, fats, waxes, resins, plastics, rubber, detergents, DDT, *etc.*, while chloroform is applied as a solvent in the pharmaceutical industry, the paint industry, in the chemical production of pesticides, oils, alkaloids, *etc.*

Some research activities, including the modelling of volumetric properties by various models (CEOS, CEOS/ G^E and empirical models) with modern mixing rules were systematically considered in previous reviews^{1,2} and in other papers particularly concerning the correlation³⁻⁸ and prediction of volumetric and other thermodynamic properties.⁹⁻¹⁵

2. VOLUMETRIC PROPERTIES

The density (ρ) of the binary systems, the molecular behaviours of which were analyzed in this work, were measured by means of a DMA 5000 digital vibrating U-tube densimeter (with automatic viscosity correction) having a stated accuracy $\pm 5 \times 10^{-3}$ kg·m⁻³. The temperature in the cell was regulated to ± 0.001 K with a built-in solid-state thermostat. To minimize errors in composition, all mixtures were prepared by mass using the cell and the procedure described previously;^{16,17} presently, a Mettler AG 204 balance with a precision of 1×10^{-4} g was employed. The uncertainty in the mole fraction calculation was less than $\pm 1 \times 10^{-4}$. All molar quantities were based on the IUPAC Relative Atomic Mass Table. The ex-

perimental uncertainty in the density was about $\pm 1 \times 10^{-2} \text{ kg}\cdot\text{m}^{-3}$, while the average uncertainty in the excess molar volume was estimated to be $\pm 3 \times 10^{-9} \text{ m}^3\cdot\text{mol}^{-1}$.

The excess molar volumes, V^E , were calculated from the equation:

$$V^E = \sum_{i=1}^n x_i M_i \left(\frac{1}{\rho} - \frac{1}{\rho_i} \right) \quad (1)$$

where n represents the number of components, x_i is the mole fraction of i -th component in the mixture, M_i its molecular weight, and ρ and ρ_i the measured densities of the mixture and the pure i -th component, respectively.

Since in previous papers^{16–25} experimental measurements of the corresponding systems were presented by V^E-x_1 curves, in this work these graphs are plotted only for the systems that are suitable for a better understanding of the complex behaviour of the chosen mixtures.

The observed values of V^E can be analyzed qualitatively in terms of the following resulting effects, which predominate in some mixtures or in a certain mole fraction region:^{26–35} (i) physical, (ii) chemical and (iii) geometrical contribution. Consequently, V^E depends on the relative strength of these effects.

The physical interactions comprise mainly dispersion forces and non-specific interactions. The chemical contribution arises mainly due to hydrogen bond rupture because of the breaking up of the hydrogen bond structure, and specific interaction such as hydrogen bond formation and charge-transfer complexes. This interaction can be considered as the reaction between an alcohol, as a Lewis acid, and an aromatic compound, as a Lewis base. It should be emphasized that the hydrogen bond energy is determined by four components:^{36,37} (i) the polarization term, (ii) the electrostatic term, (iii) the exchange repulsion term and (iv) charge transfer or delocalisation term.

The geometrical contribution occurs due to packing effects arising from interstitial accommodation of one component into the other due to differences in free volumes and molar volumes between the components.

3. ALCOHOL + AROMATIC SYSTEMS

3.1. 1-Alcohols with aromatics

Numerous articles^{36,38–43} have demonstrated that alcohols are strongly self-associated (forming clusters) through H-bonded linear chains (OH...OH interactions), with restricted rotation about the H-bonds and showing variable degrees of polymeric aggregates. The degree and strength of polymerisation decrease with increasing chain length of the carbon atoms and with branching of an alcohol.

Mixing of alcohols with other organic components enables that some molecules can dissociate from the multimers to form other kinds of H-bonds with unlike molecules. This process will depend on the proton accepting ability of the functional group in the molecule.

However, aromatic hydrocarbons are potential electron donors and electron donor–acceptor interactions between benzene and the hydrogen of alcohol hydroxyl group are of importance here.

Figure 1 shows experimental points of V^E at 308.15 K for the 1-alcohol + benzene systems reported in previous papers.^{18,19,21,24,32,44,45} These data can be explained qualitatively on the basis of different aforementioned effects predominating in certain mole fraction regions.

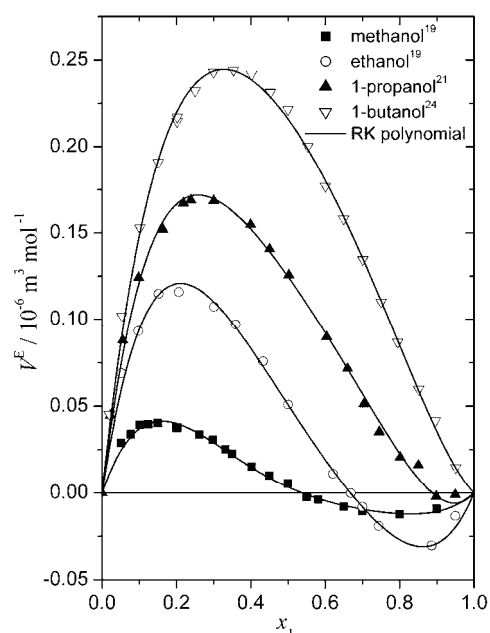


Fig. 1. Experimental values of V^E for the systems of 1-alcohols (1) with benzene (2) at 308.15 K. The symbols refer to the experimental points, while the lines present the results calculated by the Redlich–Kister polynomial.^{19,21,24}

As can be seen from this Fig. 1, the V^E of the mixtures of benzene with 1-alcohols show sigmoidal *vs.* mole fractions curves, except for the system 1-butanol + benzene for which positive V^E values were observed over the whole concentration range. When 1-alcohol molecules are added to a large amount of benzene, depolymerisation of the network of pure alcohols occurs, resulting in positive values of V^E . These V^E values indicate that there were no stronger specific interactions between the components of the mixtures but that this effect was the result of breakage of the bonds formed among the alcohol structure. This positive contribution is a consequence of hydrogen bond rupture and stretching of the self-associated molecules of the alcohols, which is insensitive to the chain length of the 1-alcohols (Fig. 1). The negative values of V^E in the alcohol-rich region indicate that complex formation occurred between the alcohols and benzene,⁴⁴ resulting in predominant electron donor–acceptor type (benzene behaves as the electron donor) of interactions between the OH group of the 1-alcohol and the π electrons of the aromatic ring of benzene. At higher mole composition of the

1-propanol + benzene mixture, the V^E values tend to be slightly negative, meaning that the breaking up of the associated alcohol aggregates is not completed and the benzene molecules are fitted into the propanol network. This situation is also clear for mixtures with methanol, where the tendency of interstitial accommodation of its molecules into benzene leads to negative values of V^E .³⁰ As can be seen from Fig. 1, the experimental data for the 1-butanol + benzene system were positive over the whole composition range at all investigated temperatures. These positive V^E values can be qualitatively explained by disruptive or stretching effects on the self-associated molecular structure of 1-butanol with physical dipole-dipole interactions between alcohol monomers and multimers, and by the disruption of the favourable orientation order of the aromatic component. The possible formation of weak intermolecular complexes between the OH group of 1-butanol and the π electron cloud of the benzene ring did not result in negative V^E values. As suggested by Assarson and Eirich,³² components of similar molecular sizes, such as 1-butanol and benzene (van der Waals volumes of 52.4 and 48.4 cm³·mol⁻¹, respectively) mix with positive values of V^E .

In addition, it is evident from the plots of 1-alcohols with benzene that, at the same temperature, the trend of increasing V^E in the positive direction in the lower alcohol region has the following order: methanol < ethanol < 1-propanol < 1-butanol. On the other hand, in the alcohol rich region, the order from negative to positive values is as follows: ethanol < methanol < 1-propanol < 1-butanol.

This behaviour of 1-alcohols can be explained in terms of the chain length of alcohols. Namely, as the mole fraction of higher 1-alcohols increases, the rupture of H-bonds of the alcohol increases from methanol to 1-butanol, and positive values of V^E become dominant. Also, interaction between the OH group of the higher 1-alcohols and the π electrons of the aromatic ring of benzene are weaker because of the decrease of their polarizability with increasing length. Structural effects leading to closer geometrical fitting of benzene into remaining structure of the higher 1-alcohols are less important. It is clear that for higher 1-alcohols, positive values of V^E are predominant. V^E measurements over a range of temperature were already performed¹⁹ and in all cases, the V^E values of the 1-alcohol + benzene systems increased with increasing temperature. It is clear that the rupture of the H-bonds of self-associated molecules of alcohols increases with increasing temperature.

1-Alcohols (methanol, ethanol, 1-propanol, 1-butanol and 1-pentanol) were mixed with other aromatic hydrocarbons with increasing size and number of substituents on the benzene ring (toluene, ethylbenzene and *p*-xylene).

The results obtained in work of Munk *et al.*⁴⁵ show that the V^E values of the mixtures with the same 1-alcohol increased with increasing of size and number of substituents, while for mixtures with the same aromatic component, V^E increased with increasing chain length of the 1-alcohols.

The measured values of V^E for mixtures of benzene with higher 1-alcohols⁴⁶ were positive over whole range of concentration. This suggests that a positive contribution from the rupture of hydrogen bonds of alcohols as well as dipole–dipole interactions between alcohol monomer and polymers were dominant in all systems. The algebraic values of V^E decreased in the order: 1-decanol \approx 1-nonanol > 1-octanol > 1-heptanol > 1-hexanol > 1-pentanol > 1-butanol > 1-propanol. In addition, it is evident that V^E increased with increasing chain length of the 1-alcohols and van der Waals interactions increased with increasing carbon chain length of the alcohols.

3.2. Branched alcohols with aromatics

Branched secondary and tertiary alcohols reflect various degrees of steric hindrance of the hydroxyl group, which directly influences the possibility of their molecules to self-associate.

First, the V^E values for the systems of benzene with 1-propanol and 2-propanol were compared.

Previously published data²¹ for the system benzene + 1-propanol at 298.15 K and those of the system benzene + 2-propanol at the same temperature⁴⁷ show that the V^E values of the former were always considerably lower at all mole fractions. This is a consequence of the branching of the alkyl group in 2-propanol, which increases the steric hindrance for the correct orientation of the benzene molecules to fit into the alcohol network.

The 1- and 2-propanol mixtures could be compared with those of other aromatic compound, for example alkylbenzenes. The introduction of two methyl groups into the benzene ring, as in the case of xylene, enhances the electron-donating power of aromatic hydrocarbons.

For 1-propanol + alkylbenzene mixtures, the V^E values have the following order: *m*-xylene > *p*-xylene \approx *o*-xylene > toluene, while for 2-propanol + alkylbenzene mixtures, the V^E values decrease in the order: *m*-xylene > *p*-xylene > toluene \approx *o*-xylene. In both cases, the V^E values in mixtures with benzene are positive over the whole composition range, having a similar magnitude as *m*-xylene in mixtures with 2-propanol, and the highest values comparing to the mixtures with 1-propanol.

From work of Singh *et al.*,⁴⁸ it is evident that alkylbenzene molecules are more or less fitted into the network of 1- and 2-propanol. This is specially the case of toluene comparing to benzene, due to its stronger electron-donating power.

On the other hand, the packing of xylene molecules is sterically hindered by the two methyl groups placed on different sites of the aromatic ring for correct orientation. Thus, a limitation of the interaction of the hydroxyl group of the alcohol with the π electron cloud of the aromatic hydrogen was realized. It is clear that the position of the methyl groups in *m*-xylene results in the maximum steric hindrance and, as a result, the maximum positive of V^E .

Finally, it can be concluded that the branching of the alkyl group in 2-propanol creates a greater geometrical contribution to fit the corresponding xylene into the alcohol network.

The V^E for all mixtures of benzene with isomeric butanols⁴⁹ are positive and follow the sequence: 1-butanol < 2-methyl-1-propanol < 2-butanol < 2-methyl-2-propanol, showing in this way that V^E becomes more positive as the branching in the alcohol molecule increases. It is the consequence of the creation of steric hindrance near the OH-group in branched alcohols, whereby it is the prevailing effect for 2-methyl-2-propanol.⁵⁰ Namely, this can be explained by postulating that steric hindrance creates the presence of one propyl group at the 1° atom in 1-butanol, one *iso*-butyl group at the 1° carbon atom in 2-methyl-1-propanol, one methyl and one ethyl group at the 2° carbon atom in 2-butanol and three methyl groups at the 3° carbon atom in 2-methyl-2-propanol.

This suggests that the appearance of steric hindrance due to the branching in an alcohol is conditioned by the strength of the interaction of unlike molecules in the order 1-butanol > 2-methyl-1-propanol > 2-butanol > 2-methyl-2-propanol. In addition, bearing in mind that the molecular sizes of the unlike components in the mixtures are similar, the packing of the molecules is not good, resulting also in positive V^E values.

In addition, it is of interest to compare the behaviour of toluene in mixtures with 1-butanol and its isomers⁴⁷ (2-butanol, 2-methyl-1-propanol, 2-methyl-2-propanol). It is known that the electron donating power of toluene is stronger than that of benzene because of the methyl group added in the benzene ring and the hydroxyl hydrogen interacts more highly with the π electron cloud of toluene than that of benzene. This results in smaller V^E values of these alcohols with toluene than those with benzene. Finally, the V^E values of the branched alcohols are higher than those for the 1-alcohols. This could be attributed explicitly to the steric hindrance caused by a change in the proportion of different structural shapes of the alcohol molecules with its changing mole fraction.

4. ALCOHOL + HALOAROMATIC OR NITROAROMATIC SYSTEMS

4.1. 1-Alcohols with haloaromatics and nitroaromatics

Methanol partially and all 1-alcohols (ethanol, 1-propanol, 1-butanol and 1-pentanol) with chlorobenzene exhibit S-shaped V^E-x_1 curves, as can be seen in Fig. 2.¹⁹ It is obvious that the maximum positive values of these systems are lower and the minimum negative values are higher than the corresponding values of 1-alcohol systems with benzene.

As in the previous cases of the systems with benzene, the positive values of V^E in the lower region of the 1-alcohols are also the result of H-bond rupture and stretching of the self-associated alcohol molecules.

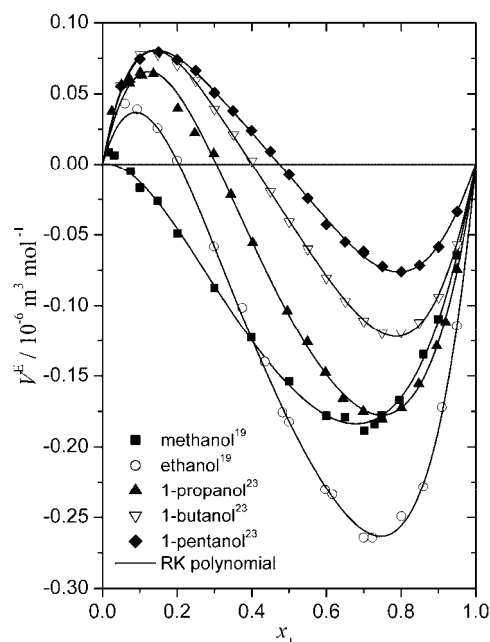


Fig. 2. Experimental values of V^E for the systems of 1-alcohols (1) with chlorobenzene (2) at 313.15 K. The symbols refer to the experimental points, while the lines present the results calculated by the Redlich–Kister polynomial.^{19,23}

Negative contributions predominate in the alcohol rich region because of dipolar complexes and changes of the free volumes in the real mixtures, as well as the geometrical fitting between unlike molecules, which are much stronger than in the systems with benzene. Here, there is an interaction between the π -electronic cloud of aromatic ring and the OH group, as in the case of the benzene mixtures, and the formation of OH–Cl hydrogen-bonded complexes between the OH group of the 1-alcohols and the electronegative Cl atom on the benzene ring.¹⁹ In addition, it is evident that the maxima of the dissociation of the polymeric aggregates of the alcohols differ slightly, since ordinary aliphatic alcohols are relatively poor proton donors. However, as the mole fraction of the higher 1-alcohol increases, the rupture of the hydrogen bonds of the alcohol increases from 1-propanol to 1-pentanol and positive volume changes appear at higher mole fraction of 1-pentanol.

The decrease in negative values of V^E with increasing chain length of the 1-alcohols could suggest that the dipole–dipole interactions are weaker in the higher 1-alcohols because of the decrease of their polarizability with increasing chain length. Bearing in mind that complexation⁵¹ is predominantly due to polarization interaction, the trend of complex formation has the following order 1-propanol > 1-butanol > 1-pentanol, which causes the increase of V^E from lower to higher 1-alcohols. Then, the relatively high electron donor capacity of chlorobenzene, because of the introduction of a Cl atom into the benzene ring, interacts more strongly with 1-propanol than with the other higher alcohols. In addition, only a

smaller fraction of hydrogen bonds are ruptured in the higher alcohols, while the steric hindrance of 1-pentanol is higher than that of 1-propanol, giving less negative values of V^E .

It is possible to include mixtures of 1-alcohols with other chlorinated benzenes, *i.e.*, 1,2-dichlorobenzene,⁵² 1,3-dichlorobenzene⁵³ and 1,2,4-trichlorobenzene⁵⁴ for comparison with mixtures of chlorobenzene + 1-alcohols. The experimental data for binary mixtures of these haloaromatics with 1-butanol, 1-pentanol, 1-hexanol, 1-heptanol and 1-octanol were measured at 303.15 K.²⁹

As in the case of the mixtures with chlorobenzene, V^E is negative in mixtures rich in 1-alcohols and positive in the region rich in both dichlorobenzene and 1,2,4-trichlorobenzene. The trend of V^E vs. the mole fraction x curve is similar for all mixtures of chlorobenzene, dichlorobenzenes and trichlorobenzene. This could be attributed to the dominant influence of the interactions between unlike molecules and the structure-making effect, which becomes remarkable due to the introduction of a second Cl atom, including its position in the benzene ring, and a third Cl atom.

In addition, it is necessary to consider mixtures of alcohols with nitrobenzene⁵⁵ and bromobenzene⁵⁶ and compare the obtained results with those of chlorobenzene. Namely, the V^E values become more negative due to the decrease in the π -electron density on the benzene ring when a halo or nitro group is introduced (nitro group deactivates the benzene ring).

When the Cl atom was replaced with a Br atom, no greater changes in V^E were observed,⁵⁷ which was to be expected bearing in mind the similar values of their dipole moments (chlorobenzene 1.6; bromobenzene 1.5) and the dipole moments of alcohols, as well as specific interactions like those of alcohol mixtures with chlorobenzene. However, the partial accommodation of linear alcohol molecules between the nitrobenzene molecules and interactions due to the high polarity of nitrobenzene (dipole moment 3.90) led to more negative V^E values, compared to those obtained with the halo compounds.⁵⁵

The small positive values of V^E in mixtures deficient in alcohols are due to the predominant H-bond stretching, as was already indicated in mixtures with chlorobenzene.

4.2. Branched alcohols with haloaromatics

The experimental V^E data of 1-butanol, 2-butanol and 2-methyl-2-propanol with chlorobenzene at 313.15 K are shown in Fig. 3.²³

As can be seen, the trend in the positive values of V^E is in the order 1-butanol < 2-butanol < 2-methyl-2-propanol, which indicates that the predominant effect is the steric hindrance due to branching. The OH group introduced at 2° carbon atom of 2-butanol and the globular shape and relative position of OH group on *tert*-butanol suggest that the structural effects of the steric hindrance are

predominant. The influence of the methyl, ethyl and propyl groups at various carbon atoms in these alcohols were already considered.¹⁹ An increase of temperature leads to an increase of the distance between the chains, the breaking of associates and sterically-hindered unlike molecules. In all cases, a positive change of volume occurs. In addition, as a consequence, the strength of the bond interaction $H\cdots Cl$ follows the order: 1-butanol > 2-butanol > 2-methyl-2-propanol, confirming the increase of V^E of the branched alcohols.

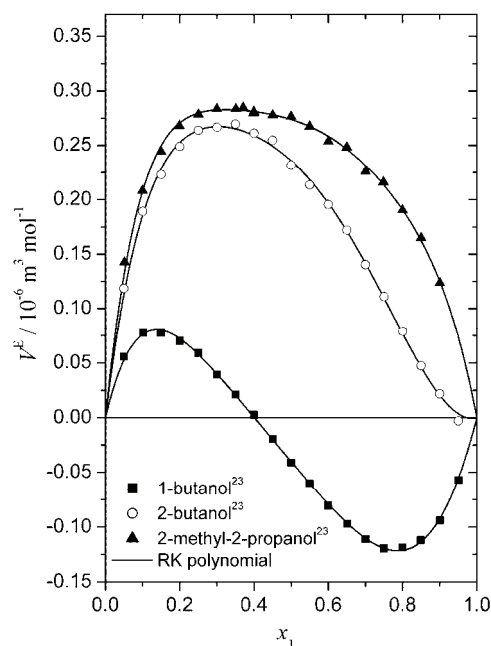


Fig. 3. Experimental values of V^E for the systems of linear or branched alcohols (1) with chlorobenzene (2) at 313.15 K. The symbols refer to the experimental points, while the lines present the results calculated by the Redlich–Kister polynomial.²³

5. ALCOHOL + HALOALIPHATIC SYSTEMS

The experimental V^E data for the 1-alcohol + chloroform systems at 308.15 K are shown in Fig. 4.^{20–22,24}

The V^E for methanol (1) + chloroform (2) mixtures are almost all negative except near the end of the dilute region for methanol. The other 1-alcohol systems with chloroform exhibit S-shaped V^E-x_1 curves with V^E positive at high mole fractions of chloroform and negative over the high mole fractions of the 1-alcohols.

For the considered systems, except methanol (1) + chloroform (2), the V^E values can be attributed qualitatively to the following contributions: (i) the positive values in the 1-alcohol lower region are caused by disruption or stretching effects on the three-dimensional, self-associated molecular structure of the alcohols; (ii) the negative values are a consequence of specific interactions between unlike molecules and (iii) the accommodation of chloroform molecules in the in-

termolecular space of 1-alcohol network structure leads to a more dense packing, affecting volume reduction in the region rich in 1-alcohols, which is, hence, a consequence of geometric factors.

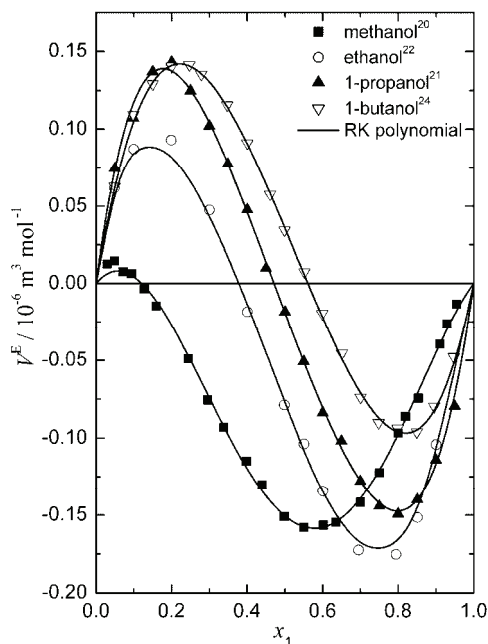


Fig. 4. Experimental values of V^E for the systems of 1-alcohols (1) with chloroform (2) at 308.15 K. The symbols refer to the experimental points, while the lines present the results calculated by the Redlich–Kister polynomial.^{20–22,24}

Concerning the alcohol mixtures with chlorobenzene (Fig. 2), unusual behaviour of the methanol + chloroform mixture was also registered. The absolute values of V^E for the same temperature at the minimum increase in the sequence ethanol > methanol > 1-propanol \approx 1-butanol. A possible explanation of this behaviour for the system with methanol could be a dominant contribution of (ii) over the factors (i) and (iii).

For the other 1-alcohol mixtures with chloroform, the positive V^E values in the 1-alcohol lower region are a consequence of the rupture of the H-bonding of the self-associated aggregates of the 1-alcohols with variable degrees of polymerization and the steric repulsion between the alkyl chain of the 1-alcohols and the Cl atom of the chloroform increasing with increasing chain length of the alcohols.

The negative V^E values in the chloroform rich region arise from changes in the free volumes in the real situation when specific interactions between unlike molecules dominate. Namely, chloroform possesses an electron-accepting hydrogen atom, which is favourable for interaction with the electron-donating oxygen atom in alcohols.

Special attention was paid to other chlorinated methanes: tetrachloromethane (CCl_4) and dichloromethane (CH_2Cl_2) in mixtures with 1-alcohols. CCl_4 is a

non-polar molecule, while the polarity of CH_2Cl_2 is larger than that of CHCl_3 . In addition, these molecules have different sizes and shapes but are structurally related, having only one C atom.⁵⁸

Comparing results for CHCl_3 with those of CCl_4 and CH_2Cl_2 mixtures with the same 1-alcohols,⁵⁹ it is evident that similar S-shaped V^E-x_1 curves were obtained for both the CH_2Cl_2 and CHCl_3 systems. It could be expected that the same three main contributions occur in the CH_2Cl_2 system as in the case when CHCl_3 was mixed with alcohols. In the case of CCl_4 , the presumption of a weak H-bond from hydroxyl group to a chlorine atom is acceptable.

The mixtures of CH_2Cl_2 with 1-alcohols showed somewhat different behaviour bearing in mind that positive values of V^E are dominant over the whole composition range, except in the region rich in some alcohols.

Two assumptions could be made for such a tendency of V^E :⁶⁰ (i) in the accommodation of CH_2Cl_2 in the H-bonded network of alcohols, the interaction of $\text{C-H}\cdots\text{H-O-R}$ is weaker than that of $\text{C-Cl}\cdots\text{H-O-R}$; (ii) it is assumed that the interaction of the C atom of CH_2Cl_2 with C-C of alcohol becomes stronger and V^E more positively increasing with increasing carbon chain length in ROH. It was concluded: (i) interaction between chlorinated methanes and R-OH are weak, except for methanol; (ii) the interactions with R-OH falls in the order $\text{CCl}_4 > \text{CHCl}_3 > \text{CH}_2\text{Cl}_2$; (iii) the tendency of interacting with C-C in ROH ascends in the order $\text{CCl}_4 \ll \text{CHCl}_3 \ll \text{CH}_2\text{Cl}_2$ and (iv) the H-bond of $\text{C-Cl}\cdots\text{H-O}$ is weaker than that of $\text{O-H}\cdots\text{O-H}$ but stronger than the interaction of C-Cl with C-C in ROH.

Branched alcohols could be also included here. For example, mixtures of CH_2Cl_2 with isomer of butanol (2-butanol, 2-methyl-1-propanol, 2-methyl-2-propanol).⁶¹

The volume of V^E ($x = 0.5$) for mixtures of 1-butanol and these isomers with CH_2Cl_2 increases in order: 1-butanol < 2-methyl-1-propanol < 2-butanol < 2-methyl-2-propanol. It is clear that a breaking of the hydrogen bonds leads to expansion of the mixtures. The positive values of V^E for the mixtures 2-butanol + chloroform²⁵ are very explicit as opposed to the S-shape of the V^E-x curve (Fig. 4) of the mixture 1-butanol + chloroform. The positive contribution of the break-up of the alcohol structure is responsible, as in the previous cases. Namely, V^E becomes more positive as the branching in the alcohols increases and negative values for the secondary and tertiary alcohols caused by the geometrical fitting into the remaining alcohol structure is less important.

6. CONCLUSIONS

It is evident that the excess molar volume V^E in the mixtures of alcohols with various types of compounds (aromatics, halo and nitroaromatics and haloaliphatics) treated in this work, showing very complex behaviour, possesses three dominant contributions. These are: (i) the positive values are caused by the break-

ing of H-bonds in the self-associated structure of the alcohol molecules, dipole–dipole interactions between monomers and polymers of the alcohols and stretching effects in the favourable orientation order of the second component; (ii) the negative values arise from changes of the “free volumes” in these real mixtures, the presence of electron donor–acceptor ability of alcohol and the other component, and OH... π electron H-bonded complexes between unlike molecules and (iii) the fitting of the other component into the intermolecular space of the network structure of the 1-alcohols or steric hindrance of the branched alcohols leads to the dense packing of the mixtures.

For the investigated mixtures, these contributions are balanced giving the corresponding values of V^E and the explained complex behaviour of the mixtures.

Acknowledgement. The authors gratefully acknowledge the financial support received from the Research Fund of Ministry of Science and Environmental Protection, Serbia and the Faculty of Technology and Metallurgy, University of Belgrade (Project No. 142064).

ИЗВОД

СТУДИЈА МОЛЕКУЛСКИХ ИНТЕРАКЦИЈА НА БАЗИ ВОЛУМЕТРИЈСКИХ СВОЈСТАВА ТЕЧНИХ БИНАРНИХ СМЕША КОЈЕ САДРЖЕ АЛКОХОЛЕ

БОЈАН Д. ЂОРЂЕВИЋ, ИВОНА Р. РАДОВИЋ, МИРЈАНА Љ. КИЈЕВЧАНИН,
АЛЕКСАНДАР Ж. ТАСИЋ и СЛОБОДАН П. ШЕРБАНОВИЋ

Технолошко–металуришки факултет, Универзитет у Београду, Карнегијева 4, 11120 Београд

У овом раду испитана је веза између волуметријских ефеката мешања и молекулских интеракција различитих молекула у бинарним смешама нормалних или разгранатих алкохола са различитим компонентама (ароматима, хало и нитроароматима, халогеним дериватима угљоводоника). Овај рад садржи преглед наших истраживања последњих година, као и резултате истраживања других аутора у циљу бољег разумевања волуметријских својстава и бољег увида у сложеност структура испитиваних смеша. Узети су у обзир и детаљно објашњени физички, хемијски и геометријски утицаји на промену V^E вредности (позитивне, сигмоидне, негативне). Утврђено је да на однос ових доприноса велики утицај има понашање молекула алкохола у контакту са другим компонентама.

(Примљено 13. јануара 2009)

REFERENCES

1. B. D. Djordjević, M. Lj. Kijevčanin, J. P. Orlović, S. P. Šerbanović, *J. Serb. Chem. Soc.* **66** (2001) 213
2. B. D. Djordjević, S. P. Šerbanović, I. R. Radović, A. Ž. Tasić, M. Lj. Kijevčanin, *J. Serb. Chem. Soc.* **72** (2007) 1437
3. S. P. Šerbanović, B. D. Djordjević, D. K. Grozdanić, *J. Chem. Eng. Japan* **27** (1994) 671
4. B. D. Djordjević, S. P. Šerbanović, D. K. Grozdanić, *Can. J. Chem. Eng.* **72** (1994) 171
5. M. Lj. Kijevčanin, B. D. Djordjević, P. S. Veselinović, S. P. Šerbanović, *J. Serb. Chem. Soc.* **63** (1998) 237
6. I. R. Grgurić, A. Ž. Tasić, B. D. Djordjević, M. Lj. Kijevčanin, S. P. Šerbanović, *J. Serb. Chem. Soc.* **68** (2003) 47

7. M. Lj. Kijevčanin, B. D. Djordjević, S. P. Šerbanović, I. R. Grgurić, A. Ž. Tasić, *Phys. Chem. Liquids* **42** (2004) 147
8. M. Lj. Kijevčanin, B. D. Djordjević, S. P. Šerbanović, I. R. Grgurić, A. Ž. Tasić, *Phys. Chem. Liquids* **44** (2006) 233
9. S. P. Šerbanović, B. D. Djordjević, D. K. Grozdanić, *Fluid Phase Equilib.* **57** (1990) 47
10. A. Ž. Tasić, B. D. Djordjević, D. K. Grozdanić, *J. Chem. Eng. Data* **37** (1992) 310
11. B. D. Djordjević, M. Lj. Kijevčanin, S. P. Šerbanović, *Fluid Phase Equilib.* **155** (1999) 205
12. M. Lj. Kijevčanin, A. B. Djordjević, I. R. Grgurić, B. D. Djordjević, S. P. Šerbanović, *J. Serb. Chem. Soc.* **68** (2003) 35
13. S. P. Šerbanović, I. R. Grgurić, M. Lj. Kijevčanin, A. Ž. Tasić, B. D. Djordjević, *Korean J. Chem. Eng.* **21** (2004) 858
14. M. Lj. Kijevčanin, S. P. Šerbanović, I. R. Radović, B. D. Djordjević, A. Ž. Tasić, *J. Serb. Chem. Soc.* **71** (2006) 807
15. I. R. Radović, M. Lj. Kijevčanin, M. Z. Gabrijel, S. P. Šerbanović, B. D. Djordjević, *Chem. Papers* **62** (2008) 302
16. N. Radojković, A. Tasić, B. Djordjević, D. Grozdanić, *J. Chem. Thermodyn.* **8** (1976) 1111
17. A. Ž. Tasić, D. K. Grozdanić, B. D. Djordjević, S. P. Šerbanović, N. Radojković, *J. Chem. Eng. Data* **40** (1995) 586
18. I. R. Grgurić, S. P. Šerbanović, M. Lj. Kijevčanin, A. Ž. Tasić, B. D. Djordjević, *Thermochim. Acta* **412** (2004) 25
19. S. P. Šerbanović, M. Lj. Kijevčanin, I. R. Radović, B. D. Djordjević, *Fluid Phase Equilib.* **239** (2006) 69
20. M. Lj. Kijevčanin, M. M. Djuriš, I. R. Radović, B. D. Djordjević, S. P. Šerbanović, *J. Chem. Eng. Data* **52** (2007) 1136
21. M. Lj. Kijevčanin, I. M. Purić, I. R. Radović, B. D. Djordjević, S. P. Šerbanović, *J. Chem. Eng. Data* **52** (2007) 2067
22. M. Lj. Kijevčanin, S. P. Šerbanović, I. R. Radović, B. D. Djordjević, A. Ž. Tasić, *Fluid Phase Equilib.* **251** (2007) 78
23. I. R. Radović, M. Lj. Kijevčanin, E. M. Djordjević, B. D. Djordjević, S. P. Šerbanović, *Fluid Phase Equilib.* **263** (2008) 205
24. J. D. Smiljanić, M. Lj. Kijevčanin, B. D. Djordjević, D. K. Grozdanić, S. P. Šerbanović, *Int. J. Thermophys.* **29** (2008) 586
25. J. D. Smiljanić, M. Lj. Kijevčanin, B. D. Djordjević, D. K. Grozdanić, S. P. Šerbanović, *J. Chem. Eng. Data* **53** (2008) 1965
26. J. M. Resa, C. Gonzalez, R. G. Concha, M. Iglesias, *Phys. Chem. Liquids* **42** (2004) 493
27. M. A. Saleh, Sh. Akhtar, M. Sh. Ahmed, *J. Mol. Liquids* **116** (2005) 147
28. R. Tanaka, S. Toyama, *J. Chem. Eng. Data* **42** (1997) 871
29. T. M. Letcher, J. A. Nevines, *J. Chem. Thermodyn.* **26** (1994) 697
30. A. Rodriguez, J. Canosa, J. Tojo, *J. Chem. Eng. Data* **44** (1999) 1298
31. M. C. S. Subha, K. C. Rao, G. Narayanaswamy, S. B. Rao, *Phys. Chem. Liquids* **18** (1988) 185
32. P. Assarsson, F. R. Eirich, *J. Phys. Chem.* **72** (1968) 2710
33. E. A. Muller, P. Rasmussen, *J. Chem. Eng. Data* **36** (1991) 214
34. A. J. Treszczanowicz, O. Kiyohara, G. C. Benson, *J. Chem. Thermodyn.* **13** (1981) 253
35. M. S. Contreras, *J. Chem. Eng. Data* **46** (2001) 1149
36. P. A. Kollman, L. C. Allen, *Chem. Reviews* **72** (1972) 283

37. S. Yamabe, K. Morokuma, *J. Am. Chem. Soc.* **97** (1975) 4458
38. R. K. Nigam, P. P. Singh, *Trans. Faraday Soc.* **65** (1969) 950
39. R. Mecke, *Discuss. Faraday Soc.* **9** (1950) 161
40. C. Bourderon, C. Sandorfy, *J. Chem. Phys.* **59** (1973) 2527
41. F. Smith, I. Brown, *Aust. J. Chem.* **26** (1973) 705
42. K. Nakanishi, H. Shirai, *Bull. Chem. Soc. Japan* **43** (1970) 1634
43. S. Figueroa-Gerstenmaier, A. Cabanas, M. Costas, *Phys. Chem. Chem. Phys.* **1** (1999) 665
44. K. N. Marsh, C. Burfitt, *J. Chem. Thermodyn.* **7** (1975) 955
45. P. Munk, A. Qin, D. E. Hoffman, *Collect. Czech. Chem. Commun.* **58** (1993) 2612
46. K. S. Kumar, N. V. Reddy, *Phys. Chem. Liquids* **39** (2001) 117
47. U. Bhardwaj, S. Maken, K. C. Singh, *J. Chem. Thermodyn.* **28** (1996) 1173
48. K. C. Singh, K. C. Kalra, S. Maken, B. L. Yadav *J. Chem. Eng. Data* **39** (1994) 241
49. A. Ali, A. K. Nain, B. Lal, D. Chand, *Int. J. Thermophys.* **25** (2004) 1835
50. B. Orge, M. Iglesias, G. Marino, M. Domínguez, M. M. Piñeiro, J. Tojo, *Fluid Phase Equilib.* **170** (2000) 151
51. K. Garabadu, G.S. Roy, S. Tripathy, B.B. Swain, *Czech. J. Phys.* **47** (1997) 765
52. T. S. Vijayalakshmi, P. R. Naidu, *J. Chem. Eng. Data* **34** (1989) 413
53. T. S. Vijayalakshmi, P. R. Naidu, *J. Chem. Eng. Data* **35** (1990) 338
54. T. S. Vijayalakshmi, P. R. Naidu, *J. Chem. Eng. Data* **37** (1992) 368
55. G. Dharmaraju, G. Narayanaswamy, G. K. Raman, *J. Chem. Thermodyn.* **12** (1980) 563
56. P. Venkateswarlu, G. Dharmaraju, G. K. Raman, *Proc. Indian Nat. Sci. Acad.* **48A** (1982) 265
57. K. Prasad, K. S. Kumar, G. Prabhakar, P. Venkateswarlu, *J. Mol. Liquids* **123** (2006)
58. H. L. Zhang, *J. Chem. Eng. Data* **48** (2003) 52
59. J. Nath, S. K. Mishra, *J. Chem. Eng. Data* **43** (1998) 196
60. H. L. Zhang, S. J. Han, *Phys. Chem. Liquids* **31** (1996) 49
61. J. Pardo, V. Rodriguez, C. Lafuente, P. M. Royo, J. S. Urieta, *J. Chem. Thermodyn.* **25** (1993) 373.



J. Serb. Chem. Soc. 74 (5) 493–502 (2009)
JSCS–3849

A mechanistic investigation of the oxidation of *N*, α -diphenylnitrones by dichloramine-T in aqueous acetonitrile medium – a non-linear Hammett plot

SUBRAMANIAN MANIVARMAN¹, GOVINDASAMY RAJARAJAN¹, GOVINDASAMY MANIKANDAN¹, MAHALIGAM SEKAR², JAYARAMAN JAYABHARATHI¹ and VENUGOPAL THANIKACHALAM^{1*}

¹Department of Chemistry, Annamalai University, Annamalainagar 608 002, Tamil Nadu and

²Department of Chemistry, Post Graduate Centre, Government Arts and Science College, Chidambaram 608 001, India

(Received 24 May 2007, revised 9 February 2009)

Abstract: The kinetics of oxidation of a number of *meta*- and *para*-substituted *N*, α -diphenylnitrones (nitrone) by dichloramine-T (DCT) was investigated in the presence of alkali in aqueous acetonitrile medium. The order with respect to DCT was one and to OH⁻ an inverse fractional order. The reaction was first order with respect to nitrone. Both electron releasing and withdrawing substituents suppress the reaction rate. The observed rate constant for the substituents were plotted against the Hammett constant, σ , and a non-linear concave downward curve was obtained. The electron withdrawing substituents fall on one side of the curve, having a negative ρ value and the electron releasing substituents fall on the other side, with a positive ρ value. A mechanism is proposed and the derived rate law is in conformity with the observed results.

Keywords: nitrones; kinetics; dichloramine-T; non-linear concave downward curve.

INTRODUCTION

Many oxidation reactions^{1–11} have been performed using dichloramine-T (DCT). DCT is an effective oxidizing and also chlorinating agent. The kinetics and oxidation of nitrone and substituted nitrones^{12–16} have already been reported. However, there is no systematic kinetic report on the oxidation of some substituted *N*, α -diphenylnitrones by *N*-halo compounds. In this paper, results on the kinetics of oxidation of some *meta*- and *para*-substituted *N*, α -diphenylnitrons with dichloramine-T (DCT) in aqueous acetonitrile in the presence of sodium hydroxide are reported.

* Corresponding author. E-mail: pvta1998@yahoo.co.in
doi: 10.2298/JSC0905493M

EXPERIMENTAL

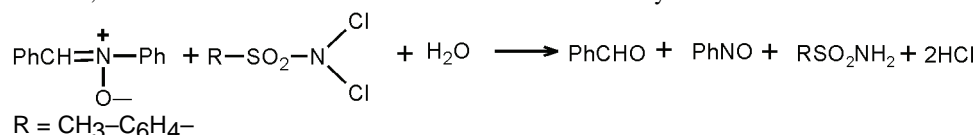
Dichloramine-T was prepared by the chlorination of *p*-toluenesulphonamide.¹⁷ *N*, α -diphenylnitron and substituted *N*, α -diphenylnitrones were prepared by literature methods.¹⁸ The purity of the nitrones were checked by their melting point, mixed melting point and the TLC method. AnalaR grade sodium hydroxide and sodium perchlorate, and purified acetonitrile were used. Doubly distilled water was employed throughout this study.

Kinetic measurements

For the kinetic runs, a measured amount of DCT pre-equilibrated at 35 °C was rapidly added to a thermally equilibrated mixture containing the appropriate amounts of the nitron, alkali, acetonitrile and water. The progress of the reaction was monitored for two half lives by the iodometric determination of unreacted DCT in a measured aliquot withdrawn at regular intervals of time. The first-order rate constants were reproducible within ± 3 %.

Stoichiometry and product analysis

Stoichiometric runs, performed with an excess of DCT in the presence of sodium hydroxide, revealed that one mole of the oxidant was consumed by one mole of nitron:



For identification of the product, an excess of oxidant was mixed with a substrate under kinetic conditions. After completion of the reaction, the reaction mixture was extracted with chloroform. The solvent was removed under reduced pressure. Two spots were obtained; products were identical with benzaldehyde and nitrosobenzene. The crude products were separated by column chromatography, benzene-chloroform as the eluent (80 % benzene-chloroform, silica gel 60-120 mesh). The melting point of the obtained solid product was found to be 67 °C which is almost identical to the melting point of the nitrosobenzene (m.p. 68 °C). The other liquid product, benzaldehyde, was confirmed by its semicarbazone (m.p. 221 °C; lit. 222 °C) and 2,4-diphenylhydrazone (m.p. 237 °C; lit. 239 °C) and 2,4-diphenylhydrazone (m.p. 237 °C; lit. 239 °C) derivatives. The recorded IR spectrum of nitrosobenzene, exhibiting three bands at 1626, 1500 and 1019 cm⁻¹, attributed to the stretching frequency of C-N, one sharp band at 1452 cm⁻¹, due to the stretching vibration of N-O, and band at 530 cm⁻¹, due to ring deformation and the CNO bending vibration, was similar to that of the authentic sample.¹⁹

RESULTS AND DISCUSSION

The reaction was found to be first order with respect to the disappearance of dichloramine-T (DCT), as evidenced by the good linearity in the plot of log titre *versus* time. The pseudo-first order rate constant increased with increasing DCT concentration (Table I).

The rate constant increased with increasing nitron concentration (Table I). The plot of log k_{obs} *versus* log $c(\text{nitron})$ for all the studied compounds was found to be linear with a slope of unity, indicating a first order kinetics with respect to nitron. The double reciprocal plot of $1/k_{\text{obs}}$ *versus* $1/c(\text{nitron})$ was linear with a finite intercept on the rate axis, indicating that the complex was formed before the rate-determining step in the reaction.

The effect of alkali has been studied by varying the concentration of OH⁻ at a given substrate concentration. The plot of log k_{obs} versus log $c(\text{OH}^-)$ showed a fractional order with respect to OH⁻ (Table II). The insignificant effects of sodium perchlorate on the reaction rate indicates that the reaction may be between dipoles (Table II) and neutral molecules.²⁰

TABLE I. Effect of $c(\text{DCT})$ and $c(\text{nitrone})$ on the reaction rate at 35 °C. $c(\text{OH}^-) = 5.0 \times 10^{-3}$ mol dm⁻³; AN-H₂O = 50 % (v/v); $c(\text{NaClO}_4) = 0.10$ mol dm⁻³

$c(\text{DCT}) / 10^{-3}$ mol dm ⁻³	$c(\text{nitrone}) / 10^{-2}$ mol dm ⁻³	$k_{\text{obs}} / 10^{-4}$ s ⁻¹
0.50	1.00	2.4
0.75	1.00	3.5
1.00	1.00	4.8
1.25	1.00	5.3
1.50	1.00	6.4
2.00	1.00	7.4
1.00	0.50	2.7
1.00	1.00	4.8
1.00	1.50	6.5
1.00	2.00	7.6
1.00	2.50	9.9
1.00	3.00	11

TABLE II. Effect of the variation of $c(\text{OH}^-)$ and $c(\text{NaClO}_4)$ on the reaction rate at 35 °C. $c(\text{DCT}) = 1.00 \times 10^{-3}$ mol dm⁻³; $c(\text{nitrone}) = 1.00 \times 10^{-2}$ mol dm⁻³; AN-H₂O = 50 % (v/v)

$c(\text{OH}^-) / 10^{-3}$ mol dm ⁻³	$c(\text{NaClO}_4) / 10^{-2}$ mol dm ⁻³	$k_{\text{obs}} / 10^{-4}$ s ⁻¹
2.50	10	3.6
3.75	10	4.0
5.00	10	4.8
6.25	10	5.8
7.50	10	6.4
5.00	2.5	4.5
5.00	8.7	4.6
5.00	10	4.8
5.00	12.5	4.9
5.00	15	5.0
5.00	18	5.4
5.00	20	5.7

The rate increased with increasing concentration of *p*-toluenesulphonamide (PTS), indicating a shift of the free hydration equilibrium towards the left during the production of HOCl (Table III). The rate increased with increasing [Cl⁻] (Table III). The rates of oxidation of nitrones were determined in solvents containing different amounts of acetonitrile. The k_{obs} value increased with increasing amount of acetonitrile in the medium (Table IV), which shows neutral and dipole interaction in the activated complex. The oxidation of nitrones by DCT in an at-

mosphere of nitrogen failed to induce polymerization of acrylonitrile. Furthermore, the addition of acrylonitrile did not affect the rate. This indicates that a one electron oxidation giving rise to free radicals is unlikely in the present reaction.^{20e}

TABLE III. Effect of *p*-toluenesulphonamide (PTS) and Cl⁻ concentration on the reaction rate at 35 °C. $c(\text{DCT}) = 1.00 \times 10^{-3} \text{ mol dm}^{-3}$; $c(\text{nitron}) = 1.00 \times 10^{-2} \text{ mol dm}^{-3}$; $c(\text{OH}^-) = 5.0 \times 10^{-3} \text{ mol dm}^{-3}$; AN-H₂O = 50 % (v/v)

$c(\text{PTS}) / 10^{-3} \text{ mol dm}^{-3}$	$c(\text{Cl}^-) / 10^{-2} \text{ mol dm}^{-3}$	$k_{\text{obs}} / 10^{-4} \text{ s}^{-1}$
0.00	–	4.8
2.5	–	6.0
5.0	–	7.1
7.5	–	10
10	–	15
–	2.5	7.6
–	5.0	7.8
–	7.5	9.1
–	10	20

TABLE IV. Effect of the dielectric constant on the reaction rate at 35 °C. $c(\text{DCT}) = 1.00 \times 10^{-3} \text{ mol dm}^{-3}$; $c(\text{nitron}) = 1.00 \times 10^{-2} \text{ mol dm}^{-3}$; $c(\text{OH}^-) = 5.0 \times 10^{-3} \text{ mol dm}^{-3}$; $c(\text{NaClO}_4) = 0.10 \text{ mol dm}^{-3}$

AN-H ₂ O, % (v/v)	$k_{\text{obs}} / 10^{-4} \text{ s}^{-1}$
35	2.8
40	3.6
45	4.2
50	4.8
55	5.8
60	6.7

In order to investigate the effect of temperature on the reaction rate, the reaction was performed at 25, 30, 35 and 40 °C. The plot of $\ln(k_2/T)$ versus $1/T$ was found to be linear.²¹ The rate constant and thermodynamic parameters are tabulated in Table V.

Mechanism and rate law

The order with respect to both DCT and nitron was unity and with respect to OH⁻ was fractional. The addition of sodium perchlorate or acrylonitrile had an insignificant effect on the rate of the reaction. The addition of toluene, PTS or Cl⁻ increased the reaction rate.

The observed stoichiometry for the reaction was 1:1 and the major oxidation products are found to be benzaldehyde and nitrosobenzene. Based on the above observations, a probable mechanism and rate law for the oxidation of *N*, α -diphenylnitrones by dichloramine-T is given below.

The substrate (nitron), which behaves as an iminium salt²², exists in two resonance forms given in Eq. (1):

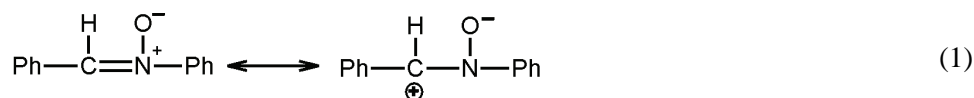
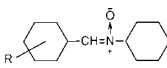
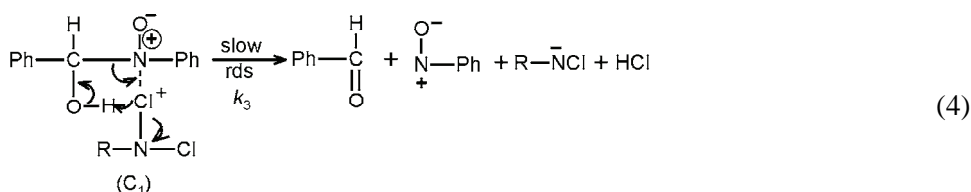
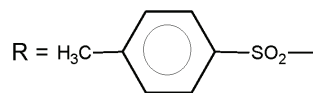
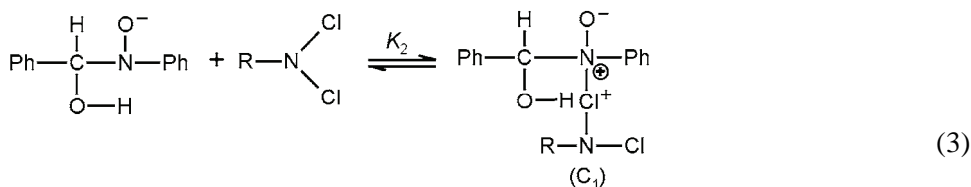
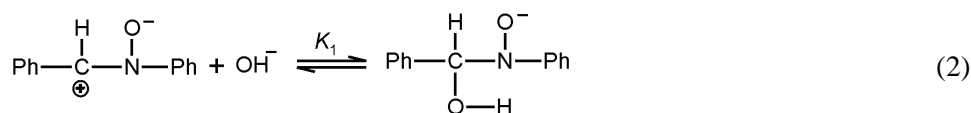
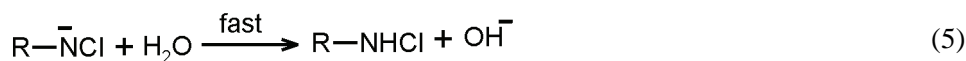


TABLE V. The rate constant and thermodynamic parameters for the oxidation of substituted nitrones by DCT. $c(\text{DCT}) = 1.00 \times 10^{-3} \text{ mol dm}^{-3}$; $c(\text{nitrone}) = 1.00 \times 10^{-2} \text{ mol dm}^{-3}$; $c(\text{OH}^-) = 5.0 \times 10^{-3} \text{ mol dm}^{-3}$; $c(\text{NaClO}_4) = 0.10 \text{ mol dm}^{-3}$

	$k_2 / 10^{-2} \text{ dm}^{-3} \text{ mol}^{-1} \text{ s}^{-1}$				ΔH^\ddagger kJ mol ⁻¹	$-\Delta S^\ddagger$ JK ⁻¹ mol ⁻¹	ΔG^\ddagger kJ mol ⁻¹	E_a kJ mol ⁻¹	R	SD
	T / K									
	303	308	313	318						
H	4.17	4.75	5.43	6.27	19.15	208.31	83.33	29.74	0.999	0.007
<i>p</i> -Me	1.33	1.60	2.37	3.11	44.49	134.51	85.92	47.07	0.990	0.064
<i>p</i> -OMe	1.18	1.38	2.92	2.91	52.88	107.73	86.00	55.46	0.922	0.218
<i>p</i> -F	2.50	2.98	4.07	5.34	38.83	147.88	84.37	41.41	0.992	0.048
<i>p</i> -Cl	2.22	2.86	3.94	5.08	42.33	137.11	84.56	45.92	0.998	0.022
<i>p</i> -Br	2.02	2.62	3.83	4.86	45.70	126.78	84.50	49.11	0.995	0.041
<i>p</i> -NO ₂	0.76	1.59	2.75	3.12	74.38	39.07	86.41	76.96	0.961	0.208
<i>m</i> -Me	2.50	3.45	4.36	5.65	40.38	142.31	84.21	42.96	0.998	0.024
<i>m</i> -F	2.03	2.61	3.79	4.66	43.55	134.47	84.96	45.93	0.994	0.046
<i>m</i> -Cl	2.08	2.50	3.28	4.41	37.52	152.72	84.56	40.40	0.992	0.046
<i>m</i> -Br	1.29	2.46	3.15	4.42	60.72	80.06	85.38	63.30	0.978	0.126
<i>m</i> -NO ₂	1.00	1.45	2.80	3.22	62.27	71.15	84.18	66.85	0.974	0.146

The attack of an electrophile occurs at the nitrogen atom rather than the carbon atom.





$$\text{Rate} = k_3 c(\text{C}_1) \quad (7)$$

$$c(\text{C}_1) = \frac{K_1 K_2 c(\text{S}_\text{T}) c(\text{OH}^-) c(\text{DCT})}{1 + K_1 c(\text{OH}^-)} \quad (8)$$

$$\frac{-d c(\text{DCT})}{dt} = \frac{K_1 K_2 k_3 c(\text{S}_\text{T}) c(\text{OH}^-) c(\text{DCT})}{1 + K_1 c(\text{OH}^-)} \quad (9)$$

$$k_{\text{obs}} = \frac{K_1 K_2 k_3 c(\text{S}_\text{T}) c(\text{OH}^-)}{1 + K_1 c(\text{OH}^-)} \quad (10)$$

or

$$\frac{1}{k_{\text{obs}}} = \frac{1}{K_1 K_2 k_3 c(\text{S}_\text{T}) c(\text{OH}^-)} + \frac{1}{K_1 k_3 c(\text{S}_\text{T})}$$

where $c(\text{S}_\text{T}) = c(\text{nitrone}_\text{T})$

A double reciprocal plot of k_{obs} versus $c(\text{OH}^-)$ is linear and the values of K_1 , K_2 and k_3 are obtained from the slope and intercept, respectively. The obtained values of $K_1 = 235$ and $K_2 k_3 = 9.33 \times 10^{-2}$ are consistent with the rate law.

Effect of substituents on the reaction rate

As an extension of the present investigation, the kinetics of the oxidation of some *meta*- and *para*-substituted *N*, α -diphenylnitrones with DCT was followed at four different temperatures (25–40 °C). The second-order rate constant and the thermodynamic parameters were calculated using the Eyring²¹ plot of $\log(k_2/T)$ against $1/T$, which were linear and the obtained data are given in Table V.

As can be seen from Table V, the entropy of oxidation was not constant for all the substituents. One of the conditions necessary for the applicability of the linear free energy relationship is the constancy of the entropy of activation.^{23,24} However, in most reaction series, this is not the case. If the Hammett equation is valid at one temperature, the condition for its validity at any other temperature is a linear relationship between the enthalpies and entropies and this is called the isokinetic relationship:^{23,24}

$$\Delta H^\ddagger = \Delta H_0^\ddagger + \beta \Delta S^\ddagger$$

A plot of ΔH^\ddagger vs. ΔS^\ddagger (Fig. 1) gave a straight line and the isokinetic temperature (β), obtained from the slope, was 326 K, which is greater than the experimental temperature, indicating that the reaction is enthalpy controlled. The linear

isokinetic correlation implies that all the nitrones are oxidized by the same mechanism and the changes in the reaction rate are governed by changes in both the enthalpy and entropy of activation. This is further supported by fact that E_a values are the lowest for the fastest reaction and higher for the slowest reaction.

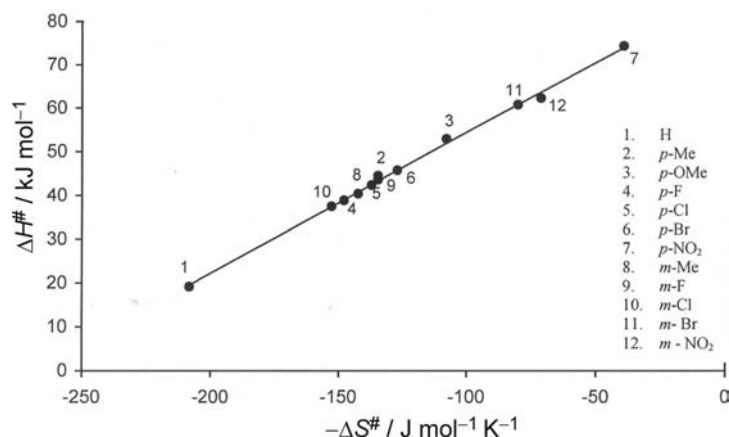


Fig. 1. The relationship between ΔH^\ddagger and ΔS^\ddagger for oxidation of nitrones by dichloramine-T.

Exner²⁵ criticized the validity of such a linear correlation between ΔH^\ddagger and ΔS^\ddagger as these quantities depend on each other. When measurements at two temperatures are made, the experimental data can be treated by the following equation:^{26,27}

$$\log k_2(T_2) = a + b \log k_2(T_1)$$

where $T_2 > T_1$.

The good correlation obtained when $\log k_2(318 \text{ K})$ was plotted against $\log k_2(308 \text{ K})$ (Fig. 2) ($R = 0.982$; slope = 0.680) shows that the reactions under investigation followed the same mechanism. The constancy of the ΔG^\ddagger values also confirms that the reactions of all the substituted compounds followed a common mechanism. The negative ΔS^\ddagger values implies the formation of an ionic transition state with an extensive charge separation, which may have a high degree of solvation and hence loss of entropy.

Deviation from the Hammett relationship

Application of the Hammett equation with the usual substituent constant σ to the $\log k_{\text{obs}}$ data of the *meta*- and *para*-substituted *N*, α -diphenylnitrones resulted in a concave downward curve (Fig. 3). Similar types of non-linear Hammett plots were observed previously in some reaction kinetics.^{28–30}

The obtained non-linear concave downwards type of Hammett plot (Fig. 3) is a composite of two straight lines, one with a positive ρ value and the other with a negative ρ value. A negative ρ value indicates the nucleophilic carbon is more

positively charged in the transition state than in the reactant, while a positive ρ value indicates dispersal of the positive charge.³ The values of the negative and positive ρ values, ρ^+ and ρ^- , respectively, at different temperature are given in Table VI.

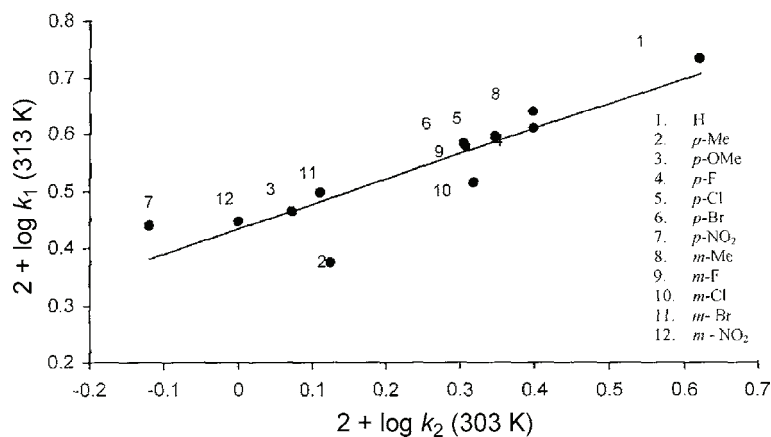


Fig. 2. Exner's plot.

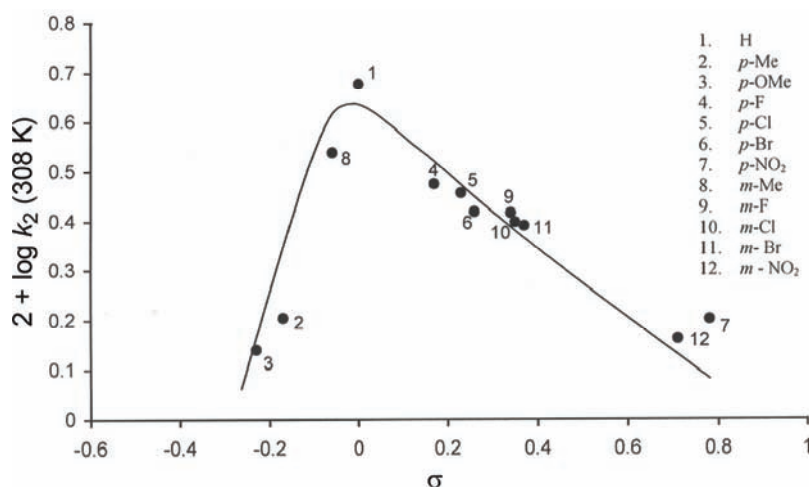


Fig. 3. Hammett plot.

TABLE VI. Values of ρ at different temperatures

$t / ^\circ\text{C}$	ρ^+	ρ^-
25	1.076	0.747
30	0.456	0.428
35	0.613	0.777
40	0.460	0.495

The reason for a break in the Hammett plot is either a change in the reaction mechanism or a change in the rate-determining step with change in the nature of the substituents.

In this reaction, a non-linear Hammett plot was obtained due to a change in the transition state in the reaction mechanism with respect to substituents because the isokinetic plot and the Exner plot gave a good correlation.

CONCLUSIONS

The oxidation of nitrones by DTC is of fractional order with respect to OH⁻ and first order with respect to DTC and nitron. Under the employed experimental conditions, nitrones are oxidized to benzaldehyde and nitrosobenzene. The high negative entropy of activation suggests the formation of a complex in the slow step. The isokinetic and Exner plots show that the oxidations of all the studied nitrones follow a common mechanism. The obtained concave Hammett plot indicates a change of the transition state with respect to the substituent on the benzene nucleus under the employed experimental conditions.

ИЗВОД

МЕХАНИСТИЧКО ПРОУЧАВАЊЕ ОКСИДАЦИЈЕ *N*, α -ДИФЕНИЛНИТРОНА ПОМОЋУ ДИХЛОРАМИНА-Г У ВОДЕНОМ РАСТВОРУ АЦЕТОНИТРИЛА: НЕЛИНЕАРНИ ХАММЕТТ-ОВ ГРАФИК

S. MANIVARMAN¹, G. RAJARAJAN¹, G. MANIKANDAN¹, M. SEKAR²,
J. JAYABHARATHI¹ и V. THANIKACHALAM¹

¹Department of Chemistry, Annamalai University, Annamalainagar-608 002, Tamil Nadu и ²Department of Chemistry, Post Graduate Centre, Government Arts and Science College, Chidambaram-608 001, India

Кинетика оксидације серије *мета*- и *пара*-супституисаних *N*, α -дифенилнитрона (нитрон) помоћу дихлорамина-Г (ДСТ) проучавана је воденом раствору ацетонитрила у присуству базе. Реакција је првог реда у односу на ДСТ, и инверзног фракционог реда у односу на ОН⁻. Реакција је првог реда у односу на нитрон. Како електрон-донорски, тако и електрон-привлачни супституенти, смањују брзину реакције. Када су константе брзине за супституенте дате у односу на Hammett-ову константу σ , добијена је нелинеарна силазна конкавна крива. Електрон-привлачни супституенти налазе се са једне стране криве са негативном ρ вредношћу, док су електрон-донорски супституенти са друге стране криве са позитивном ρ вредношћу. Предложени механизам и изведена брзина реакције су у сагласности са добијеним резултатима.

(Примљено 24. маја 2007, ревидирано 9. фебруара 2009)

REFERENCES

1. E. Bishop, V. J. Jennings, *Talanta* **1** (1958) 197
2. T. Higuchi, K. Ikeda, A. Hussain, *J. Chem. Soc. B* (1967) 546
3. T. Higuchi, A. Hussain, *J. Chem. Soc. B* (1967) 549
4. H. M. K. Naidu, D. S. Mahadevappa, *Indian J. Chem.* **13** (1975) 976
5. N. M. Made Gowda, A. A. Anamlamurthy, D. S. Mahadevappa, *Indian Acad. Sci.* **44** (1975) 5

6. H. M. K. Naidu, D. S. Mahadevappa, *Curr. Sci.* **45** (1976) 216
7. Rangaswamy, D. S. Mahadevappa, *J. Indian Chem. Soc.* **55** (1978) 60
8. H. S. Yathirajan, Rangaswamy, D.S. Mahadevappa, *J. Indian Chem. Soc.* **56** (1979) 421
9. H. S. Yathirajan, D. S. Mahadevappa, Rangaswamy, *Talanta* **27** (1980) 52
10. B. Thimme Gowda, J. Ishwara Bhatt, *J. Indian Chem. Soc.* **65** (1987) 159
11. B. Thimme Gowda, N. S. Sherigara, *Indian J. Chem.* **26A** (1987) 930
12. M. Uma, M. Gopalakrishnan, J. Jayabharathi, V. Thanikachalam, *Indian J. Chem.* **34B** (1995) 612
13. M. Uma, M. Gopalakrishnan, J. Jayabharathi, V. Thanikachalam, *J. Indian Chem. Soc.* **73** (1996) 92
14. M. Gopalakrishnan, J. Jayabharathi, V. Thanikachalam, *Asian J. Chem.* **11** (1999) 1459
15. M. Gopalakrishnan, M. Uma, J. Jayabharathi, V. Thanikachalam, *Afinidad* **59** (2002) 688
16. M. Uma, M. Gopalakrishnan, J. Jayabharathi, V. Thanikachalam, *Oxid. Commun.* **30** (2007) 625
17. a) O. Tomicek, J. Valcha, *Collect. Czech. Chem. Commun.* **16** (1951) 113; b) J. E. Leffler, *J. Org. Chem.* **20** (1955) 1202
18. a) H. Studinger, K. Niescher, *Helv. Chim. Acta* **2** (1919) 554; b) P. Grammaticakis, *Bull. Soc. Chim. Fr.* (1951) 889; c) Chem. Abstr. **46** (1952) 11133; d) V. Bellavita, *Gazz. Chim. Ital.* **65** (1935) 889; e) Chem. Abstr. **30** (1936) 3419; f) E. Bamberger, *Ber. Dtsch. Chem. Ges.* **57** (1924) 2082; g) J. E. Leffler, *J. Chem. Phys.* **23** (1955) 2199
19. a) G. M. Bradley, H. L. Strauss, *J. Phys. Chem.* **79** (1975) 1953; b) R. C. Peterson, *J. Org. Chem.* **29** (1964) 3133
20. a) J. E. Quinlan, E. Amis, *J. Am. Chem. Soc.* **77** (1955) 4187; b) P. D. Sharma, Y. K. Gupta, *J. Chem. Soc., Dalton Trans.* (1972) 52; c) K. S. Gupta, S. Mittal, S. P. Ghosh, *Indian J. Chem.* **19A** (1980) 869; d) C. D. Ritchie, W. F. Sager, *Prog. Phys. Org. Chem.* **2** (1964) 323; e) J. S. Litaler, W. A. Waters, *J. Chem. Soc.* (1959) 1299
21. W. F. K. Wynne-Jones, H. Eyring, *J. Chem. Phys.* **3** (1935) 492
22. H. Bohme, M. Haake, *Adv. Org. Chem.* **9** (1976) 107
23. J. E. Leffler, *J. Org. Chem.* **20** (1955) 1202
24. N. R. Gilkerson, C. A. Gallup, M. M. Jones, *Trans. Kansas Acad. Sci.* **57** (1954) 391
25. a) J. E. Leffler, *J. Chem. Phys.* **23** (1955) 2199; b) O. Exner, *Collect. Czech. Chem. Commun.* **29** (1964) 488; c) O. Exner, *Nature* **201** (1964) 488; d) D. Noyce, A. Bottini, S. Smith, *J. Org. Chem.* **23** (1958) 752
26. B. H. Anderson, W. P. Jancks, *J. Chem. Soc.* **82** (1960) 1773
27. E. Pratt, M. J. Kamlet, *J. Org. Chem.* **28** (1963) 1366
28. J. Hoffmann, J. Klicnar, V. Sterba, M. Vecera, *Collect. Czech. Chem. Commun.* **35** (1970) 1387
29. J. F. Burneu, R. E. Zahler, *Chem. Rev.* **49** (1951) 294
30. S. Meenakshisundaram, M. Amutha, *J. Chem. Res. S* **2** (1999), *J. Chem. Res. M* (1999) 0219.



J. Serb. Chem. Soc. 74 (5) 503–511 (2009)
JSCS–3850

Effects of various nitric oxide synthase inhibitors on AlCl₃-induced neuronal injury in rats

IVANA STEVANOVIĆ^{1*}, MARINA JOVANOVIĆ¹, ANKICA JELENKOVIĆ²,
MIODRAG ČOLIĆ¹ and MILICA NINKOVIĆ¹

¹Military Medical Academy, Institute for Medical Research, Crnotravska 17, Belgrade and

²Institute for Biological Research, Belgrade, Serbia

(Received 1 October, revised 9 December 2008)

Abstract: The present study was aimed at determining the effectiveness of nitric oxide synthase (NOS) inhibitors: *N*-nitro-*L*-arginine methyl ester, 7-nitroindazole and aminoguanidine in modulating the toxicity of AlCl₃ on superoxide production and the malondialdehyde concentration of Wistar rats. The animals were sacrificed 10 min and 3 days after the treatment and the forebrain cortex was removed. The results show that AlCl₃ exposure promotes oxidative stress in different neural areas. The biochemical changes observed in the neuronal tissues show that aluminum acts as pro-oxidant, while NOS inhibitors exert an anti-oxidant action in AlCl₃-treated animals.

Keywords: aluminum; forebrain cortex; NOS inhibitors; superoxide production; lipid peroxidation.

INTRODUCTION

Aluminum has the ability to produce neurotoxicity by many mechanisms. In addition to the promotion of insoluble beta-amyloid (A beta) and hyperphosphorylated tau protein formation and accumulation, Al can alter neuronal signal transduction pathways associated with glutamate receptors.^{1,2} In cerebella neurons in culture, long term-exposure to Al added *in vitro* impaired the glutamate (Glu)–nitric oxide (NO)–cyclic GMP (cGMP) pathway, reducing the glutamate-induced activation of NO synthase (NOS) and NO-induced activation of the cGMP generating enzyme, guanylate cyclase. These findings suggest that the impairment of the Glu–NO–cGMP pathway in the brain may be responsible for some of the neurological alteration induced by Al.^{3–5}

Free radicals (oxidative toxins) have been implicated in the destruction of cells through the process of lipid peroxidative damage of the cell membranes. Aluminum has been shown to alter the Ca²⁺ flux and homeostasis, and facilitate

* Corresponding author. E-mail: ivanav13@yahoo.ca
doi: 10.2298/JSC0905503S

peroxidation of membrane lipids.⁶ After exposure to Al, a statistically significant increase in malondialdehyde (MDA), an index of lipid peroxidation, was observed.^{7,8}

Molecular oxygen is the primary biological electron acceptor that plays vital roles in fundamental cellular functions. However, the beneficial properties of O₂ are accompanied by the inadvertent formation of reactive oxygen species (ROS), such as superoxide (O₂⁻), hydrogen peroxide (H₂O₂), and hydroxyl radicals (OH•).^{9,10} Evidence is being amassed that iron (Fe) accumulates in the brain and catalyzes O₂⁻ formation, which reacts with NO to form the very harmful peroxy-nitrite ion (ONOO⁻), that nitrates tyrosine residues to form nitrotyrosine.¹¹

The NO-synthesizing enzyme NOS is present in the mammalian brain in three different isoforms, two constitutive enzymes (*i.e.*, neuronal nNOS and endothelial eNOS) and one inducible enzyme (iNOS). All three isoforms are aberrantly expressed after Al intoxication giving rise to elevated levels of NO, which is apparently involved in neurodegeneration by various different mechanisms, including oxidative stress and activation of intracellular signaling mechanisms.¹²

Cell death and changes in neurite morphology were partly reduced when NO production was inhibited by NOS inhibitors.^{13–17} In view of the above, the present study was undertaken to examine whether O₂⁻ production and MDA concentration after receiving intracerebral injections of AlCl₃ can be modulated by the co-administration with various NOS inhibitors: non-specific inhibitor NOS (*N*-nitro-L-arginine methyl ester – L-NAME) and specific inhibitors: neuronal NOS inhibitor (7-nitroindazol – 7-NI) and inducible NOS inhibitor (aminoguanidine – AG).^{18–20}

EXPERIMENTAL

Materials and animals

The employed chemicals, all analytical grade, were purchased from Sigma (St. Louis, MO, USA). All drug solutions were prepared on the day of the experiment.

Male adult Wistar rats with a body mass 500 ± 50 g were used for the experiments. Groups of two or three rats per cage (Erath, FRG), were housed in an air-conditioned room at a temperature of 23±2 °C with 55±10 % humidity and with lights on 12 h/day (07.00–19.00 h). The animals were given a commercial rat diet and tap water *ad libitum*. The animals used for the procedure were treated in strict accordance with the NIH Guide for Care and Use of Laboratory Animals (1985).

Experimental procedure

For biochemical analysis, the rats were divided into eight basic groups (according to drug treatment). Each basic group consisted of two different subgroups (according to survival times – 10 min and 3 days) and each subgroup consisted of 10 animals. Animals were anesthetized by intraperitoneal injections of sodium pentobarbital (0.04 g/kg b.w.). Using a stereotaxic instrument for small animals, the chemicals were administered by a Hamilton microsyringe and injected into the CA1 sector of the hippocampus (coordinates: 2.5 A; 4.2 L; 2.4 V).²¹ The NOS inhibitors (L-NAME, 7-NI or AG) were immediately applied before a neuro-

toxin/saline solution. In all treated animals, the injected intracerebral volume was 10 μ l (Table I) and it was always injected into the same left side. All animals were decapitated and the heads were immediately frozen in liquid nitrogen and stored at -70 °C until use. Then the ipsilateral and contralateral forebrain cortex (FC) was quickly isolated and homogenized in ice-cold buffer containing 0.25 M sucrose, 0.10 mM EDTA, 50 mM K-Na phosphate buffer, pH 7.2. The homogenates were centrifuged twice at 1580 rpm for 15 min at 4 °C. The supernatant (crude mitochondrial fraction) obtained by this procedure was then frozen and stored at -70 °C.²²

Table I. All the experimental animal groups with the applied dosage for the appropriate treatment

Number	Group	Dosage
1	Control	0.9% saline solution
2	AlCl ₃	3.7×10^{-4} g/kg b.w. dissolved in 0.010 ml of deionized water
3	L-NAME + AlCl ₃	1×10^{-4} g dissolved in saline solution + AlCl ₃
4	7-NI + AlCl ₃	1×10^{-4} g dissolved in olive oil + AlCl ₃
5	AG + AlCl ₃	1×10^{-4} g dissolved in saline solution + AlCl ₃
6	L-NAME	1×10^{-4} g dissolved in saline solution + saline solution
7	7-NI	1×10^{-4} g dissolved in saline solution + saline solution
8	AG	1×10^{-4} g dissolved in saline solution + saline solution

Biochemical analysis

The superoxide anion content was determined through the reduction of nitro blue tetrazolium (Merck, Darmstadt, Germany) in a nitrogen saturated alkaline medium. Kinetic analysis was performed at 550 nm.²³

The lipid peroxidation index was measured as the quantity of produced malondialdehyde (MDA). Thiobarbituric acid reagent (TBAR–15 % trichloroacetic acid (Merck, Darmstadt) + 0.375 % TBA + 0.25 % mol HCl) reacted with MDA, which had been produced from polyunsaturated fatty acids in the process of peroxidation. The product of reaction – MDA, was measured spectrophotometrically at 533 nm.²⁴

The protein content in the rat brain homogenates (forebrain cortex-FC, ipsilateral and contralateral) was measured by the Lowry method using bovine serum albumin (Sigma) as the standard.²⁵

Data presentation and analysis

Statistical analysis was performed using the statistical software program, Statistic 5.0 for Windows. Descriptive data are expressed as the mean \pm standard deviation (*SD*). The statistical significance was determined as $p < 0.05$ using either the Student's *t*-test or ANOVA followed by the Tukey's *t*-test.

RESULTS

Superoxide production in the rat forebrain cortex (FC)

The O₂⁻ levels (μ M red. NBT min⁻¹ mg⁻¹ proteins) bilaterally in the rat FC homogenates at 10 min (Fig. 1A) and 3 days (Fig. 1B) after the treatment are presented in Fig. 1. At the early tested time (10 min), AlCl₃ injection resulted in higher levels of O₂⁻ production in the contralateral FC, compared to the control animals ($p < 0.05$). Also, 7-NI + AlCl₃ application, as well as L-NAME injection and AG injection, resulted in an increase in the production of O₂⁻ bilaterally in

the FC after 10 min, compared to the control groups. However, after 3 days, L-NAME + AICl₃ and 7-NI + AICl₃ injection resulted in lower levels of O₂⁻ production bilaterally in the same brain structure, compared to the control groups. At 10 min after 7-NI + AICl₃ application, the O₂⁻ levels showed increase in the ipsilateral FC, compared with the AICl₃-treated animals. L-NAME application resulted in an increase of the O₂⁻ levels ipsilaterally in the FC after 10 min and bilaterally in this brain structure after 3 days, compared to the L-NAME + AICl₃-treated groups. Also, AG injection resulted in an increase of O₂⁻ production in the ipsilateral FC after 10 min, compared to the AG + AICl₃-treated group. However, 7-NI injection resulted in a decrease of O₂⁻ production bilaterally in the FC after 10 min, compared to the 7-NI + AICl₃-treated groups (Fig. 1).

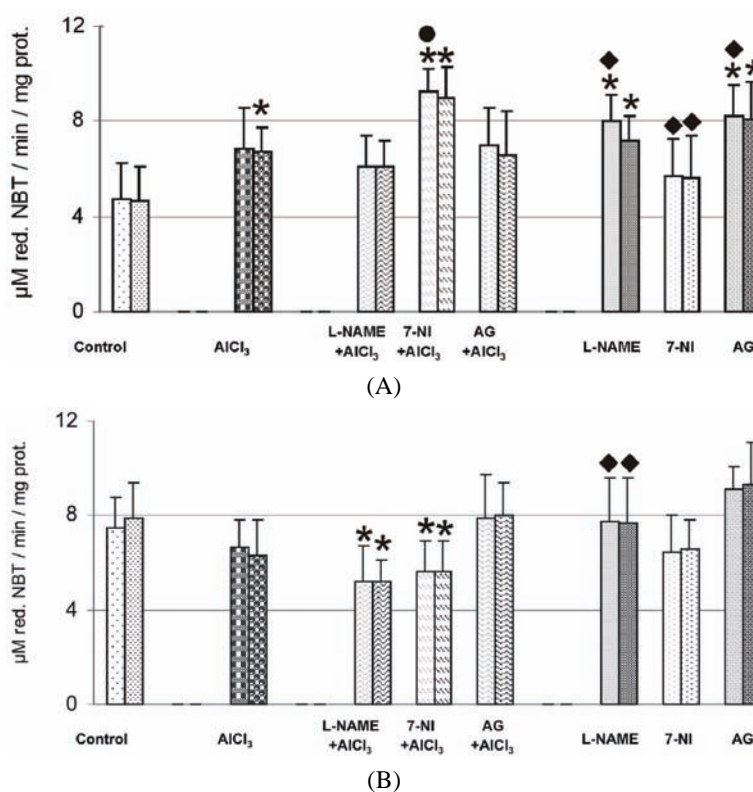


Fig. 1. The effect of intrahippocampal drug injection on O₂⁻ production (µM red. NBT/min/mg protein) in the rat ipsilateral and contralateral FC at different survival times – 10 min (A) and 3 days (B) after treatment. Data are means ±SD of 10 animals. *A statistically significant difference between the treated (AICl₃-, NOS inhibitors + AICl₃- and NOS inhibitors-treated) and the control (sham-operated) animals ($p < 0.05$). •A statistically significant difference between the NOS inhibitors + AICl₃-treated and the AICl₃-treated animals ($p < 0.05$).

♦A statistically significant difference between the NOS inhibitors-treated and the NOS inhibitors + AICl₃-treated animals ($p < 0.05$).

Malondialdehyde concentration in the rat forebrain cortex (FC)

The MDA concentration (nM MDA h⁻¹ mg⁻¹ proteins) in the ipsilateral and contralateral FC homogenates at 10 min (Fig. 2A) and 3 days (Fig. 2B) after the treatment are shown in Fig. 2. Ten minutes after the injection of AlCl₃ injection and of L-NAME, the MDA concentration was bilaterally increased in the FC compared to controls, with the difference being statistically significant (Student's *t*-test; *p* < 0.05). Also, in the same brain structure, after 3 days, the MDA concentration was increased bilaterally after 7-NI+AlCl₃ and AG injection, as well as ipsilaterally after L-NAME and 7-NI application, compared to the control groups.

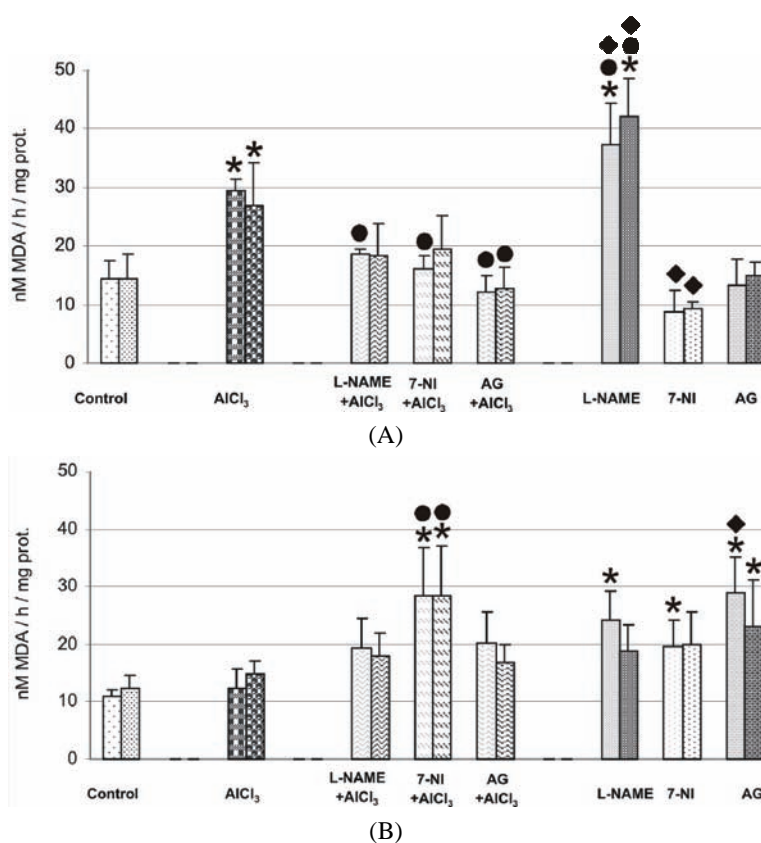


Fig. 2. The effect of intrahippocampal drug injection on the MDA concentration (nM MDA/h/mg protein) in the rat ipsilateral and contralateral FC at different survival times – 10 min (A) and 3 days (B) after treatment. Data are means \pm SD of 10 animals. *A statistically significant difference between treated (AlCl₃-, NOS inhibitors + AlCl₃- and NOS inhibitors-treated) and the control (sham-operated) animals (*p* < 0.05). •A statistically significant difference between the treated (NOS inhibitors + AlCl₃- and NOS inhibitors-treated) and the AlCl₃-treated animals (*p* < 0.05). ♦A statistically significant difference between the NOS inhibitors-treated and the NOS inhibitors + AlCl₃-treated animals (*p* < 0.05).

Ten minutes after L-NAME + AlCl₃ and 7-NI + AlCl₃ injection, lower MDA concentrations were measured in the ipsilateral FC, and after AG + AlCl₃ injection in the ipsilateral and contralateral FC, compared to the AlCl₃-treated group. However, after 3 days, 7-NI + AlCl₃ injection resulted in a higher MDA concentration bilaterally in the same brain structure, compared to the AlCl₃-treated group. At the early tested time (10 min), L-NAME application resulted in an increase in the MDA concentration bilaterally in the FC, compared with the AlCl₃-treated animals, as well as compared to the L-NAME + AlCl₃-treated groups ($p < 0.05$). Also, AG injection resulted in an increase in the MDA concentration in the ipsilateral FC after 3 days, compared to the AG + AlCl₃-treated group. However, 7-NI injection resulted in a decrease in the MDA concentration bilaterally in the FC after 10 min, compared to the 7-NI + AlCl₃-treated group (Fig. 2).

DISCUSSION

The application of AlCl₃ to the CA1 sector of the hippocampus resulted in a significant increase in O₂⁻ production and the MDA concentration in the FC. This suggests that inhibition of NOS by L-NAME, 7-NI or AG can modulate AlCl₃ poisoning and, therefore, may limit the retrograde and anterograde spread of toxicity.

In this study, AlCl₃ application produced a rapid (within 10 min) increase in O₂⁻ production contralaterally in the FC, compared to the control (Fig. 1A). Literature data suggest that Al is suspected to be associated with oxidative stress, possibly due to the pro-oxidant properties of A beta in the senile plaques.^{26,27} The underlying mechanism by which this occurs is not well understood although interactions between amyloid and Fe have been proposed. The presence of low molecular weight Fe compounds can stimulate free radical production in the brain. Both Al and A beta can potentiate free radical formation by stabilizing Fe in its more damaging ferrous (Fe²⁺) form, which can promote the Fenton reaction. The rate at which Fe²⁺ is spontaneously oxidized to Fe³⁺ was significantly slower in the presence of Al salts.²⁸

There are several lines of evidence that show a key role of ROS in both intracellular signaling and intracellular communication, processes involved in maintaining homeostasis. Some experimental data indicate that ROS-mediated lipid peroxidation, protein oxidation and oxidative alterations to nucleic acids are crucial events of the unfavorable actions of ROS.^{29,30} Lipid peroxidation is a measure of tissue destruction. Literature data suggest that Al may facilitate increases in intracellular Ca²⁺ and ROS, and potentially contribute to neurotoxicity induced by other neurotoxicants.⁶ In this study, it was shown that 10 min after intrahippocampal AlCl₃ injection, the application of a neurotoxicant produced an increase in the MDA concentration bilaterally in the FC, compared to control animals (Fig. 2A).

Neuropharmacological data indicate that A beta toxicity is mediated by an excitotoxic cascade involving blockage of astroglial glutamate uptake, sustained activation of NMDA receptors and an overt intracellular Ca²⁺ influx.³¹ These changes are associated with increased NOS activity in cortical target areas that may directly lead to the generation of free radicals. A sustained overproduction of NO *via* NOS expression may be responsible, at least in part, for some of the neurodegenerative changes caused by stress and support a possible role for NOS inhibitors in this situation.³²

Decreased O₂⁻ production bilaterally in the FC at 3 days in the L-NAME + AlCl₃ group and the 7-NI + AlCl₃ group compared to the controls (Fig. 1B), along with decreased SOD activity (results not shown) confirm the achieved anti-oxidative defense.

In addition, the decreased MDA concentration ipsilaterally in the same brain structure at 10 min in the NOS inhibitors + AlCl₃ groups, compared to the AlCl₃-treated animals, (Fig. 2A), suggests activation of the anti-oxidative system, resulting in an aggressive blockage of the oxidative mechanisms initiated by neurotoxicant application.

The significant increase in O₂⁻ production after L-NAME and after AG injection (at 10 min bilaterally in the FC, compared to the controls), which correlates with unchanged O₂⁻ levels after 7-NI application in the same brain structure (Fig. 1A), indicates the permanent and long-lasting effect of nNOS blocking at the early tested time. These findings suggest that treatment with 7-NI leads to the protection of brain neurons against neuronal injuries by impairment of cellular energy metabolism and oxidative stress.³³⁻³⁵

The present data, which indicates an increased MDA concentration 10 min after L-NAME application bilaterally in the FC compared to the controls (Fig. 2A), suggests that NOS inhibition exhibits protective effects for cellular membrane. This only occurs during the presence of oxidative stress caused by AlCl₃, meaning that peroxidation after L-NAME application is not developed through NO, but through the creation of •OH from O₂⁻ and H₂O₂.³⁶

In addition, it was shown in this study that L-NAME injection after 10 min produced an increase in the MDA concentration, compared to the L-NAME + AlCl₃-treated group (Fig. 2A). It is known³⁷ that glutamate excitotoxicity, oxidative stress, and mitochondrial dysfunctions are common features leading to neuronal death after Al intoxication. Nitric oxide, alone or in cooperation with O₂⁻ and ONOO⁻, is emerging as a predominant effector of neurodegeneration.

CONCLUSIONS

In conclusion, the present data revealed that NO is included in the toxicity induced by AlCl₃ application in the CA1 hippocampal sector, resulting in both

temporal and spatial spreading of damage to the FC, so that NOS inhibitors (L-NAME, 7-NI, AG) could have potentially beneficial effects.

ИЗВОД

ЕФЕКТИ РАЗЛИЧИТИХ ИНХИБИТОРА АЗОТ-ОКСИД-СИНТАЗЕ НА
ОШТЕЋЕЊЕ НЕУРОНА ИЗАЗВАНО $AlCl_3$

ИВАНА СТЕВАНОВИЋ¹, МАРИНА ЈОВАНОВИЋ¹, АНКИЦА ЈЕЛЕНКОВИЋ²,
МИОДРАГ ЧОЛИЋ¹ и МИЛИЦА НИНКОВИЋ¹

¹Војномедицинска академија, Институт за медицинска истраживања, Црнобравска 17, Београд и

²Институт за биолошка истраживања Београд

У експерименту је одређивана ефикасност инхибитора азот-оксид-синтазе (NOS): метил-естра *N*-нитро-L-аргинина, 7-нитроиндазола и аминокванидина у модулацији токсичности $AlCl_3$ на стварање супероксидног анјона и концентрацију малондиалдехида код Wistar пацова. Животиње су жртвоване 10 min и 3 дана након третмана и изолована је кора великог мозга. Резултати показују да излагање $AlCl_3$ покреће оксидативни стрес у различитим можданим регионима. Биохемијске промене описане у неуронском ткиву показују да алуминијум делује као про-оксидант, док инхибитори NOS имају антиоксидативно дејство код животиња третираних $AlCl_3$.

(Примљено 1. октобра, ревидирано 9. децембра 2008)

REFERENCES

1. P. C. Ferreira, A. Piai Kde, A. M. Takayanagui, S. I. Segura-Muñoz, *Rev. Lat. Am. Enfermagem.* **16** (2008) 151
2. L. F. Rodella, F. Ricci, E. Borsani, A. Stacchiotti, E. Foglio, G. Favero, R. Rezzani, C. Mariani, R. Bianchi, *Histol. Histopathol.* **23** (2008) 433
3. J. J. Canales, R. Corbalan, C. Montoliu, M. Liansola, P. Monfort, S. Erceg, M. Hernandez-Viadell, V. Felipo, *J. Inorg. Biochem.* **87** (2001) 63
4. M. Liansola, M. D. Minana, C. Montoliu, R. Saez, R. Corbalan, L. Manzo, V. Felipo, *J. Neurochem.* **73** (1999) 712
5. C. R. Hermenegildo, C. Saez, L. Minoia, L. Manzo, V. Felipo, *Neurochem Internat.* **34** (1999) 245
6. W. R. Mundy, T. M. Fraudenrich, P. R. Kodavanti, *Mol. Chem. Neuropathol.* **32** (1997) 41
7. H. Tanino, S. Shimohama, Y. Sasaki, Y. Sumida, S. Fujimoto, *Biochem. Biophys. Res. Commun.* **271** (2000) 620
8. P. Zatta, E. Lain, C. Cagnolini, *Eur. J. Biochem.* **267** (2000) 3049
9. J. G. Scandalios, *Braz. J. Med. Biol. Res.* **38** (2005) 995
10. S. Hara, T. Mukai, K. Kurosaki, H. Mizukami, F. Kuriwa, T. Endo, *Toxicology* **239** (2007) 136
11. S. Johnson, *Med. Hypotheses* **56** (2001) 595
12. H. J. Luth, M. Holzer, U. Gartner, M. Staufenbiel, T. Arendt, *Brain Res.* **913** (2001) 57
13. G. Munch, J. Gašić-Milenković, S. Dukić-Stefanović, B. Kuhla, K. Heinrich, P. Riederer, H. J. Huttunen, H. Founds, G. Sajithlal, *Exp. Brain Res.* **150** (2003) 1
14. S. N. Yang, W. Y. Hsieh, D. D. Liu, L. M. Tsai, C. S. Tung, J. N. Wu, *Chin. J. Physiol.* **41** (1998) 175
15. N. Matsumura, K. Kikuchi-Utsumi, T. Nakaki, *J. Pharmacol. Exp. Ther.* **325** (2008) 357

16. M. Djukić, M. C. Jovanović, M. Ninković, I. Vasiljević, M. Jovanović, *Ann. Agric. Environ. Med.* **14** (2007) 247
17. M. Ninković, Ž. Maličević, A. Jelenković, M. D. Jovanović, M. Dukić, I. Vasiljević, *Acta Physiol. Hung.* **93** (2006) 315
18. M. Jovanović, A. Jelenković, I. Vasiljević, D. Bokonjić, M. Čolić, S. Marinković, D. Stanimirović, in *Neurobiological Studies – From Genes to Behaviour*, S. Ruždijić, Lj. Rakić, Eds., Research Signpost, Kerala, 2006, p. 259
19. I. Vasiljević, M. Jovanović, M. Ninković, Ž. Maličević, *Acta Vet.* **52** (2002) 79
20. I. Stevanović, M. Jovanović, A. Jelenković, M. Čolić, I. Stojanović, M. Ninković, *Bulg. J. Vet. Med.* **11** (2008) 37
21. J. F. R. König, R. A. Klippel, *The Rat Brain*, The Williams and Wilkins Company, Baltimore, MD, 1963
22. J. W. Gurd, L. R. Jones, H. R. Mahler, W. J. Moore, *J. Neurochem.* **22** (1974) 281
23. C. Auclair, E. Voisin, in *Handbook of Methods for Oxygen Radical Research*, R. A. Greenwald, Ed., CRC Press, Boca Raton, 1985, p. 123
24. A. Villacara, K. Kumami, T. Yamamoto, B. B. Mršulja, M. Spatz, *J. Neurochem.* **53** (1989) 595
25. O. H. Lowry, J. V. Passonneau, *A Flexible System of Enzymatic Analysis*, Academic Press, New York, 1974
26. C. Exley, *J. Alzheim. Dis.* **12** (2007) 313
27. J. R. Walton, *J. Inorg. Biochem.* **101** (2007) 1275
28. E. Y. Yang, S. X. Guo-Ross, S. C. Bondy, *Brain Res.* **839** (1999) 221
29. A. Campbell, S. C. Bondy, *Cell. Mol. Biol.* **46** (2000) 721
30. I. Juranek, S. Bezek, *Gen. Physiol. Biophys.* **24** (2005) 263
31. T. Harkany, B. Penke, P. G. Luiten, *Ann. N.Y. Acad. Sci.* **903** (2000) 374
32. R. Olivenza, R. M. A. Moro, I. Lizasoain, P. Lorenzo, A. P. Fernandez, J. Rodrigo, L. Bosca, J. C. Leza, *J. Neurochem.* **74** (2000) 785
33. A. K. Strorch, A. C. Burkhardt, L. Ludolph, J. Schwarz, *J. Neurochem.* **75** (2000) 2259
34. V. L. Thorns, L. Hansen, E. Masliah, *Exp. Neurol.* **150** (1998) 14
35. M. Hartlage-Rubsamen, P. Apelt, R. Schliebs, *Neurosci. Lett.* **302** (2001) 73
36. M. P. Mattson, W. A. Pedersen, *Int. J. Dev. Neurosci.* **16** (1998) 737
37. P. E. Chabrier, C. Demerle-Pallardy, M. Auguet, *Cell. Mol. Life Sci.* **55** (1999) 1029.



J. Serb. Chem. Soc. 74 (5) 513–522 (2009)
JSCS–3851

Isolation and characterization of the 68 kD allergen from house dust mite *Dermatophagoides pteronyssinus*

KATARINA MILOVANOVIĆ¹, LIDIJA BURAZER¹, OLGA VUČKOVIĆ¹,
MARINA ATANASKOVIĆ-MARKOVIĆ², TANJA ĆIRKOVIĆ VELIČKOVIĆ^{3#},
RATKO M. JANKOV^{3#} and MARIJA GAVROVIĆ-JANKULOVIĆ^{3*#}

¹Institute of Virology, Vaccines and Sera, Torlak, Belgrade, ²University Children's Hospital, Medical Faculty, University of Belgrade, Belgrade and ³Biochemistry Department, Faculty of Chemistry, University of Belgrade, Belgrade, Serbia

(Received 4 November 2008, revised 6 February 2009)

Abstract: House dust mites (HDM) represent a major source of allergens, contributing to the increasing incidence of type I hypersensitivity disease worldwide. Over 30 different IgE-binding proteins from the HDM extract were detected. Although group 1 and 2 have been identified as major allergens, due to the safety and efficacy of allergy diagnosis and immunotherapy, there is a need to carefully evaluate the clinical relevance of other allergens present in the HDM extract. In regard to this, a high molecular mass allergen of about 68 kD was purified from the HDM extract using a combination of gel permeation chromatography and reversed-phase chromatography. The IgG and IgE reactivity of the purified protein were preserved during the purification process, as confirmed by Western blot analysis with polyclonal rabbit antibodies and dot blot analysis with a pool of sera from subjects with house dust mite allergy, respectively. In addition, the IgE reactivity was confirmed using ELISA testing with nine patient sera. The biological potency of the 68 kD allergen was confirmed by skin prick testing in five allergic subjects, suggesting that the high molecular mass allergen is a good candidate for component-resolved diagnosis of house dust mite allergy and eventual therapeutic treatment.

Keywords: HDM; *Dermatophagoides pteronyssinus*; allergens; isolation.

INTRODUCTION

House dust mites (HDM) represent a major source of aeroallergens contributing to the increasing incidence of type I hypersensitivity disease worldwide.^{1,2} More than 50 % of allergic patients and up to 80 % of asthmatic children are sensitized to mite allergens.³ The HDM extract used in allergy diagnosis and therapy is a complex mixture of allergens and non-allergen components from mite

* Corresponding author. E-mail: mgavrov@chem.bg.ac.rs

Serbian Chemical Society member.

doi: 10.2298/JSC0905513M

bodies, fecal pellets and eggs.⁴ Over 30 different proteins from mite extract bind IgE and 21 of them have been characterized.⁵ Major IgE binding was reported for the group 1–3, 9, 11, 14 and 15 allergens.⁶ One of the problems in standardization of HDM extracts is the presence of proteolytic enzymes, which are important allergens, the presence of which can, nevertheless, compromise the quality of the allergen extract. Allergens with proteolytic activity which have been found in the HDM extract are Der p1 – a cysteine protease, Der p3 with trypsin activity, Der p6 chymotrypsin, and Der p9 a collagenolytic serine protease. Group 1 and 2 represent the most important allergens as they are recognized by the majority of mite-allergic patients.⁷ Nevertheless, about 20 % of mite allergic subjects do not produce IgE to the group 1 and 2, and given the high frequency of mite allergy, this constitutes a respectable number of patients.⁶ In addition, sensitivity to one of the major allergens can be under- or over-represented in a limited group of patients,⁸ and very often, it is dependent on the geographical region and environmental exposure to the allergen source. Moreover, the sequence polymorphisms of the major group 1 and 2 allergens produced by environmental mites can have an impact on the T-cell response to peptides containing different amino acid substitutions.⁹ Therefore, structural features, as well as immunoreactivity of all allergens present in the HDM extract have to be considered and carefully evaluated.

Novel approaches based on a defined content of structurally defined individual allergens that can be applied in diagnosis and treatment of allergies are termed component-resolved diagnosis (CRD) and component-resolved immunotherapy¹⁰ (CRI), respectively. Such an immunotherapeutic approach enables patient-tailored specific allergy treatment without risk of side effects and additional sensitization, especially in the pediatric population.¹¹

The aim of this study was to isolate and examine the diagnostic potential of a high molecular mass protein of about 68 kD from house dust mite *Dermatophagoides pteronyssinus* in terms of its IgE-binding properties and biological activity in a group of Serbian HDM allergic persons.

EXPERIMENTAL

HDM allergen extract preparation

Dried house dust mites (*Dermatophagoides pteronyssinus*), 5 % (w/v), were extracted in 0.15 M phosphate-buffered saline (PBS), pH 7.6, by stirring overnight at 4–8 °C. After centrifugation at 6000 rpm for 30 min and filtration through a 0.22 µm membrane filter (Pall Europe Limited Portsmouth, England), the extract was lyophilized and stored at –70 °C. The protein concentration of the extract was determined by the Bradford method¹² using bovine serum albumin (BSA) as the standard.

Size-exclusion chromatography

The HDM extract was resolved by size-exclusion chromatography using a Superdex 200 column in 20 column volumes (850 mm×16 mm, Pharmacia, Uppsalla, Sweden), after equilibration of the column with 20 mM PBS, pH 8.0. The protein fractions were pooled and analyzed by SDS-PAGE.

Reversed-phase chromatography

Following size-exclusion chromatography, the pooled fractions containing a high-molecular mass allergen were further purified by reversed-phase chromatography (100 mm×4.6 mm C5 HPLC column, Supelco, Bellefonte, PA, USA), and analyzed by SDS-PAGE.

SDS-PAGE

The quality of the HDM extract was analyzed by 12 % SDS-PAGE and the resolved proteins were stained with Coomassie Brilliant Blue R-250 (Serva, Heidelberg, Germany), as outlined by Laemmli *et al.*¹³

Production of the polyclonal antibodies to HDM extract

Two rabbits were immunized according to the protocol described by Harlow and Lane.¹⁴ In brief, 0.25 mL of the HDM extract (0.50 mg mL⁻¹) was mixed with 0.25 mL FCA (Freund's complete adjuvant) for the first immunization. Every 15 days, for six months, the rabbits were boosted with a mixture of 0.25 mL of the HDM extract and 0.25 mL of FCA. Each rabbit was subcutaneously immunized with 0.50 mL of the emulsion. After six months, sera were collected and the antibodies were purified using Protein A Sepharose¹⁵ (Pharmacia, Uppsala, Sweden) according to the manufacturer's instructions.

Patients' sera

Patients allergic to house dust mites ($n = 17$; 10 male and 7 female) were selected according to their case history, positive skin prick test and specific IgE for *D. pteronyssinus* extract (CAP-FEIA System, Unicap 100; Phadia, Uppsala, Sweden). Sera from three non-allergic individuals were pooled and used for control purposes.

Western blot

Proteins of the HDM (*D. pteronyssinus*) extract or isolated 68 kD protein were resolved by SDS-PAGE and electro-transferred onto a nitrocellulose membrane (0.45 μ m Serva, Heidelberg, Germany).¹⁶ The pattern of the IgE reactivity was determined with individual patient's sera (dilution 1:5, in 50 mM sodium phosphate, pH 7.4, containing 100 mM NaCl, 0.50 % (v/v) Tween-20; 0.50 % (w/v) bovine serum albumin (BSA) and alkaline-phosphatase labeled monoclonal anti-human IgE (Sigma Chemical Co., St. Louis, MO, USA) as the secondary antibody. Rabbit polyclonal anti-HDM antibodies were used to evaluate the IgG reactivity profile and alkaline-phosphatase labeled goat anti-rabbit IgG (Sigma Chemical Co., St. Louis, MO, USA) was used as the secondary antibody. The IgE and IgG binding patterns were visualized with a substrate solution of 1.5 mg BCIP (5-bromo-4-chloro-3-indolyl phosphate, Serva, Heidelberg, Germany) and 3.0 mg NBT (nitro blue tetrazolium, Serva, Heidelberg, Germany) in 10 mL of 100 mM Tris buffer containing 150 mM NaCl and 5 mM MgCl₂, pH 9.6, according to Harlow and Lane.¹⁴

Dot blot

Purified 68 kD allergen or HDM extract were dotted (2.0 μ L, $c = 0.50$ mg mL⁻¹) onto nitrocellulose membrane strips (0.45 μ m Serva, Heidelberg, Germany). Subsequently, the membrane was blocked with buffer A (50 mM sodium phosphate, pH 7.4, 100 mM NaCl, 0.50 % (v/v) Tween-20, 0.5 % (w/v) bovine serum albumin (BSA) and 0.05 % (w/v) sodium azide) for one hour at room temperature and incubated with patients sera at a 1:5 dilution in buffer A for 3 h at room temperature. The bound IgE was detected with alkaline-phosphatase labeled monoclonal anti-human IgE antibodies (Sigma Chemical Co., St. Louis, MO, USA). The binding patterns were visualized with a BCIP/NBT substrate solution.

IgE ELISA

A MaxiSorp ELISA plate (Sigma-Aldrich, Steinheim, Germany) was coated with the purified 68 kD protein ($10 \mu\text{g mL}^{-1}$, $100 \mu\text{L}$ *per* well) in $15 \text{ mM Na}_2\text{CO}_3/35 \text{ mM NaHCO}_3$, pH 9.5, overnight at $4 \text{ }^\circ\text{C}$. The plate was washed ($3 \times 10 \text{ min}$) with TBS containing 0.010% (v/v) Tween 20 (TTBS). After blocking for 2 h at room temperature with 1.0% BSA in TTBS, the individual patient sera ($1:5$ dilution in 0.10% (w/v) BSA in TTBS) were added to the plate and incubated overnight at $4 \text{ }^\circ\text{C}$. The bound IgE was detected using alkaline-phosphatase labeled anti-human IgE ($1:1000$ Sigma Chemical Co., St. Louis, MO, USA). Following a 2 h incubation, the plate was subsequently incubated for 1 h with a substrate solution (1.0 mg mL^{-1} *p*-nitrophenyl phosphate in 100 mM diethanolamine buffer, pH 9.6), and the absorbance was measured at 405 nm . Absorbance values were considered positive if they exceeded the mean $A_{405 \text{ nm}}$ of the negative control by $>3 \text{ SD}$. Due to the lack of sufficient sera, patients No. 7, 9, and 17 were not tested using ELISA.

Skin prick testing

For skin prick test (SPT), the 68 kD allergen ($20 \mu\text{g mL}^{-1}$) was prepared in PBS, as previously described.¹⁷ Histamine phosphate at 1.0 mg mL^{-1} and PBS were used as the positive and negative control, respectively. The results of the SPTs were evaluated after 20 min and a wheal of at least 3 mm was considered positive. The skin prick testing was performed with the approval of the Ethics Committee of the University Children's Hospital and informed written consent was given by all patients.

RESULTS AND DISCUSSION

IgE reactivity of house dust mite extract

To examine the pattern of IgE reactivity in the Serbian population, seventeen individuals with a positive clinical history of HDM allergy were selected. Their clinical data are presented in Table I. A specific IgE to house dust mite allergens

TABLE I. Clinical and serological characterization of the house dust mite allergic subjects; ND – not determined

Patient	Sex	CAP class	Symptoms and diagnosis	Sensitization	ELISA 68 kD allergen
1. JM	M	6	Rhinoconjunctivitis	Dermatophagoides, g×1	+
2. NN	F	6	Asthma	Dermatophagoides	+
3. TS	M	6	Atopic dermatitis	Dermatophagoides	–
4. SM	F	6	Asthma	Dermatophagoides	+
5. SB	M	6	Rhinitis	Dermatophagoides, w3	+
6. TM	M	6	Asthma	Dermatophagoides	+
7. MM	M	5	Rhinitis, Asthma	Dermatophagoides	ND
8. ĆS	F	5	Rhinitis	Dermatophagoides	–
9. ĆI	F	5	Asthma	Dermatophagoides	ND
10. MF	M	5	Rhinitis	Dermatophagoides	–
11. MD	F	5	Rhinitis	Dermatophagoides	–
12. KD	M	5	Rhinitis	Dermatophagoides, w6	+
13. KI	M	5	Asthma	Dermatophagoides	+
14. ĆB	M	4	Rhinitis	Dermatophagoides, g×1, w×1	ND
15. SJ	F	4	Rhinosinusitis	Dermatophagoides, w×1, w×3	+
16. MG	M	4	Rhinitis	Dermatophagoides, g×1, w×1, t×5	+
17. PS	F	4	Asthma	Dermatophagoides	ND

determined by ImmunoCAP was scored as: class 6 in six patients, class 5 in seven patients and class 4 in four patients. From the seventeen HDM allergic patients, six were co-sensitized to weed, grass and/or tree pollen. The pattern of the IgE reactivity in Western blot analysis with individual patient sera is shown in Fig. 1. The HDM extract showed a complex IgE-binding pattern with bands of various molecular mass ranging from 116–10 kD. The major allergens in this population of HDM allergic subjects with IgE reactivity by more than 50 % were proteins with molecular mass of about 14, 27, 47, 68 and 116 kD. The band at about 14 kD showed the strongest intensity in the IgE binding, probably representing Der p 2, and/or Der p 5.^{2,18} The IgE binding in the range of 20–35 kD may represent Der p 6, Der p 7, Der p 8, and Der p 9. A strong IgE binding of the 68 kD protein was observed in four patients with a high specific IgE (patients 1, 2, 5, and 6).

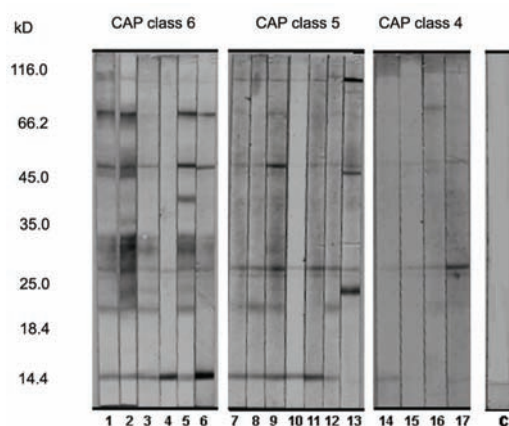


Fig. 1. IgE reactivity profile to HDM allergen extract obtained with HDM patients' sera.

Isolation of the 68 kD allergen

The 68 kD allergen was isolated from the HDM extract by a combination of size-exclusion chromatography on a Superdex 200 column and subsequent reversed-phase chromatography on a C5 column. The HDM proteins were resolved into three peaks by gel permeation chromatography, pooled according to the chromatogram fractions: 11–12, 35–54 and 57–63 (Fig. 2a), and analyzed by SDS PAGE and Western blot (Fig. 3). Pool A contained high molecular mass proteins of about 60–116 kD and 30–40 kD, pool B contained a doublet of about 25–30 kD and low-molecular mass proteins of 15–20 kD and 25–40 kD, while pool C contained proteins with molecular masses of about 14 and 35 kD. Pool A was applied on the C5 column and a 68 kD protein was eluted with 79 % acetonitrile containing 0.10 % TFA (Fig. 2b), and was analyzed by SDS-PAGE (Fig. 3a) and Western blot (Fig. 3b). According to the literature, 21 allergens⁵ from *Dermatophagoides pteronyssinus* house dust mite, with a wide range of molecular

masses (7–177 kD),^{6,19} have been identified. Recently, two recombinant house dust mite allergens, Der p 15, with a molecular mass of about 60 kD, and Der p 18, of about 50 kD, were characterized.²⁰ However, there is no report in the literature on the properties of a 68 kD house dust mite protein.

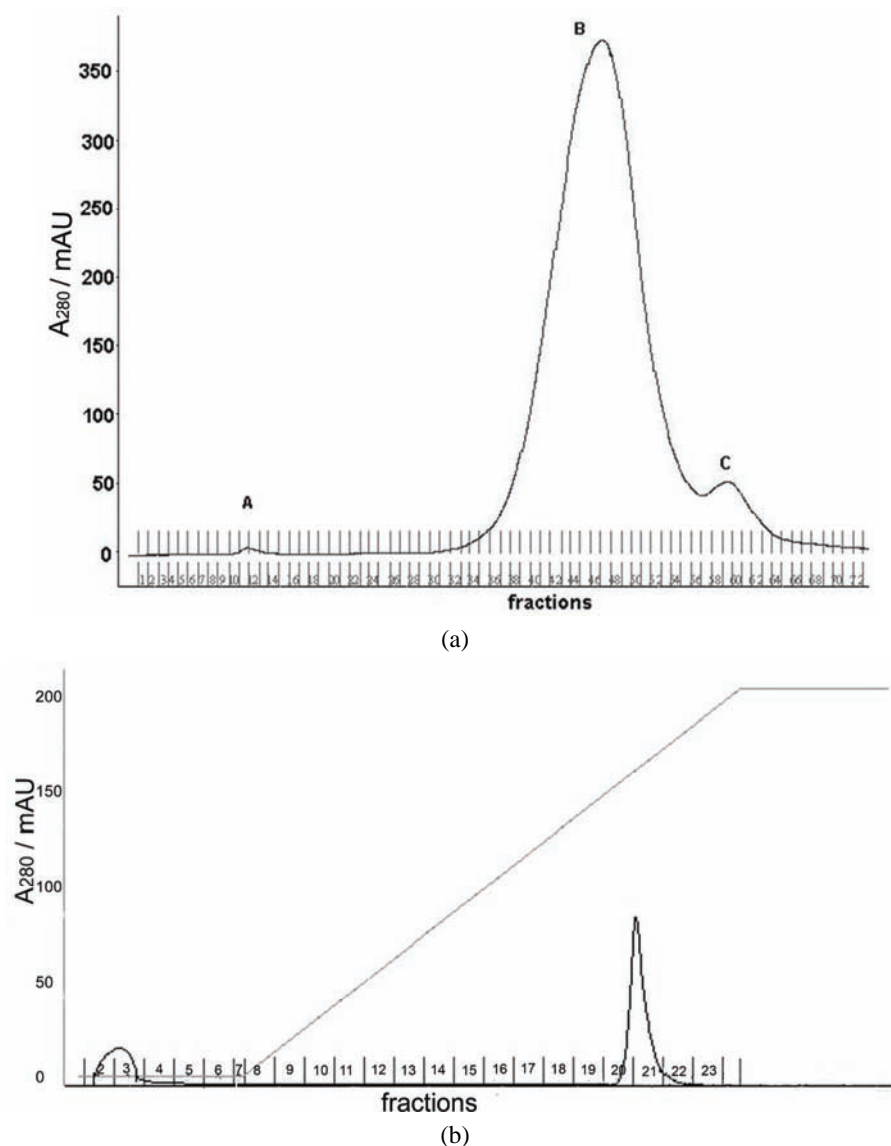


Fig. 2. Separation of the HDM extract by a) size-exclusion chromatography on a Superdex 200 column and b) reversed-phase chromatography on a C5 column.

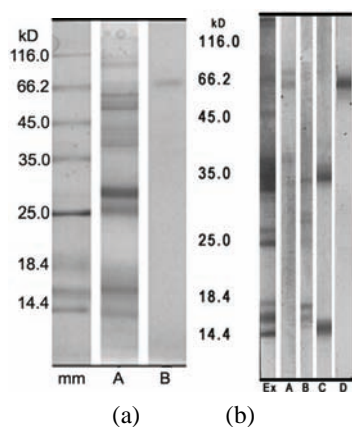


Fig. 3. Isolation of the 68 kD protein: a) SDS PAGE analysis: HDM extract (A), purified 68 kD protein (B); molecular mass proteins (mm) and b) Western blot: HDM extract (Ex), A pool of 11-12 fractions (A), B pool of 35-54 fractions (B), C pool of 57-63 fractions (C), A pool after C5 reversed-phase chromatography (D).

IgE and IgG reactivity of the 68 kD allergen

IgE and IgG reactivity of the 68 kD allergen was confirmed using dot blot analysis (Fig. 4) with a pool of patient sera and rabbit polyclonal antibodies, respectively. In addition, IgE reactivity was evaluated with sera from individual patients using ELISA (Fig. 5). These results suggest that the IgE binding epitopes of the isolated 68 kD allergen were preserved during the purification process and nine from fourteen tested patients (64 %) showed a specific IgE reactivity (Table I) to the 68 kD allergen.

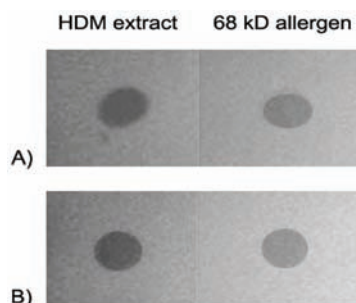


Fig. 4. IgG (A) and IgE (B) reactivity of dot-blotted HDM extract and 68 kD allergen.

For the evaluation of the biological activity, five patients were skin prick tested with a solution containing the 68 kD allergen ($20 \mu\text{g mL}^{-1}$). The positive results in all the tested patients (Table II) suggested that the 68 kD allergen is capable of bridging specific IgE antibodies on the mast cells and triggering the release of preformed biologically active mediators, such as histamine. It is noteworthy that the isolated allergen induced a larger skin prick test reaction compared to the HDM extract in three patients. Taking into consideration the prevalence of IgE reactivity in the tested group of HDM allergic subjects, the 68 kD allergen is a good candidate for component-resolved allergy diagnosis, or at least for patients from the Serbian climate.

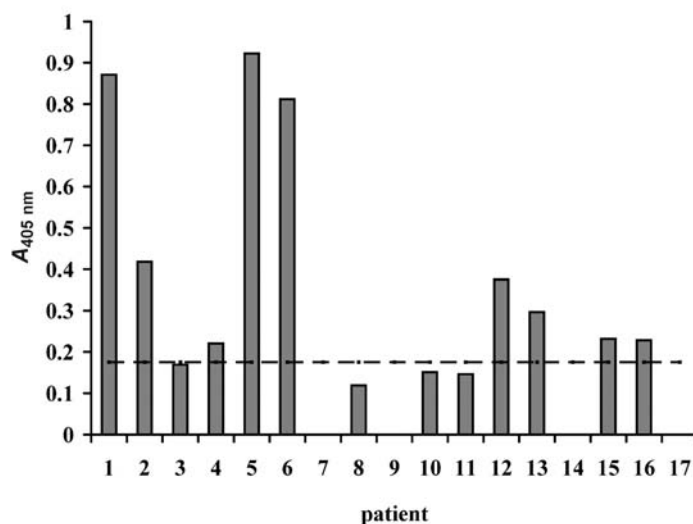


Fig. 5. Histogram: IgE ELISA to 68 kD allergen.

Table II. Skin prick test reactivity (wheal×flare, mm²) to HDM extract and 68 kD allergen

Allergen	Patient No.				
	1	2	3	4	5
HDM extract	8×20	5×10	4×15	8×30	10×35
68 kD allergen	9×30	7×10	4×0	9×30	9×30
Histamine	5×20	5×10	5×25	4×0	–

CONCLUSIONS

A high-molecular mass allergen of about 68 kD was isolated from a HDM extract and its IgE reactivity was evaluated. Using a combination of two biochemical methods, gel permeation chromatography and reversed-phase chromatography, a 68 kD protein was isolated. The strong IgE binding of the 68 kD allergen was observed in patients with a high level of specific IgE (CAP class 6). IgE reactivity was confirmed in 64 % of the tested HDM allergic patients by ELISA and its biological activity was confirmed in five HDM allergic subjects. According to these results, the 68 kD allergen is a good candidate for component-resolved allergy diagnosis of house dust mite allergy. Further biochemical characterization, such as amino acid sequence determination, should provide more data on its structural features. Additional clinical studies should evaluate its allergenic potency in HDM allergic patients with lower level of specific IgE (CAP class < 4), as well as its diagnostic potential in the pediatric population.

Acknowledgments. The study was supported by Grant 142020 from the Ministry of Science and Environmental Protection, Republic of Serbia.

ИЗВОД

ИЗОЛОВАЊЕ И КАРАКТЕРИЗАЦИЈА 68 kD АЛЕРГЕНА ИЗ ЕКСТРАКТА КУЋНИХ ГРИЊА

КАТАРИНА МИЛОВАНОВИЋ¹, ЛИДИЈА БУРАЗЕР¹, ОЛГА ВУЧКОВИЋ¹, МАРИНА АТАНАСКОВИЋ-МАРКОВИЋ², ТАЊА ЂИРКОВИЋ ВЕЛИЧКОВИЋ³, РАТКО М. ЈАНКОВ³ И МАРИЈА ГАВРОВИЋ-ЈАНКУЛОВИЋ³

¹Институт за вирусологију, вакцине и серуме, Торлак, Београд, ²Универзитетска дечја клиника, Медицински факултет и ³Катедра за биохемију, Хемијски факултет, Универзитет у Београду

Гриње из кућне прашине представљају један од главних извора алергена који су у значајној мери допринели порасту првог типа преосетљивости. Преко 30 IgE-везујућих протеина из кућне прашине је детектовано до данас. Алергени групе 1 и 2 означени су као главни алергени кућне прашине. Међутим, да би се побољшала сигурност и ефикасност дијагнозе и терапије алергијских обољења изазваних грињама из кућне прашине, неопходно је одредити клинички значај свих алергена из овог алергенског извора. У овом раду изолован је алерген високе молекулске масе од 68 kD из екстракта кућне прашине комбинавањем гел-пермеационе хроматографије и реверсно-фазне хроматографије. IgG и IgE реактивност пречишћеног протеина је проверена у «Western blot»-у и «dot blot»-у са поликлонским зечијим антителима на екстракт кућне прашине и «pool»-ом серума особа алергичних на кућну прашину, редом. 64 % пацијената је показало IgE реактивност на пречишћени протеин у ELISA тесту. Биолошка реактивност пречишћеног алергена је потврђена у кожним пробама на пет пацијената, указујући да је пречишћен алерген добар кандидат за дијагнозу алергије на кућну прашину појединачним компонентама и евентуални терапеутски третман.

(Примљено 4. новембра 2008, ревидирано 6. фебруара 2009)

REFERENCES

1. F. de Blay, G. Pauli, M. Velten, J. C. Bessot, *J. Allergy. Clin. Immunol.* **93** (1994) 136
2. M. Weghofer, W. R. Thomas, G. Pittner, F. Horak, R. Valenta, S. Vrtala, *Clin. Exp. Allergy* **35** (2005) 1384
3. L.-P. Boulet, H. Turcotte, C. Laprise, C. Lavertu, P.-M. Bedard, A. Lavoie, J. Hebert, *Clin. Exp. Allergy* **27** (1997) 52
4. T. Batard, A. Hrabina, X. Z. Bi, H. Chabre, P. Lemoine, M.-N. Couret, D. Faccenda, B. Villet, P. Harzic, F. Andre, S. Y. Goh, C. Andre, F. T. Chew, P. Moingeon, *Int. Arch. Allergy Immunol.* **140** (2006) 140
5. M. Weghofer, Y. Dall'Antonia, M. Grote, A. Stöcklinger, M. Kneidinger, N. Balic, M.-T. Krauth, E. Fernández-Caldas, W. R. Thomas, M. van Hage, S. Vieths, S. Spitzauer, F. Horak, D. I. Svergun, P. V. Konarev, P. Valent, J. Thalhamer, W. Keller, R. Valenta, S. Vrtala, *Allergy* **63** (2008) 758
6. W. R. Thomas, W. A. Smith, B. J. Hales, K. L. Mills, R. M. O'sBrien, *Int. Arch. Allergy Immunol.* **129** (2002) 1
7. W. R. Thomas, B. J. Hales, H.-D. Shen, W. Smith, *Int. Arch. Allergy Immunol.* **118** (1999) 214
8. R. van Ree, *ACI International* **11** (1999) 55
9. W.-A. Smith, B. J. Hales, A. G. Jarnicki, W. R. Thomas, *J. Allergy Clin. Immunol.* **107** (2001) 985
10. R. Valenta, J. Lidholm, V. Niederberger, B. Hayek, D. Kraft, H. Gronlund, *Clin. Exp. Allergy* **29** (1999) 896

11. G. Pittner, S. Vrtala, W. R. Thomas, M. Weghofer, M. Kundi, F. Horak, D. Kraft, R. Valenta, *Clin. Exp. Allergy* **34** (2004) 597
12. M. M. Bradford, *Anal. Biochem.* **72** (1976) 248
13. U. K Laemmli, *Nature* **227** (1970) 680
14. E. Harlow, D. Lane, *Antibodies: A Laboratory Manual*, Cold Spring Harbor Laboratory, New York, 1988, p. 410
15. Amersham Pharmacia Biotech, *Antibody Purification Handbook*, 18-1037-46
16. H. Towbin, T. Staehelin, J. Gordon, *Proc. Natl. Acad. Sci. USA* **76** (1979) 4350
17. L. Heinzerling, A. J. Frew, C. Bindslev-Jensen, S. Bonini, J. Bousquet, M. Bresciani, K.-H. Carlsen, P. Cauwenberge, U. Darsow, W. J. Fokkens, T. Haahtela, H. Hoecke, B. Jessberger, M. L. Kowalski, T. Kopp, C. N. Lahoz, K. C. Lodrup Carlsen, N. G. Papadopoulos, J. Ring, P. Schmid-Grendelmeier, A. M. Vignola, S. Wöhrl, T. Zuberbier, *Allergy* **60** (2005) 1287
18. A. M. Smith, D. C. Benjamin, N. Hozic, U. Derewenda, W.-A. Smith, W. R. Thomas, G. Gafvelin, M. van Hage-Hamsten, M. Chapman, *J. Allergy Clin. Immunol.* **107** (2001) 977
19. E. Tovey, B. Baldo, *J. Allergy Clin. Immunol.* **79** (1987) 93
20. S. E.O'Neil, T. K. Heinrich, B. J. Hales, L. A. Hazell, D. C. Holt, K. Fischer, W. R. Thomas, *Clin. Exp. Allergy* **36** (2006) 831.



J. Serb. Chem. Soc. 74 (5) 523–535 (2009)
JSCS–3852

Structural and antimicrobial studies of coordination compounds of VO(II), Co(II), Ni(II) and Cu(II) with some Schiff bases involving 2-amino-4-chlorophenol

A. P. MISHRA*, R. K. MISHRA and S. P. SHRIVASTAVA

*Bio-coordination Laboratories, Department of Chemistry,
Dr. H. S. Gour University Sagar-470003, India*

(Received 5 August, revised 9 December 2008)

Abstract: Complexes of tailor-made ligands with life essential metal ions may be an emerging area to answer the problem of multi-drug resistance (MDR). The coordination complexes of VO(II), Co(II), Ni(II) and Cu(II) with the Schiff bases derived from 2-hydroxyacetophenone/2-chlorobenzaldehyde with 2-amino-4-chlorophenol were synthesized and characterized by elemental analysis, molar conductance, electronic spectra, FT-IR, ESR, FAB mass, thermal and magnetic susceptibility measurements. The FAB mass and thermal data show degradation of the complexes. The ligand **A** (2-hydroxyacetophenone-2-amino-4-chlorophenol) behaved as tridentate and ligand **B** (2-chlorobenzylidene-2-amino-4-chlorophenol) as bidentate, coordinating through O and N donors. The complexes [VO(**A**)(H₂O)]·xH₂O, [M(**A**)(H₂O)_n]·xH₂O for Co and Ni, [Cu(**A**)(H₂O)] and [VO(**B**)₂]·xH₂O, [M(**B**)₂(H₂O)_n] for Co and Cu and [Ni(**B**)₂] exhibited coordination numbers 4, 5 or 6. X-ray powder diffraction data ($a = 11.00417 \text{ \AA}$, $b = 11.706081 \text{ \AA}$ and $c = 54.46780 \text{ \AA}$) showed that [Cu(CACP)₂(H₂O)₂], complex **8**, crystallized in the orthorhombic system. The *in vitro* biological screening effects of the investigated compounds were tested against the bacteria *Escherichia coli*, *Staphylococcus aureus* and *Streptococcus fecalis* and the fungi *Aspergillus niger*, *Trichoderma polysporum* and *Candida albicans* by the serial dilution method. A comparative study of the MIC values of the Schiff base and their [M(**B**)₂(H₂O)₂] complexes (Co(II), complex **6** and Cu(II), complex **8**), indicated that the metal complexes exhibited a higher or lower antimicrobial activity than 2-chlorobenzylidene-2-amino-4-chlorophenol as the free ligand (**B**).

Keywords: Schiff base; 2-amino-4-chlorophenol; 2-hydroxyacetophenone; metal complexes; spectral studies; antimicrobial activity.

* Corresponding author. E-mail: apm19@rediffmail.com; rudra_25g@yahoo.co.in
doi: 10.2298/JSC0905523M

INTRODUCTION

Some transition metals are essential for the normal function of living organisms. Metallo-drugs are becoming an interesting research area after the discovery of cisplatin.¹ Since then, many complexes have been synthesized and tested on a number of biological systems. Copper complexes are known to have a broad spectrum of biological action,^{2,3} but its concentration as free metal ion inside cells should be lower than 10^{-15} M (calculated)/ 10^{-12} M (observed). A concentration higher than 10^{-9} M in the cytoplasm can be poisonous.⁴ The chemistry of vanadium with multidentate ligands has achieved a special status in the last decade because of its catalytic^{5,6} and medicinal⁷ input. Structural and functional models for vanadate-dependent haloperoxidases and nitrogenases have further stimulated vanadium coordination chemistry.⁸

The structures of the active site of the vanadate-dependent haloperoxidases have been revealed by X-ray diffraction studies. Accordingly, the vanadate ion is distorted towards a trigonal pyramid, thus providing a fifth coordination site to be occupied by the >NH of a histidine, thus covalently linking the vanadate ion to the protein.⁹⁻¹¹

The chemistry of nickel Schiff base complexes has obtained a significant place in bioinorganic chemistry and redox enzyme systems.¹¹ Morrow and Kolasala¹² reported the cleavage of plasmid DNA by square planar nickel-salen [*bis*-(salicylidene)ethylenediamine] complex in the presence of either magnesium monoperoxyphthalic acid (MPPA) or iodosulbenzene.

In this paper, the preparation and structures of VO(II), Co(II), Ni(II) and Cu(II) complexes with some synthesized Schiff base ligands, *i.e.*, 2-hydroxyacetophenone-2-amino-4-chlorophenol (HACP) (**A**) and 2-chlorobenzylidene-2-amino-4-chlorophenol (CACP) (**B**), is described (Fig. 1). The antimicrobial activity of these ligands and complexes is also reported.

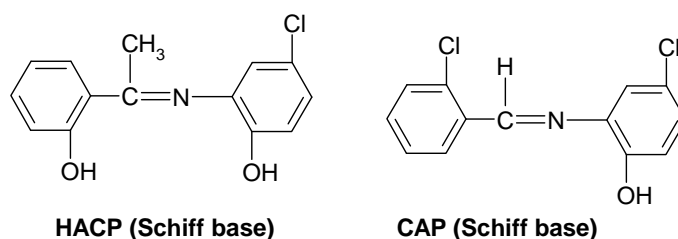


Fig. 1. HACP and CAP Schiff bases.

EXPERIMENTAL

Apparatus and reagents

All the used chemicals and solvents were of Analar grade. Oxovanadium(IV), cobalt(II), nickel(II) and copper (II) chloride/sulphate were obtained from Loba Chemie. Elemental analysis and FAB (Fast Atom Bombardment) mass spectra were realised at SAIF-CDRI,

Lucknow. Molecular weights were determined by the Rast method. Magnetic measurement was made by the Gouy method. Electronic spectra (in MeOH), were recorded on a Perkin-Elmer Lambda-2B-Spectrophotometer. Molar conductance (10^{-3} M) was measured using an Elico-conductivity bridge at room temperature. The FT-IR spectra (in KBr) were recorded at SAIF, IIT, Dehli. X-Ray powder diffraction analysis ($\text{CuK}\alpha$, 1.54060\AA) was performed at SAIF, Punjab University, Chandigarh. The ESR (electron spin resonance) spectra were recorded at SAIF, IIT, Mumbai. Thermal heating of the complexes was performed in a muffle furnace at four temperatures, *i.e.*, 100, 300, 500 and $750\text{ }^\circ\text{C}$.

Synthesis of the Schiff bases (ligands)

Two Schiff bases (HACP, CACP) were synthesized by adding a methanolic solution of 2-hydroxy-acetophenone/2-chloro-benzaldehyde (0.060 mol/0.070 mol) to a methanolic solution of 2-amino 4-chlorophenol (0.060 mol/0.070 mol). The reaction mixture was then refluxed on a water bath for about 5–6 h. The condensation product was filtered, washed thoroughly with ethanol and petroleum ether, recrystallized and dried under vacuum. The purity of the synthesized compounds was monitored by TLC (Thin Layer Chromatography) using silica gel (yield **(A)** = 79.5 % and yield **(B)** = 87.6 %).

Preparation of the metal complexes

All the complexes were prepared by mixing a methanolic solution of $\text{MCl}_2/\text{SO}_4 \cdot n\text{H}_2\text{O}$ (5.0 mmol/3.0 mmol) with the methanolic solution of Schiff bases HACP-(**A**)/CACP-(**B**) in a 1:1 or 1:2 molar ratio. The resulting mixture was refluxed on a water bath for 8–9 h. A coloured product appeared on standing and cooling the solution. The complexes were filtered, washed with petroleum ether and dried under reduced pressure over anhydrous CaCl_2 in a desiccator. They were further dried in an electric oven at $60\text{--}70\text{ }^\circ\text{C}$.

Antimicrobial activity

The *in vitro* biological screening effects of the investigated compounds were tested against *Escherichia coli*, *Staphylococcus aureus* and *Streptococcus fecalis* by the well diffusion method^{13,14} using agar nutrient as the medium and gentamycin as the control.

The *in vitro* antifungal assay was performed by the disc diffusion method.^{13,14} The complexes and ligand were tested against the fungi *Aspergillus niger*, *Trichoderma polysporum* and *Candida albicans*, cultured on potato dextrose agar as the medium. In a typical procedure, a well was created on the agar medium and nystatin as the control was inoculated with the fungi. The well was filled with the test solution, which diffuses and the growth of the inoculated fungi is affected. The inhibition zone which developed on the plate was measured. The *MIC* values of the complexes were determined by the serial dilution technique.

RESULTS AND DISCUSSION

All the metal chelates are coloured, solid and stable towards air and moisture. They decompose at high temperatures ($90\text{--}100\text{ }^\circ\text{C}$) and they are more or less soluble in methanol, acetone, ethanol and chloroform as solvents. The analytical data of the complexes are consistent with the proposed molecular formulae (Fig. 2). All the metal chelates have 1:1 and 1:2 (metal:ligand) stoichiometry. The molar conductance values of the complexes in methanol (10^{-3} M) suggest a non-electrolytic nature, due to the low conductivity values.^{15,16} The analytical results of the complexes are presented in Table I.

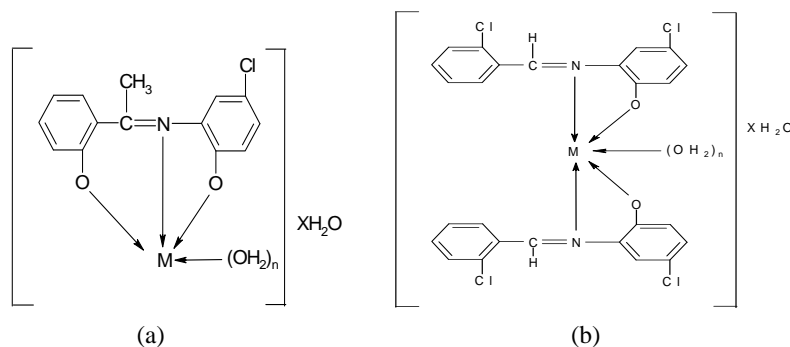


Fig. 2. Structures of the synthesized complexes with Schiff base (ligand):
a) **A** ($n = 1,2,3$; $x = 0,1,2$) and b) **B** ($n = 0,1,2$; $x = 0,1,2$).

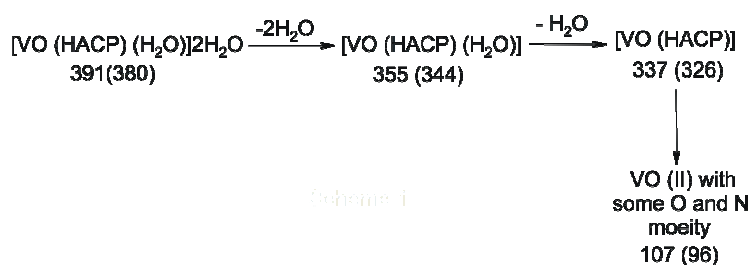
FAB mass spectrum

The FAB mass spectrum of the $[\text{VO}(\text{HACP})(\text{H}_2\text{O})]2\text{H}_2\text{O}$ (**1**) complex was studied as a representative case. Peaks of appreciable intensity were observed at m/z values 391, 355, 337, 259 and 105, suggesting the fragmentation pattern given in Scheme 1.¹⁷ The m/z value 391 corresponds to nearest composition

TABLE I. Physical characterization, analytical, molar conductance and magnetic susceptibility data of HACP (**A**) and CACP (**B**) Schiff base ligands and their metal complexes

Compound	M_r g mol ⁻¹	Colour	Yield %	Elemental analysis				μ_{eff} μ_B	Λ S m ⁻¹ mol ⁻¹
				Found (Calcd.), %					
				C	H	N	M		
(C ₁₄ H ₁₂ NO ₂ Cl) (A)	261.7	Yellow bricks	79.5	64.15 (64.19)	4.53 (4.58)	5.29 (5.34)	–	–	–
[VO(A)(H ₂ O)]·2H ₂ O (1)	380.7	Black	67.7	44.08 (44.12)	4.17 (4.20)	3.62 (3.67)	17.57 (17.59)	1.71	7.3
[Co(A)(H ₂ O) ₃] (2)	372.6	Black	69.9	45.02 (45.07)	4.24 (4.29)	3.71 (3.75)	15.82 (15.80)	5.10	16.2
[Ni(A)(H ₂ O) ₃] (3)	372.4	Light green	69.5	45.06 (45.11)	4.25 (4.29)	3.69 (3.75)	15.75 (15.76)	3.37	14.5
[Cu(A)(H ₂ O)] (4)	341.2	Black	79.7	49.19 (49.23)	3.47 (3.51)	4.06 (4.10)	18.58 (18.61)	1.86	19.3
(C ₁₃ H ₉ NOCl ₂) (B)	265.5	Yellow	87.6	58.71 (58.74)	3.33 (3.38)	5.23 (5.27)	–	–	–
[VO(B) ₂]·2H ₂ O (5)	632.1	Black	67.7	49.31 (49.35)	3.12 (3.16)	4.36 (4.42)	9.98 (10.59)	1.73	14.5
[Co(B) ₂ (H ₂ O) ₂] (6)	624.0	Dark brown	72.6	49.98 (50.00)	3.16 (3.20)	4.42 (4.48)	9.38 (9.43)	5.04	18.9
[Ni(B)] (7)	588.0	Black	74.0	53.02 (53.06)	2.67 (2.72)	4.71 (4.76)	9.95 (9.98)	Diamag- netic	8.1
[Cu(B) ₂ (H ₂ O) ₂] (8)	628.6	Black	75.7	49.59 (49.63)	3.11 (3.18)	4.39 (4.45)	10.08 (10.10)	2.29	17.4

[VO(A)(H₂O)]₂H₂O, 355 to [VO(A)H₂O], 327 to [VO(A)], 259 to the ligand alone and 107 to VO with a chelated ligand moiety.



Scheme 1.

Infrared spectra

A careful comparison of the spectra of the ligands with those of their complexes resulted in the following information regarding various groups. The IR spectrum of the synthesized HACP (A) Schiff base showed absorption band at 1605 cm⁻¹ due to the azomethine group. It was shifted towards higher frequencies (1617±5 cm⁻¹) in the complexes, suggesting coordination through the azomethine nitrogen.¹⁸ The ligand spectrum showed bands at 3375 and 1360 cm⁻¹ due to the deformation stretching vibration of the phenolic OH group, which were absent in the spectra of the complexes. An intense ligand band at about 1202 cm⁻¹ (phenolic C–O) was shifted to higher frequencies (1235±5 cm⁻¹) in the complexes. This suggests deprotonation of the phenolic OH group after its chelation with the metal ion.^{19,20} The appearance of a broad band around 3344±20 cm⁻¹ in the spectra of the complexes suggests the presence of water molecules. A band of weak intensity at 810–820 cm⁻¹ suggests the presence of coordinated water in all four complexes. The IR spectra of the complexes showed some new bands in the region 525±5 and 475±10 cm⁻¹, which are probably due to the n(M–O) and n(M–N) modes, respectively.^{20–23} A characteristic non-ligand sharp band at 968 cm⁻¹ in the spectra of the VO(II) complex was assigned to (V=O), Table II.

TABLE II. IR spectral data (cm⁻¹) of the metal complexes of HACP (A)

Compound	$\nu(\text{O-H})$	$\nu(\text{C=N})$	$\nu(\text{C-O})$	$\nu(\text{C=C})$	$\nu(\text{M-O})$	$\nu(\text{M-N})$	$\nu(\text{V=O})$
HACP (A)	3375 1360	1605	1202	1486	–	–	–
[VO(A)(H ₂ O)] ₂ H ₂ O (1)	–	1618	1240	1475	520	480	968
[Co(A)(H ₂ O) ₃] (2)	–	1617	1235	1472	525	475	–
[Ni(A)(H ₂ O) ₃] (3)	–	1620	1238	1470	528	467	–
[Cu(A)(H ₂ O)] (4)	–	1615	1240	1476	525	486	–

The IR spectrum of the CACP (**B**) Schiff base showed a band at about 1616 cm^{-1} due to ($>\text{C}=\text{N}$) azomethine group. The complexes displayed lower frequency shift of about 5–10 cm^{-1} , suggesting coordination through the azomethine nitrogen. The ligand spectrum showed bands at 3369 and 1361 cm^{-1} due to the stretching deformation of the phenolic OH. These are absent in the spectra of the complexes. A medium intensity ligand band at about 1266 cm^{-1} (phenolic C–O) shifted to higher frequencies and appeared at 1279 \pm 5 cm^{-1} in the metal complexes. This indicates its involvement in chelation. The appearance of broad bands around 3372 \pm 20 cm^{-1} in the spectra of complexes may be due to water molecules. A band of medium intensity at 835 \pm 10 cm^{-1} (OH rocking) suggests the presence of coordinated water in the VO(II), Co(II) and Cu(II) complexes. This band is absent in the Ni(II) complex. New bands of weak intensity at 528 \pm 5 and 475 \pm 10 cm^{-1} in the metal complexes were tentatively assigned to the $\nu(\text{M}-\text{O})$ and $\nu(\text{M}-\text{N})$ modes, respectively.^{5,19,24–27} A characteristic non-ligand sharp band in the spectra of the VO(II) complex at 984 cm^{-1} was assigned to ($\text{V}=\text{O}$), Table III.

Table III. IR spectral data (cm^{-1}) of the metal complexes of CACP (**B**)

Compound	$\nu(\text{O}-\text{H})$	$\nu(\text{C}=\text{N})$	$\nu(\text{C}-\text{O})$	$\nu(\text{C}=\text{C})$	$\nu(\text{M}-\text{O})$	$\nu(\text{M}-\text{N})$	$\nu(\text{V}=\text{O})$
CACP (B)	3369 1361	1616	1266	1480	–	–	–
[VO(B) ₂] \cdot 2H ₂ O (5)	–	1610	1279	1475	528	475	984
[Co(B) ₂ (H ₂ O) ₂] (6)	–	1605	1282	1476	525	470	–
[Ni(B) ₂] (7)	–	1602	1278	1473	530	482	–
[Cu(B) ₂ (H ₂ O) ₂] (8)	–	1608	1277	1473	530	480	–

Electronic spectra

The electronic spectra of the [VO(**A**)(H₂O)] \cdot 2H₂O (**1**) and [VO(**B**)₂] \cdot 2H₂O (**5**) complexes were recorded in methanol as solvent. They displayed three bands at 666.6–657.8 nm, 588.2–555.5 nm and 454.5–416.6 nm, assignable to the transitions ${}^2\text{B}_2 \rightarrow {}^2\text{E}$ (n_1), ${}^2\text{B}_2 \rightarrow {}^2\text{B}_1$ (n_2) and ${}^2\text{B}_2 \rightarrow {}^2\text{A}_1$ (n_3), respectively. The suggested geometry for these complexes may be trigonal bipyramidal based on a coordination number five.²⁷ The values of the magnetic moments for these complexes are 1.71 and 1.73 μ_{B} , respectively, indicating the presence of one unpaired electron.^{27,28}

The electronic spectra of the [Co(**A**)(H₂O)₃] (**2**) and [Co(**B**)₂(2H₂O)] (**6**) complexes displayed two main bands at 666.6–625.1 and 526.3–476.1 nm. These were assigned to ${}^4\text{T}_{1\text{g}}(\text{F}) \rightarrow {}^4\text{A}_{2\text{g}}(\text{F})$ (n_2) and ${}^4\text{T}_{1\text{g}}(\text{F}) \rightarrow {}^4\text{T}_{1\text{g}}(\text{P})$ (n_3) transitions, respectively. The various ligand field parameters: $10 Dq$, B , β , $\beta\%$, ν_2/ν_1 , λ and LFSE were calculated to be: 8612 and 8748 cm^{-1} ; 1029 and 957 cm^{-1} ; 0.91

and 0.85; 8.1 and 14.55; 2.2 and 2.2, (-)669 and (-)646 cm^{-1} , 82.31 and 83.61 kJ mol^{-1} , respectively. The ν_1 transition was expected to appear at larger λ (below 10000 cm^{-1}) and hence it could not be observed. The magnetic moment values of the complexes were 5.10 and 5.04 μ_B . The observed transitions are consistent with an octahedral geometry.²⁹⁻³¹

The electronic spectrum of the $[\text{Ni}(\mathbf{A})(\text{H}_2\text{O})_3]$ (**3**) complex, recorded in methanol, showed two bands at 490.0 and 420.0 nm. These bands were tentatively assigned to ${}^3\text{A}_{2g} \rightarrow {}^3\text{T}_{1g}(\text{F})$ (n_2) and ${}^3\text{A}_{2g} \rightarrow {}^3\text{A}_{1g}(\text{P})$ (n_3) transitions, respectively, which are characteristic for hexa-coordinated Ni(II). The value of the various ligand field parameters $10 Dq$, B , β , ν_2/ν_1 , λ and LFSE were calculated to be: 11337 cm^{-1} , 680 cm^{-1} , 0.62, 1.8, (-)540 cm^{-1} and 162 kJ mol^{-1} . Since the value of the magnetic moment is 3.37 μ_B , a high-spin octahedral geometry for Ni(II) is proposed.³²⁻³⁴

The electronic spectrum of the $[\text{Ni}(\mathbf{B})_2]$ (**7**) complex displayed two bands at 710.0 and 460.0 nm, which are assignable to ${}^1\text{A}_{1g} \rightarrow {}^1\text{E}_g$ (n_1) and ${}^1\text{A}_{1g} \rightarrow {}^1\text{B}_{2g}$ (n_2) transitions, respectively. This complex is diamagnetic in nature. Therefore, a square-planar geometry is suggested.^{29,35-37}

The electronic spectrum of the $[\text{Cu}(\mathbf{A})(\text{H}_2\text{O})]$ (**4**) complex exhibited two bands at 520.0 and 440.0 nm, assignable to ${}^2\text{B}_{1g} \rightarrow {}^2\text{B}_{2g}$ and ${}^2\text{B}_{1g} \rightarrow {}^2\text{E}_g$ transitions, respectively. Since the value of the magnetic moment was 1.86 μ_B , square planar geometry is suggested.^{29,35-37}

The electronic spectrum of a methanolic solution of the $[\text{Cu}(\mathbf{B})(\text{H}_2\text{O})_2]$ (**8**) complex exhibited a broad band at 490.0 nm, which was assigned to the ${}^2\text{E}_g \rightarrow {}^2\text{T}_{2g}$ transition. The various ligand field parameters, *viz.*: $10 Dq$, λ and LFSE were calculated to be 14492 cm^{-1} , (-)670 cm^{-1} and 103.88 kJ mol^{-1} , respectively. The magnetic moment value was 1.89 μ_B . Based on this, an octahedral geometry is suggested for this Cu(II) complex.^{27,35}

ESR spectra

Based on hyperfine and superhyperfine structures, the ESR spectrum of metal complexes provides information about the environment of the metal ion within the complexes, *i.e.*, the geometry and nature of the ligating sites of the Schiff base and the metal. The ESR spectra of the Cu(II) (**4**) and VO(II) (**5**) complexes were recorded at room temperature. The Cu chelate showed two peaks, one in the low field region and the other in the high field region, from which g_{\parallel} and g_{\perp} were calculated. The g_{\parallel} value (< 2.3) indicates a covalent character of the metal-ligand bond.³⁸ The covalent nature of the metal-ligand bond in the complex is further supported by the G value,³⁹ which was < 4.0 . The value $g_{\parallel} > g_{\perp}$ is well consistent with a primarily $d_{x^2-y^2}$ ground state having an elongated tetragonal or square planar structure, Table IV.^{40,41}

TABLE IV. ESR parameters of the Cu(II) (**4**) and VO(II) (**5**) complexes

Metal complex	g_{\parallel}	G_{\perp}	g_{av}	Δg	G
4	2.2147	2.1206	2.1520	0.0941	1.7934
5	1.9387	1.9665	1.9572	0.0278	–

The x-band ESR spectra of the oxovanadium(IV) (**5**) (d^1 , ^{51}V , $I = 7/2$) complex was not resolved enough at room temperature to exhibit all eight hyperfine lines. The calculated values of g_{\parallel} , g_{\perp} , g_{av} and Δg for the VO(II) (**5**) complex are given in Table IV. The g_{av} value is one-third of $(2g_{\perp} + g_{\parallel})$ value. The values are typical of the spectrum displayed by the square pyramidal VO(II) (**5**) complex with one unpaired electron in an orbital of mostly d_{xy} character. The g_{av} values determined from the spectra are nearer to the spin only value. A slight variation may be the result spin-orbit coupling. In square pyramidal complexes with C_4V symmetry, the V=O band is along the z and the other four donor atoms (O_2N_2) are along the x, y axes. An anisotropic ESR spectrum is expected, exhibiting two g values ($g_z = g_{\parallel} < g_{\perp} = g_x = g_y$).^{42–46}

Powder X-ray diffraction analysis

The X-ray powder diffractogram of the $[\text{Cu}(\mathbf{B})_2(\text{H}_2\text{O})_2]$ (**8**) complex was recorded using $\text{CuK}\alpha$ as the source in the 2θ range $5\text{--}74^\circ$. The data reveal that the complex had crystallized in the orthorhombic system (Table V). Eight reflections of 2θ between 16.10 to 57.53° with a maximum $2\theta = 16.10^\circ$ and $d = 5.50 \text{ \AA}$ were observed. $\sin^2\theta$ and hkl values for different lattice planes were calculated. The crystal data for the $[\text{Cu}(\mathbf{B})_2(\text{H}_2\text{O})_2]$ (**8**) complex are: $a = 11.004173 \text{ \AA}$, $b = 11.706081 \text{ \AA}$, $c = 54.46780 \text{ \AA}$, $D_{\text{obs}} = 1.49680 \text{ gm/cm}^3$ and $D_{\text{cal}} = 1.496015 \text{ gm/cm}^3$. The observed and calculated values of the density and $\sin^2\theta$ show good agreement. The calculated values of the cell volume and particle size are 7016.30 \AA^3 and 1.324 nm , respectively. The number of molecules (n) per unit cell was also calculated using the equation $D = nM/NV$; the value is 10 molecules per unit cell (Fig. 3).

TABLE V. XRD data of the $[\text{Cu}(\mathbf{B})_2(\text{H}_2\text{O})_2]$ (**8**) complex

Peak No.	d -Spacing \AA	Relative intensity $I/I_0 \times 100$	$\sin^2\theta$		
			Observed	Cald.	hkl
1	5.504	100.00	0.0916	0.0196	200
2	4.011	59.16	0.0369	0.0369	220
3	3.104	60.02	0.0616	0.0616	320
4	2.752	51.62	0.0784	0.0784	400
5	2.685	96.99	0.0825	0.0827	410
6	2.229	28.90	0.1195	0.1191	433
7	2.000	30.02	0.1485	0.1484	442
8	1.600	22.32	0.2316	0.2314	522

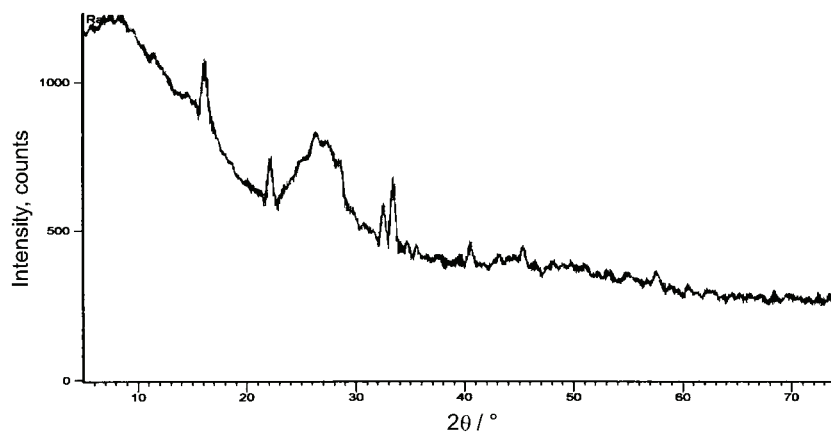


Fig. 3. X-Ray powder diffractogram of the $[\text{Cu}(\mathbf{B})_2(\text{H}_2\text{O})_2]$ (**8**).

Thermal decomposition

The complexes **1–4** of HACP (**A**) and the complexes **5–8** of CACP (**B**) were heated at four temperatures (100, 300, 500 and 750 °C) in a muffle furnace for 20–30 min. The resulting weights were measured. The weight loss at 100 °C corresponds to the loss of lattice water molecules from the complexes.^{17,46,47} The weight measured after heating at 300 °C indicates the loss of coordinated water molecules from the complexes. On heating at 500 °C, the remaining weight indicates the loss of parts of the ligand moiety. The weight of the pyrolysis product after heating at 750 °C corresponds to metal oxide.

Antimicrobial activity

The *in vitro* anti-microbial activity of the investigated compounds was, tested against the micro-organisms *E. coli*, *S. aureus*, *S. fecalis*, *A. niger*, *T. polysporum* and *C. albicans* by the serial dilution method. The minimum inhibitory concentration (*MIC*) values of the compounds against the growth of the micro-organisms are summarized in Table VI. A comparative study of the ligand and its cobalt(II) and copper(II) complexes (*MIC* values) indicated that both complexes **6** and **8** exhibited either higher or lower antimicrobial activity than the free ligand **A**.^{48,49}

The complexes **6** and **8** exhibited better antibacterial activity than their SB-ligand **A** against *E. coli* and *S. aureus*. Against *S. fecalis*, complex **6** showed better activity than its SB-ligand **A** while complex **8** was less active.

The complexes **6** and **8** exhibited better antifungal activity in comparison to SB-ligand **A** against all three fungi, Table VI.

These observations showed that the majority of the complexes were more active than their respective Schiff base ligands. In some cases, Schiff bases are more active than their metal complexes against bacteria. The chelation either enhances or reduces the antimicrobial activity; sometimes it remains neutral. Thus,

TABLE VI. Antimicrobial data (MIC value; diameter of inhibition zone, mm) of the investigated compounds

Compound	E. coli		S. aureus		S. fecalis		A. niger		T. polysporum		C. albicans						
	25	50	100	25	50	100	25	50	100	25	50	100					
CACP (6)	13	13	15	i/nm ^a	10	13	17	23	10	14	22	15	17	19	13	16	18
[Co(6) ₂ (H ₂ O) ₂] (6)	20	24	28	11	12	20	17	20	16	12	16	25	18	19	21	15	19
[Cu(6) ₂ (H ₂ O) ₂] (8)	22	25	32	13	15	19	10	15	19	10	15	23	17	20	22	14	18
Nystatin	-	-	-	-	-	-	-	-	-	20	23	24	23	24	20	21	20
Gentamycin	18	20	19	19	22	20	18	21	23	-	-	-	-	-	-	-	-
Standard DMSO	i/nm	i/nm	i/nm	i/nm	i/nm	i/nm	i/nm	i/nm	i/nm	i/nm	i/nm	i/nm	i/nm	i/nm	i/nm	i/nm	i/nm

^aInactive/not measurable

metal chelation may increase or decrease/suppress the therapeutic value of organic compounds (drugs). It may maintain the property intact by further stabilizing the drug and/or reducing the biodegradability/metabolic decay of the organic ligands through chelation.

CONCLUSIONS

The coordination complexes of VO(II), Co(II), Ni(II) and Cu(II) with two new tridentate and bidentate Schiff base ligands, *i.e.*, 2-hydroxy acetophenone-2-amino-4-chlorophenol (**A**) and 2-chlorobenzylidene-2-amino-4-chlorophenol (**B**), were synthesized and characterized. The ligands coordinated with the metal ions through N or O donors. The complexes exhibited a geometry based on the coordination numbers 4, 5 or 6. A comparative study of the *MIC* value of the ligands and their complexes indicated that the chelation might be helpful in tailoring the structure and monitoring the antimicrobial activity and therapeutic potential of a drug; thus giving a new thrust area in the field of metallo-drugs (bio-inorganic chemistry) through molecular biology. The synthesized metal complexes may also function as single molecule nanoprecursors.

ИЗВОД

СТРУКТУРНО И АНТИМИКРОБНО ПРОУЧАВАЊЕ КООРДИНАЦИОНИХ ЈЕДИЊЕЊА VO(II), Co(II), Ni(II) И Cu(II) СА НЕКИМ ШИФОВИМ БАЗАМА КОЈЕ УКЉУЧУЈУ 2-АМИНО-4-ХЛОРОФЕНОЛ

A. P. MISHRA, R. K. MISHRA и S. P. SHRIVASTAVA

Bio-coordination Laboratories, Department of Chemistry, Dr. H. S. Gour University Sagar-470003, India

Комплекси са есенцијалним металним јонима могу дати одговор на проблем отпорности на више лекова. Координациона једињења VO(II), Co(II), Ni(II) и Cu(II) са Шифовим базама изведеним из 2-хидроксиацетофенон/2-хлоробензалдехида са 2-амино-4-хлорофенилом су синтетисана и окарактерисана елементалном анализом, моларном проводљивошћу, електронским спектрима, FT-IR, ESR, FAB масеним спектрима, термичким мерењима и одређивањем магнетне суспектибилности. FAB масени и термички подаци показују деградацију комплекса. Лиганд **A**, 2-хидроксиацетофенон-2-амино-4-хлорофенол, понаша се као тридентат, а лиганд **B**, 2-хлорбензилиден-2-амино-4-хлорофенол, као бидентат који се координира преко O и N донора. Комплекси [VO(**A**)(H₂O)]·xH₂O, [M(**A**)(H₂O)_n]·xH₂O за Co и Ni, [Cu(**A**)(H₂O)] и [VO(**B**)₂]·xH₂O, [M(**B**)₂(H₂O)_n] за Co и Cu, [Ni(**B**)₂] имају координационе бројеве 4, 5 или 6. Резултати дифракције x-зрака за прах (*a* = 11.00417 Å, *b* = 11.706081 Å и *c* = 54.46780 Å) показују да [Cu(CACP)₂(H₂O)₂] кристалише у орторомбичном систему. *In vitro* биолошка проучавања изучаваних једињења вршена су према бактеријама *Escherichia coli*, *Staphylococcus aureus* и *Streptococcus fecalis* и гљивицама *Aspergillus niger*, *Trichoderma polysporum* и *Candida albicans* серијском методом разблажења. Упоредно проучавање *MIC* вредности Шифове базе и њених [M(**B**)₂(H₂O)₂] (M = Co(II) или Cu(II)) комплекса, указују да метални комплекси имају већу или мању антимикробну активност у односу на 2-хлоробензилиден-2-амино-4-хлорофенол као слободни лиганд (**B**).

(Примљено 5. августа, ревидирано 9. децембра 2008)

REFERENCES

1. M. C. Orving, J. Abrams, *Chem. Rev.* **99** (1999) 2201
2. N. Raman, S. Johnson, *J. Serb. Chem.* **72** (2007) 983
3. R. K. Crouch, T. W. Kensler, T. W. Oberley, J. R. J. Sorenson, in *Possible medicinal use of copper complexes; Biological and inorganic copper chemistry*, K. D. Karlin, J. Zubietta, Eds., Adenine Press, NT, 1986
4. R. J. P. Williams, J. J. R. Frausto da Silva, *Coord. Chem. Rev.* **200** (2000) 247
5. M. R. Maurya, S. Khurana, C. Schulzke, D. Rehder, *Eur. J. Inorg. Chem.* (2001) 779
6. A. Butler, M. J. Clauge, G. E. Meister, *Chem. Rev.* **94** (1994) 625
7. J. H. McNeil, V. G. Yuen, H. R. Hoveyda, C. Orvig, *J. Med. Chem.* **35** (1992) 489
8. D. Rehder, *Coord. Chem. Rev.* **182** (1999) 297
9. M. Weyand, H. J. Hecht, M. Kieß, M. F. Liaud, H. Vilter, D. Schomburg, *J. Mol. Biol.* **293** (1999) 595
10. S. Macedo-Ribeiro, W. Hemrika, R. Reniric, R. Wever, A. Messerschmidt, *J. Bio. Inorg. Chem.* **4** (1999) 209
11. A. Majumdar, G. M. Rosair, A. Mallick, N. Chattopadhyay, S. Mitra, *Polyhedron* **25** (2006) 1753
12. J. R. Morrow, K. A. Kolasa, *Inorg. Chim. Acta* **195** (1992) 245
13. S. C. Prescott, C. G. Duan, *Industrial Microbiology*, 3rd ed., McGraw Hill, Koyakesha, 1949, p. 519
14. W. Barrows, *Text Book of Microbiology*, 16th ed., W. B. Saunders Co., London, 1954, p. 8
15. S. F. A. Kettle, *Coordination Compounds*, Thomas Nelson & Sons, Nashville, TN, 1969
16. C. P. J. Piriz Macoll, *J. Chem. Edu.* (1951) 303
17. A. P. Mishra, L. R. Pandey, *Indian J. Chem.* **44A** (2005) 94
18. V. Shrivastava, S. K. Shrivastava, A. P. Mishra, *J. Indian Chem. Soc.* **22** (1995) 434
19. K. Nakamoto, *Infrared and Raman Spectra of Inorganic and Coordination Compounds*, 4th Ed., John Wiley & Sons, New York, 1986, p. 227
20. R. S. Drago, *Physical Methods in Inorganic Chemistry*, Student Ed., Affiliated East West, Darya Ganj, 1978, pp. 85, 139, 339
21. K. Dey, D. Bandyopadhyay, *Indian J. Chem.* **31A** (1992) 34
22. R. M. Silverstein, G. C. Bassaler, T. C. Morill, *Spectrometric Identification of Organic Compounds*, 4th Ed., John Wiley & Sons, New York, 1981, p. 95
23. J. R. Dyer, *Application of Absorption Spectroscopy of Organic Compounds*, Prentice Hall, New Delhi, 1984
24. L. J. Bellamy, *Infrared Spectra of Complex Molecules*, Wiley, New York, 1954
25. A. K. Dey, *J. Indian Chem. Soc.* **63** (1986) 357
26. N. K. Singh, N. R. Agrawal, *Indian J. Chem.* **37** (1998) 276
27. B. N. Figgis, *Introduction to Ligand Field Theory*, 2nd Ed., Wiley East, New Delhi, 1976
28. M. Calligaris, L. Randaccio, in *Comprehensive Coordination Chemistry*, Vol. 2, G. Wilkinson, Ed., Pergamon Press, Oxford, 1987, p. 715
29. A. B. P. Lever, *Inorganic Electronic Spectroscopy*, 2nd Ed., Elsevier, Amsterdam, 1984, p. 479, 507, 553, 736
30. A. D Liether, *J. Phys. Chem.* **67** (1967) 1314
31. T. A. Khan and A. Shahjahan, *Synth. React. Inorg. Met. Org. Chem.* **31** (2001) 1023
32. A. M. A. Hassaan, *Trans. Met. Chem.* **15** (1990) 283
33. G. G. Mohamed, M. M. Omar, A. M. Hindy, *Turk J. Chem.* **30** (2006) 361

34. M. S. Masoud, A. M. Hindawy, A. S. Soayed, *Trans. Met. Chem.* **16** (1991) 372
35. D. F. Shriver, P. W. Atkins, C. H. Langford, *Inorganic Chemistry*, Oxford University Press, Oxford, 1990, p. 434
36. B. J. Hathway, in *Comprehensive Coordination Chemistry*, Vol. 2, G. Wilkinson, Ed., Pergamon Press, Oxford, 1987, p. 413
37. B. N. Figgis, in *Comprehensive Coordination Chemistry*, Vol. 2, G. Wilkinson, Ed., Pergamon Press, Oxford, 1987, p. 413
38. D. Kivelson, R. Neeman, *J. Chem. Phys.* **35** (1961) 149
39. A. Syamal, *Chem. Edu.* **62** (1985) 143
40. M. F. El-Shazly, L. S. Retaat, *Trans. Met. Chem.* **6** (1981) 10
41. J. Viroopakshappa, D. Vithal Rao, *J. Indian Chem. Soc.* **73** (1996) 513
42. S. K. Sengupta, O. P. Pandey, J. K. Pandey, G. K. Pandey, *Indian J. Chem.* **40A** (2001) 887
43. S. Bhattacharya, T. Ghosh, *Indian J. Chem.* **38A** (1999) 601
44. M. R. Maurya, S. Khurana, W. Zhang, D. Rehder, *Eur. J. Inorg. Chem.* (2002) 1749
45. R. L. Dutta, A. Symal, *Elements of Magneto Chemistry*, 2nd ed., Affil East-West Press Pvt. Ltd., New Delhi, 1993
46. A. P. Mishra, M. Khare, S. K. Gautam, *Synth. React. Inorg. Met-Org Chem.* **32** (2002) 1485
47. P. R. Mandik, M. B. More, A. S. Aswar, *Indian J. Chem.* **42A** (2003) 1064
48. N. Raman, J. Joseph, S. K. Velan, C. Pothiraj, *Microbiology* **34** (2006) 214
49. N. Raman, R. Johnson, *J. Serb. Chem. Soc.* **72** (2007) 983.



J. Serb. Chem. Soc. 74 (5) 537–548 (2009)
JSCS–3853

Preparation, characterization and antibacterial effect of 2-methoxy-6-(5-H/Me/Cl/NO₂-1H-benzimidazol-2-yl)phenols and some transition metal complexes

AYDIN TAVMAN^{1*}, SERKAN IKIZ², A. FUNDA BAGCIGIL²,
N. YAKUT ÖZGÜR² and SEYYAL AK²

¹Istanbul University, Faculty of Engineering, Department of Chemistry, 34320 Avcilar,
Istanbul and ²Istanbul University, Veterinary Faculty, Department of Microbiology,
34320 Avcilar, Istanbul, Turkey

(Received 10 June, revised 28 November 2008)

Abstract: 2-Methoxy-6-(5-H/methyl/chloro/nitro-1H-benzimidazol-2-yl)phenols (HL_x; x = 1–4, respectively) ligands and HL₁ complexes with Fe(NO₃)₃, Cu(NO₃)₂, AgNO₃ and Zn(NO₃)₂ were synthesized and characterized. The structures of the compounds were confirmed based on elemental analysis, molar conductivity, magnetic moment, FT-IR, ¹H- and ¹³C-NMR. The antibacterial activity and minimum inhibitory concentration (MIC) of the free ligands, their hydrochloride salts and the complexes were evaluated using the disk diffusion method in dimethyl sulfoxide (DMSO) and the dilution method, respectively, against 9 bacteria. HL₁ and HL₃, as well as the Cu(II) and Zn(II) complexes, showed antibacterial activity against Gram-positive bacteria.

Keywords: benzimidazolylphenols; complexes; antibacterial activity.

INTRODUCTION

Benzimidazole and its derivatives possess a wide variety of useful biological properties due to their structural similarities with the common nucleobases.^{1–4} While some are important potent antiviral agents,^{5,6} many are the active components of biocides, such as fungicides, and insecticides.⁷ For instance, 2-(4-thiazolyl)benzimidazole, known as thiabendazole, and several of its coordination compounds aroused considerable interest in medicine due to their strong antimicrobial activity.^{8,9} Also in this range, 5-methoxy-2-[(4-methoxy-3,5-dimethylpyridin-2-yl)methyl]sulphonyl}-1H-benzimidazole (omeprazole) is used as the prototype antisecretory agent.¹⁰ The compounds albendazole, mebendazole and flubendazole are effective anthelmintics.^{11,12} Others, such as astemizole, are non-sedating antihistamines¹³ and fenbendazole is effective against gastrointestinal nematode parasites.¹⁴

* Corresponding author. E-mail: atavman@istanbul.edu.tr
doi: 10.2298/JSC0905537T

Investigation of the biological activity of complex compounds is a field that has developed over the years. When the ligands coordinate to transition metals, it is believed that the selectivity towards certain biological systems is improved.^{15–18} In this work, 2-methoxy-6-(5-H/methyl/chloro/nitro-1*H*-benzimidazol-2-yl)-phenols (Fig. 1) ligands and the iron(III), copper(II), silver(I) and zinc(II) nitrate complexes with 2-methoxy-6-(1*H*-benzimidazol-2-yl)-phenol are reported. The antibacterial activities of the ligands and the complexes were evaluated by the disk diffusion method against nine bacteria.

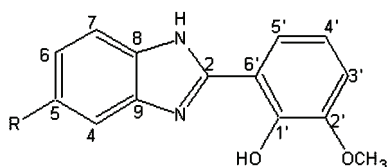


Fig. 1. Schematic view of the structure of the ligands; R = H in HL₁; R = CH₃ in HL₂; R = Cl in HL₃; R = NO₂ in HL₄.

EXPERIMENTAL

Materials and apparatus

All chemicals and solvents were of reagent grade and were used as purchased without further purification. Melting points were determined using a Gallenkamp melting point apparatus. The C,H,N content was determined on a Thermo Finnigan Flash EA 1112 analyzer (Istanbul University, Advanced Analyses Laboratory, Istanbul). The molar conductivity of the complexes was measured on a WPA CMD750 conductivity meter in dimethyl sulfoxide (DMSO, $c = 10^{-3}$ mol/L) at 25 ± 1 °C. The ¹H- and ¹³C-NMR spectra were recorded on a Varian Unity Inova 500 NMR spectrometer (in DMSO-*d*₆, $c \approx 10^{-4}$ mol/L). The residual DMSO-*d*₆ signal was used as an internal reference. The FT-IR spectra were recorded in KBr disks on a Mattson 1000 FT-IR spectrometer. The electronic spectra were recorded on a Perkin Elmer Lambda 25 UV/Visible Spectrometer. The magnetic measurements were performed on a Sherwood Scientific apparatus at room temperature by the Gouy method using CuSO₄·5H₂O as the calibrant and were corrected for diamagnetism by applying Pascal's constants.¹⁹

Syntheses of the ligands

The ligands were prepared according to literature procedures.^{20,21}

2-Methoxy-6-(1*H*-benzimidazol-2-yl)phenol (HL₁) was prepared by reacting 2-hydroxy-3-methoxybenzaldehyde (1.52 g, 10.0 mmol) and an equivalent amount of NaHSO₃ (1.04 g, 10.0 mmol) at room temperature in ethanol (25 ml) for 4–5 h. The mixture was treated with 1,2-phenylenediamine (1.08 g, 10.0 mmol) in dimethylformamide (15 ml) and gently refluxed for 2 h. The reaction mixture was then poured into iced water (500 ml), filtered and crystallized from ethanol. Yield: 1.9 g; ≈ 80 %.

2-Methoxy-6-(5-methyl-1*H*-benzimidazol-2-yl)phenol (HL₂) was synthesized by a procedure similar to that employed for HL₁ but using 2-hydroxy-3-methoxybenzaldehyde (305 mg, 2.00 mmol), NaHSO₃ (210 mg, 2.00 mmol) and 4-methyl-1,2-phenylenediamine (250 mg, 2.00 mmol). Yield: 355 mg; ≈ 70.0 %.

2-Methoxy-6-(5-chloro-1*H*-benzimidazol-2-yl)phenol (HL₃) was synthesized by a procedure similar to that employed for HL₁ but using 2-hydroxy-3-methoxybenzaldehyde (305 mg,

2.00 mmol), NaHSO₃ (210 mg, 2.00 mmol) and 4-chloro-1,2-phenylenediamine (285 mg, 2.00 mmol). Yield: 360 mg; ≈ 65.0 %.

2-Methoxy-6-(5-nitro-1H-benzimidazol-2-yl)phenol (HL₄) was synthesized by a procedure similar to that employed for HL₁ but using 2-hydroxy-3-methoxybenzaldehyde (305 mg, 2.00 mmol), NaHSO₃ (210 mg, 2.00 mmol) and 4-nitro-1,2-phenylenediamine (306 mg, 2.00 mmol). Yield: 430 mg; ≈ 75.0 %.

Syntheses of the complexes

[Fe(L₁)(OH)(H₂O)₂]NO₃ was prepared by treating a hot solution of the ligand HL₁ (120 mg, 0.500 mmol) in iso-propanol (10 ml) with Fe(NO₃)₃·9H₂O (222 mg, 0.550 mmol) in iso-propanol (5.0 ml) at ≈ 60 °C for 3–4 h. The solution mixture was allowed to stand at ≈ 4 °C for several days whereby black solid products precipitated, which were collected by filtration and dried under vacuum over anhydrous calcium chloride. Yield: 180 mg; ≈ 95.0 %.

[Cu(L₁)₂]·2H₂O was prepared by reacting 120 mg HL₁ (0.500 mmol) and 133 mg Cu(NO₃)₂·3H₂O (0.550 mmol) in 10 ml methanol. After 4 h-reflux, the formed precipitate was filtered and dried at ≈ 80 °C. Yield: 150 mg; ≈ 65.0 %.

[Ag(L₁)] was synthesized by reacting 120 mg HL₁ (0.500 mmol) and 94 mg AgNO₃ (0.550 mmol) in 10 ml ethanol at room temperature for 6 h with stirring. The obtained precipitate was filtered and dried at ≈ 80 °C. Yield: 135 mg; ≈ 80.0 %.

[Zn(L₁)(H₂O)₂]NO₃ was prepared by adding 164 mg Zn(NO₃)₂·6H₂O (0.550 mmol) in 15 ml ethyl acetate to 120 mg HL₁ (0.500 mmol) suspended in ethyl acetate and refluxing the mixture for 2 h. The obtained dark yellow precipitate was filtered and dried under vacuum over calcium chloride. Yield: 145 mg; ≈ 75.0 %.

Determination of antimicrobial activity

The antimicrobial activities were evaluated against Gram-positive (*Staphylococcus aureus*, ATCC 29213, *Bacillus cereus*, ATCC 11778, *Bacillus subtilis*, ATCC 6633, *Staphylococcus epidermidis*, ATCC 12228) and Gram-negative (*Escherichia coli*, ATCC 25922, *Klebsiella pneumoniae*, ATCC 4352, *Pseudomonas aeruginosa*, ATCC 27853, *Salmonella enteritidis*, KUEN 349, *Proteus mirabilis*, CCM 1944) bacteria. The strains were provided by the Centre for Research and Application of Culture Collections of Microorganisms, Istanbul University (KUKENS).

Mueller–Hinton Agar (Fluka 70191) was used for the detection of the qualitative antibacterial effect and to maintain the strains. For the detection of the quantitative antibacterial effect, Mueller–Hinton broth (Fluka 70192) (CAMBH) with MgCl₂·2H₂O (10 mg Mg²⁺/L) and CaCl₂·6H₂O (20 mg Ca²⁺/L) was used as the medium.

The disc diffusion method was used for the detection of the qualitative antibacterial effect of the chemical agents.²² For this purpose, filter papers (Whatman, No:1) with 6 mm diameter were autoclaved and dried at 37 °C overnight. Each chemical agent (21.27 mg) was dissolved in DMSO and 23.5 µl of this solution (containing 500 µg chemical agent) were soaked onto the sterile discs. Bacterial suspension with 1–2×10⁸ cfu/ml (McFarland 0.5) were prepared from each bacterial strain and streaked onto the agar. The discs impregnated with the chemical agents were placed onto the agar surface and incubated at 37 °C for 24 h. Chemical agents with growth inhibition zones were used for the further examinations.

For the detection of the antibacterial effect of the chemical agents, quantitatively, the macro-dilution broth method according to clinical and laboratory standards institute (formerly NCCLS) was performed.²³ Serial dilutions of the chemical agents between 531.75–0.26 µg/ml with CAMBH were prepared in sterile tubes. A bacterial suspension with 10⁷ cfu/ml final

concentration was inoculated. Positive (without tested chemical agent) and negative (without bacterial suspension) tubes were used at the end of each organism tested. The tubes were incubated at 37 °C for 24 h. The minimum inhibitory concentration, *MIC*, value was defined as the lowest concentration of the chemical agent giving complete inhibition of visible growth.

RESULTS AND DISCUSSION

Physical properties

The analytical data and physical properties of the ligands and the complexes are summarized in Table I. The melting points of the ligands HL₂–HL₄ suggest that a methyl substitution on the 5-position of the benzimidazole moiety decreases the melting point and a chloro or nitro group increases it with respect to the HL₁ ligand.

TABLE I. The analytical data and physical properties of the HL₁–HL₄ ligands and the complexes

Compound	Found (Calcd.), %			M.p. °C	Color	Λ^a S cm ² mol ⁻¹
	C	H	N			
HL ₁ (C ₁₄ H ₁₂ N ₂ O ₂)	70.3 (70.0)	4.8 (5.0)	11.4 (11.7)	278	White	–
HL ₂ (C ₁₅ H ₁₄ N ₂ O ₂)	70.5 (70.8)	5.8 (5.6)	10.6 (11.0)	259	White	–
HL ₃ (C ₁₄ H ₁₁ ClN ₂ O ₂)	61.5 (61.2)	3.9 (4.0)	9.9 (10.2)	304	Dirty white	–
HL ₄ (C ₁₄ H ₁₁ N ₃ O ₄)	59.2 (58.9)	4.1 (3.9)	14.4 (14.7)	329	Greenish yellow	–
[Fe(L ₁)(OH)(H ₂ O) ₂] ₂ NO ₃ ^b C ₁₄ H ₁₆ FeN ₃ O ₈	40.7 (41.0)	3.6 (3.9)	9.9 (10.2)	227	Black	37
[Cu(L ₁) ₂].2H ₂ O ^b C ₂₈ H ₂₆ CuN ₄ O ₆	57.8 (58.2)	3.9 (4.5)	10.3 (9.7)	212	Khaki- green	12
[Ag(L ₁) ₂] C ₁₄ H ₁₂ AgN ₃ O ₅	48.8 (48.4)	3.2 (3.2)	8.5 (8.1)	184	Grey	9
[Zn(L ₁)(H ₂ O) ₂] ₂ NO ₃ C ₁₄ H ₁₃ N ₃ O ₆ Zn	41.5 (41.8)	3.2 (3.7)	10.8 (10.4)	322	Dark- yellow	35

^aIn DMSO, $t = 25 \pm 1$ °C; ^b μ_{eff} values for [Fe(L₁)(OH)(H₂O)₂]₂NO₃ and [Cu(L₁)₂].2H₂O are 3.85 and 1.61 μ_{B} , respectively

The molar conductivity values of the complexes were 37 and 35 S cm² mol⁻¹ for the Fe(III) and Zn(II) complexes, respectively. These results are indicative for 1:1 electrolyte complexes. The Cu(II) and Ag(I) complexes had a non-ionic character according to the molar conductivity measurements.^{24,25}

The magnetic moment value of the [Fe(L₁)(OH)(H₂O)₂]₂(NO₃) complex was 3.85 μ_{B} , which is lower than the spin only value of $\approx 5.90 \mu_{\text{B}}$ for Fe(III) d⁵ with $s = 5/2$ (high spin under a weak field) and higher than the spin only value of $\approx 2.0 \mu_{\text{B}}$ in the case of $s = 1/2$ (low spin in the presence of a strong field). The intermediate value of the magnetic moment indicates stabilization of the species having an intermediate ferric spin ($s = 3/2$) state for this complex. The occurrence of

such an intermediate spin state is typical for five coordinated Fe(III) d⁵ ferric complexes.^{26,27} The magnetic moment value of the [Cu(L₁)₂].2H₂O complex was 1.63 μ_B, which is to be expected for a typical d⁹ Cu(II) complex.

Electronic spectra

UV-visible spectral data of the ligands and the complexes are given in Table II. The electronic spectra of the ligands and the complexes exhibit intense bands in the 220–310 nm region, which may be assignable to n → p* and p → p* transitions.

TABLE II. UV-visible spectral data of the HL₁–HL₄ ligands and the complexes (in methanol)

Compound	Wavelength, nm
HL ₁	245, 283, 306, 361
[Fe(L ₁)(OH)(H ₂ O) ₂]NO ₃	258, 318, 367, 381, 575
[Cu(L ₁) ₂].2H ₂ O	251, 298, 305, 357, 456, 645
[Ag(L ₁)]	285, 293, 303, 341
[Zn(L ₁)(H ₂ O) ₂]NO ₃	274, 302, 335, 390, 445
HL ₂	236, 265, 290, 371
HL ₃	221, 300, 310, 352
HL ₄	265, 295, 345, 363, 401, 415

The electronic spectra of the Fe(III) complex is of little help in the present case, since the d → d transitions are masked by broad strong charge-transfer bands (575 nm, L → Fe, charge transfer).²⁸ The broad band at 445 nm in the spectrum of the Zn(II) complex is a charge-transfer band.

The electronic spectra of the Cu(II) complex showed three bands at 645, 456 and 357 nm. The 357 nm-band is assigned to a metal–ligand charge transfer. The other two bands are assigned to a ²B_{1g} → ²A_{1g} and ²B_{1g} → ²E_g transition, respectively. These assignments are typically characteristic for a square-planar geometry of Cu(II) complexes (Fig. 2).^{29,30}

FT-IR spectra

FT-IR spectral data of the ligands and the complexes are given in Table III. The characteristic ν(O–H) and ν(N–H) vibrations of the ligands exhibit only a single strong band at ca. 3290 cm⁻¹ in the IR spectra, which is probably caused by doubly intramolecular hydrogen bonding between the phenoxyl hydrogen atom and one of the imine nitrogen atoms (Table III, Fig. 2).^{15,31,32} The 3295 cm⁻¹ band in HL₁ changed significantly upon metal complexation, indicating deprotonation and subsequent involvement of the phenoxyl group in metal coordination. The coordination of the phenolic oxygen atom could also be supported by the appearance of medium-to-strong bands at a lower frequency region, ca. 500 cm⁻¹, assignable to ν(M–OC) vibration.³³

The appearance of a strong broad band at *ca.* 3400 cm^{-1} in the Fe(III), Cu(II) and Zn(II) complexes strongly supports the presence of coordinated water molecules (Fig. 3). The characteristic $\nu(\text{C-H})$ and $\delta(\text{C-H})$ modes of the ring residues and aliphatic groups (methyl and methoxy substituents) are observed in the wavelength region between 3100–2940 cm^{-1} and 1500–800 cm^{-1} (Table III). The $\nu(\text{C=C})$ frequencies of the ring residue are expected to appear at *ca.* 1630 cm^{-1} with their own characteristics for the ligands in the IR spectra. These frequencies are expected to shift to lower frequencies upon complex formation. Similarly, the $\nu(\text{C=N})$ asymmetric stretching frequencies are expected to appear at *ca.* 1590 cm^{-1} . Thus, the IR band at 1593 cm^{-1} in the spectrum of the HL₁ ligand shifts to *ca.* 1600 cm^{-1} upon complex formation. These frequency changes may support the argument that coordination possibly occurs *via* an imine nitrogen atom.

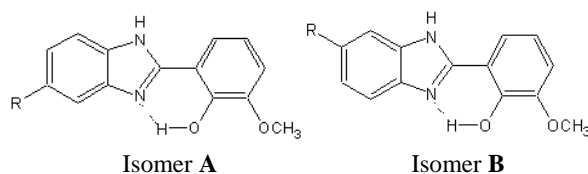


Fig. 2. Schematic presentation of the isomeric structures for the HL₂ (isomer **A**) and HL₄ (isomer **B**) ligands (R = CH₃, NO₂).

Fe(III) and Zn(II) complexes show strong bands at 1386 cm^{-1} in their IR spectra, supporting the presence of an uncoordinated nitrate ion, which was also confirmed by conductivity data.^{28,34}

TABLE III. Prominent IR bands for the HL₁–HL₄ ligands and the complexes

Compound	Frequency, cm^{-1}
HL ₁	3295 <i>s</i> , 3068 <i>w</i> , 2930 <i>w</i> , 1628 <i>m</i> , 1593 <i>m</i> , 1478 <i>s</i> , 1424 <i>m</i> , 1255 <i>s</i> , 1062 <i>m</i> , 781 <i>m</i> , 743 <i>m</i> , 605 <i>m</i> , 502 <i>w</i> , 433 <i>w</i>
[Fe(L ₁)(OH)(H ₂ O) ₂] ₂ NO ₃	3411 <i>m,br</i> , 3276 <i>m, br</i> , 2933 <i>w</i> , 1621 <i>m</i> , 1605 <i>sh</i> , 1562 <i>m</i> , 1547 <i>m</i> , 1493 <i>m</i> , 1478 <i>m</i> , 1386 <i>s</i> , 1305 <i>m</i> , 1278 <i>m</i> , 1066 <i>w</i> , 793 <i>w</i> , 746 <i>m</i> , 589 <i>m</i> , 508 <i>w</i> , 458 <i>w</i>
[Cu(L ₁) ₂] ₂ ·2H ₂ O	3423 <i>m, br</i> , 3254 <i>m, br</i> , 2946 <i>m</i> , 1623 <i>m</i> , 1608 <i>m</i> , 1538 <i>w</i> , 1485 <i>s</i> , 1462 <i>m</i> , 1315 <i>m</i> , 1246 <i>m</i> , 1208 <i>m</i> , 1069 <i>m</i> , 854 <i>w</i> , 746 <i>m</i> , 572 <i>m</i> , 517 <i>m</i> , 445 <i>w</i>
[Ag(L ₁)]	3434 <i>m, br</i> , 3361 <i>m, br</i> , 3280 <i>m, br</i> , 3049 <i>w</i> , 2934 <i>w</i> , 1621 <i>m</i> , 1594 <i>m</i> , 1532 <i>m</i> , 1497 <i>m</i> , 1447 <i>m</i> , 1255 <i>s</i> , 1070 <i>s</i> , 750 <i>s</i> , 735 <i>m</i> , 654 <i>m</i> , 604 <i>m</i> , 445 <i>w</i>
[Zn(L ₁)(H ₂ O) ₂] ₂ NO ₃	3449 <i>m, br</i> , 3307 <i>m, br</i> , 2941 <i>w</i> , 1624 <i>m</i> , 1605 <i>w</i> , 1497 <i>s</i> , 1482 <i>s</i> , 1386 <i>s</i> , 1312 <i>s</i> , 1286 <i>m</i> , 1243 <i>m</i> , 1197 <i>m</i> , 1112 <i>m</i> , 1066 <i>m</i> , 793 <i>m</i> , 743 <i>m</i> , 572 <i>w</i> , 517 <i>m</i> , 445 <i>w</i>
HL ₂	3291 <i>s</i> , 3076 <i>w</i> , 2933 <i>w</i> , 1632 <i>m</i> , 1593 <i>m</i> , 1482 <i>s</i> , 1424 <i>m</i> , 1255 <i>s</i> , 1062 <i>m</i> , 789 <i>m</i> , 735 <i>m</i> , 604 <i>m</i>
HL ₃	3295 <i>s</i> , 3072 <i>w</i> , 2937 <i>w</i> , 1628 <i>w</i> , 1594 <i>m</i> , 1482 <i>s</i> , 1424 <i>m</i> , 1386 <i>m</i> , 1255 <i>s</i> , 1058 <i>m</i> , 935 <i>m</i> , 739 <i>m</i> , 735 <i>m</i> , 608 <i>m</i>
HL ₄	3291 <i>s</i> , 3087 <i>w</i> , 2941 <i>w</i> , 1632 <i>m</i> , 1593 <i>m</i> , 1520 <i>s</i> , 1478 <i>m</i> , 1424 <i>m</i> , 1336 <i>s</i> , 1255 <i>s</i> , 1055 <i>m</i> , 843 <i>m</i> , 792 <i>m</i> , 739 <i>s</i> , 608 <i>m</i>

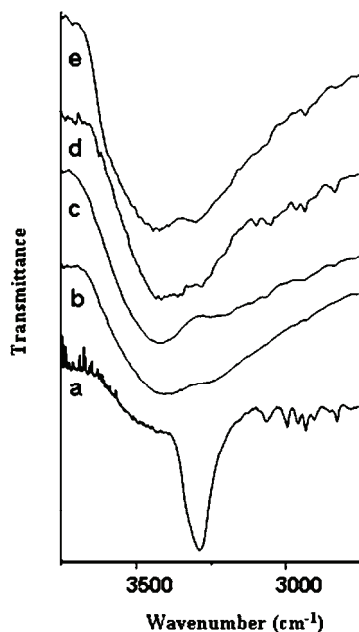


Fig. 3. FT-IR spectra of HL₁ and its complexes in the 3750–2750 cm⁻¹ region.

- a, HL₁;
 b, [Fe(L₁)(OH)(H₂O)₂]NO₃;
 c, [Cu(L₁)₂]·2H₂O; d, [Ag(L₁)];
 e, [Zn(L₁)(H₂O)₂]NO₃.

NMR spectra

The ¹H- and ¹³C-NMR spectral data are given in Tables IV and V, respectively. The ligands HL₂ and HL₄ have two isomeric forms according to their ¹H-NMR spectra (Figs. 2 and 4, Table IV). The isomer structures are observed for the benzimidazole protons only. The OH and NH protons show only a broad single band in the spectra of HL₁. This observation results from strong hydrogen bonding between the imine nitrogen with a double bond and the phenolic hydrogen atoms (Fig. 2).^{35,36} The other ligands, HL₂, HL₃ and HL₄ give two broad bands for the OH and NH protons, probably because of the 5-position substitutions (Fig. 4). This means that these ligands have weaker hydrogen bonding than HL₁ in DMSO-*d*₆.

In the ¹H-NMR spectra of the Ag(I) and Zn(II) complexes, considerable changes are observed. The broad signal in the ¹H-NMR spectrum of HL₁ at 13.15 ppm, due to the NH and OH protons sharpens on complexation and its intensity changes to only single proton, namely the NH proton (Fig. 5). The OH proton signal is absent in the ¹H-NMR spectra of the complexes. This is evidence that the phenolic oxygen is coordinated to the metal ions and that the phenolic hydrogen is eliminated on complexation (Fig. 6).

The benzimidazole moiety protons of the Ag(I) and Zn(II) complexes show broad signals in the ¹H-NMR spectra because of the perturbing effect of the metal ion. On complexation, the acidic character of the benzimidazole moiety protons is increased.

TABLE IV. ¹H-NMR spectral data of the HL₁–HL₄ ligands, and the Ag(I) and Zn(II) complexes (in DMSO-*d*₆)

Compound	Benzimidazole protons					Phenolic protons				
	H4	H5	H6	H7	NH	H3'	H4'	H5'	OH	OCH ₃
HL ₁	7.65 <i>m</i>	7.29 <i>m</i>	7.29 <i>m</i>	7.65 <i>m</i>	13.15 <i>s, br</i>	7.65 <i>m</i>	6.95 <i>t</i> <i>J</i> ^a = 7.8, 8.3	7.08 <i>d-d</i> <i>J</i> = 8.3, 1.5	13.15 <i>s, br</i>	3.84 <i>s</i>
A ^b	7.64 <i>d</i> <i>J</i> = 7.8	7.29 <i>s, br</i>	7.29 <i>s, br</i>	7.64 <i>d</i> <i>J</i> = 7.8	13.16 <i>s, br</i>	7.10 <i>d</i> <i>J</i> = 8.2	6.96 <i>t</i> <i>J</i> = 8.2, 7.8	7.10 <i>d</i> <i>J</i> = 8.2	–	3.84 <i>s</i>
B ^c	8.73 <i>s</i>	7.22 <i>s, br</i>	7.22 <i>s, br</i>	7.98 <i>s, br</i>	13.49 <i>s, br</i>	7.61 <i>s</i>	7.30 <i>d, br</i> <i>J</i> = 7.3	7.56 <i>d</i> <i>J</i> = 7.3	–	3.85 <i>s</i>
HL ₂ , Isomer A (54 %)	7.48 <i>d</i> <i>J</i> = 7.8	7.12 <i>d</i> <i>J</i> = 7.8	2.46 ^d <i>s</i>	7.52 <i>s</i>	13.30 <i>s, br</i>	7.61 <i>d</i> <i>J</i> = 7.8	6.94 <i>t</i> <i>J</i> = 7.8, 8.3	7.08 <i>m</i>	13.04 <i>s, br</i>	3.83 <i>s</i>
HL ₂ , Isomer B (46 %)	7.38 <i>s</i>	2.43 ^d <i>s</i>	7.08 <i>m</i>	7.59 <i>d, br</i> <i>J</i> = 6.8	13.34 <i>s, br</i>	7.61 <i>d</i> <i>J</i> = 7.8	6.94 <i>t</i> <i>J</i> = 7.8, 8.3	7.08 <i>m</i>	13.07 <i>s, br</i>	3.83 <i>s</i>
HL ₃	7.68 <i>s, br</i>	–	7.66 <i>d, br</i>	7.30 <i>d-d</i> <i>J</i> = 8.3, 1.9	13.26 <i>s, br</i>	7.63 <i>d-d</i> <i>J</i> = 7.8, 1.5	6.97 <i>t</i> <i>J</i> = 7.8, 7.8	7.11 <i>d-d</i> <i>J</i> = 7.8, 1.5	12.88 <i>s, br</i>	3.84 <i>s</i>
HL ₄ , Isomer A (60 %)	7.79 <i>s, br</i>	8.17 <i>s, br</i>	–	8.45 <i>s, br</i>	13.63 <i>s, br</i>	7.68 <i>d</i> <i>J</i> = 7.4	7.00 <i>t</i> <i>J</i> = 7.8, 7.8	7.16 <i>d</i> <i>J</i> = 7.8	12.40 <i>s, br</i>	3.86 <i>s</i>
HL ₄ , Isomer B (40 %)	8.61 <i>s, br</i>	–	8.17 <i>s, br</i>	7.87 <i>s, br</i>	13.56 <i>s, br</i>	7.68 <i>d</i> <i>J</i> = 7.4	7.00 <i>t</i> <i>J</i> = 7.8, 7.8	7.16 <i>d</i> <i>J</i> = 7.8	12.29 <i>s, br</i>	3.86 <i>s</i>

^aIn Hz; ^b[Ag(L₁)]; ^c[Zn(L₁)(H₂O)₂]NO₃; ^d3H (CH₃)

TABLE V. ¹³C-NMR spectral data of HL₁ and its Ag(II) and Zn(II) complexes

Compound	Chemical shift in DMSO- <i>d</i> ₆ (δ _C / ppm)
HL ₁	152.64, 149.30, 149.09, 124.62, 119.39, 118.35, 114.69, 113.24, 56.45
[Ag(L ₁)]	152.95, 149.05, 148.85, 124.30, 119.20, 118.50, 114.20, 113.40, 56.35
[Zn(L ₁)(H ₂ O) ₂]NO ₃	155.70, 148.60, 148.10, 124.20, 122.40, 120.75, 115.50, 114.12, 57.85

In the ¹³C-NMR spectra of HL₁ and its Ag(I) and Zn(II) complexes, the signal around 152.64, 152.95 and 155.70 ppm, respectively, belongs to the imidazole C=N (C-2) carbon atom. The low ppm signal, 56.45, 56.35 and 57.85 ppm, respectively, is due to the methoxy carbon atom in HL₁ and its Ag(I) and Zn(II) complexes. The signals around 149 ppm are due to C-8, C-9, C-2', C-1' carbon atoms of the HL₁ ligand and the complexes. The other signals belong to the benzimidazole benzene and phenol ring carbon atoms (Table V).

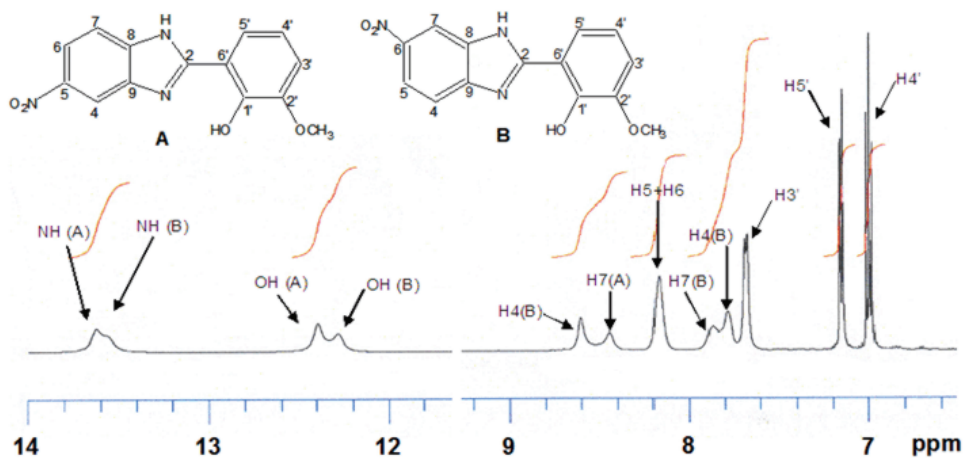


Fig. 4. ¹H-NMR spectra of the HL₄ isomers (A and B) in the 6.5–14 ppm region.

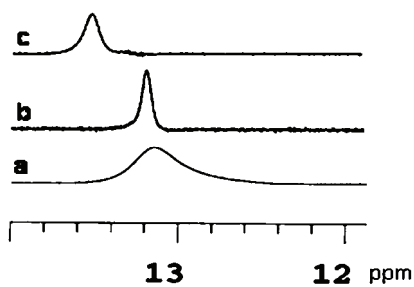


Fig. 5. ¹H-NMR spectra of HL₁ and its Ag(I) and Zn(II) complexes in the 12–14 ppm region. a, HL₁; b, [Ag(L₁)]; c, [Zn(L₁)(H₂O)₂]NO₃.

In conclusion, the optimized structures for the complexes presented in Fig. 6 are in best accord with the experimental data obtained from the analytical data, molar conductivity, magnetic moments, FT-IR and NMR spectroscopic measurements.

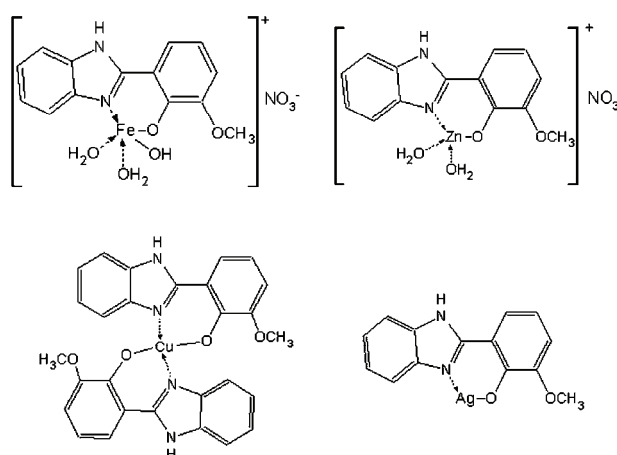


Fig. 6. Schematic view of the proposal structures of the studied complexes.

Antibacterial activity

The results concerning the *in vitro* antibacterial activity of the ligand and their complexes, together with the inhibition zone (mm) and *MIC* values, are presented in Tables VI and VII.

TABLE VI. *In vitro* antimicrobial activity of the compounds (inhibition zone, mm)

Compound	Microorganisms ^a								
	1	2	3	4	5	6	7	8	9
HL ₁	– ^b	–	–	–	–	8	–	–	8
HL ₁ ·HCl	–	–	–	–	–	8	–	–	–
HL ₃	14	–	–	–	–	–	10	8	–
HL ₃ ·HCl	12	–	–	–	–	–	–	–	–
HL ₄	14	–	–	–	–	–	–	–	–
[Fe(L ₁)(OH)(H ₂ O) ₂]NO ₃	14	–	>20	–	–	–	–	–	–
[Cu(L ₁) ₂]·2H ₂ O	–	–	–	–	–	–	8	8	–
[Ag(L ₁)]	10	–	10	–	12	–	12	8	–
[Zn(L ₁)(H ₂ O) ₂]NO ₃	–	–	–	–	8	–	8	10	10
Fe(NO ₃) ₃ ·9H ₂ O	–	–	–	–	7	–	–	–	–
Cu(NO ₃) ₂ ·3H ₂ O	10	7	7	7	–	7	7	10	12
AgNO ₃	–	–	10	–	10	–	–	8	8
Zn(NO ₃) ₂ ·6H ₂ O	–	12	7	–	10	7	–	12	16

^a1 – *P. aeruginosa*, 2 – *S. enteritidis*, 3 – *E. coli*, 4 – *P. mirabilis*, 5 – *K. pneumoniae*, 6 – *B. cereus*, 7 – *S. epidermidis*, 8 – *S. aureus*, 9 – *B. subtilis*; ^bzone did not form

TABLE VII. *In vitro* antimicrobial activity of the compounds (*MIC* / μg ml⁻¹)

Compound	Microorganisms								
	1	2	3	4	5	6	7	8	9
HL ₁	– ^a	–	–	–	–	532	–	–	* ^b
HL ₁ ·HCl	–	–	–	–	–	532	–	–	–
HL ₃	*	–	–	–	–	–	66.5	66.5	–
HL ₃ ·HCl	*	–	–	–	–	–	–	–	–
HL ₄	532	–	–	–	–	–	–	–	–
[Fe(L ₁)(OH)(H ₂ O) ₂]NO ₃	532	–	*	–	–	–	–	–	–
[Cu(L ₁) ₂]·2H ₂ O	–	–	–	–	–	–	*	532	–
[Ag(L ₁)]	66.5	–	33.2	–	66.5	–	33.2	66.5	–
[Zn(L ₁)(H ₂ O) ₂]NO ₃	–	–	–	–	*	–	*	133	*

^aNo antibacterial activity qualitatively; ^b*MIC* value was not detected in the test concentrations (< 532 μg/ml)

The chloride substituted ligand, HL₃, and the [Ag(L₁)] and [Zn(L₁)(H₂O)₂](NO₃) complexes exhibit moderate antibacterial activity. Of all the compounds tested, the ligands and some complexes show antibacterial activity against Gram-positive bacteria. As an example, the inhibition zone and *MIC* values of HL₁, HL₃, [Cu(L₁)₂]·2H₂O and [Zn(L₁)(H₂O)₂]NO₃ for the *B. cereus*, *S. epidermidis*, *S.*

aureus and *B. subtilis* (Gram+) organisms are exceptionally effective compared with the other compounds (Tables VI and VII, microorganisms 6–9).

A noteworthy result is that the Cu(II), Zn(II) and Ag(I) complexes show antibacterial activity toward *S. epidermidis* and *S. aureus* while the HL₁ ligand has no activity on them. On the other hand, it was observed that AgNO₃ has no activity on *P. aeruginosa* and *S. epidermidis*; however the [Ag(L₁)] complex has considerable antibacterial activity toward these two bacteria. The Fe(III) complex exhibited antibacterial activity against *P. aeruginosa* and *E. coli* while Fe(NO₃)₃·9H₂O itself did not show any antibacterial effect on them.

Acknowledgement. This work was supported by Istanbul University Research Fund, Project number: 262/23082004.

ИЗВОД

ДОБИЈАЊЕ, КАРАКТЕРИЗАЦИЈА И АНТИБАКТЕРИЈСКИ ЕФЕКАТ
2-МЕТОКСИ-6(5-Н/МЕ/СЛ/НО₂-1Н-БЕНЗИМИДАЗОЛ-2-ИЛ)-ФЕНОЛА
И КОМПЛЕКСА НЕКИХ ПРЕЛАЗНИХ МЕТАЛА

AYDIN TAVMAN¹, SERKAN IKIZ², A. FUNDA BAGCIGIL², N. YAKUT ÖZGÜR² и SEYYAL AK²

¹Istanbul University, Faculty of Engineering, Department of Chemistry, 34320 Avcilar, Istanbul u ²Istanbul University, Veterinary Faculty, Department of Microbiology, 34320 Avcilar, Istanbul, Turkey

Добијени су и окарактерисани 2-метокси-6-(5-Н/метил/хлоро/нитро-1Н-бензимидазол-2-ил)-фенолни (HL_x; x = 1–4, редом) лиганди и HL₁ комплекси са Fe(NO₃)₃, Cu(NO₃)₂, AgNO₃, Zn(NO₃)₂. Структуре комплекса су потврђене на основу елементалне анализе, моларне проводљивости, магнетног момента, FT-IR, ¹H- и ¹³C-NMR. Антибактеријаска активност слободних лиганата, њихових хидрохлоридних соли и комплекса је проверена коришћењем диск дифузионе методе у диметил-сулфоксиду (DMSO) као и минимална инхибиторска концентрација (MIC) методом разблажења, према 9 сојева бактерија. HL₁, HL₃, Cu(II) и Zn(II) комплекси показују антибактеријску активност према Грам-позитивним бактеријама.

(Примљено 10. јуна, ревидирано 28. новембра 2008)

REFERENCES

1. V. Klimesova, J. Koci, K. Waisser, J. Kaustova, *Farmaco* **57** (2002) 259
2. N. M. Agh-Atabay, B. Dülger, F. Gücin, *Eur. J. Med. Chem.* **38** (2003) 875
3. F. Gümüş, O. Algül, G. Eren, H. Eroglu, N. Diril, S. Gür, A. Özkul, *Eur. J. Med. Chem.* **38** (2003) 473
4. H. Göker, M. Tuncbilek, G. Ayhan, N. Altanlar, *Farmaco* **53** (1998) 415
5. S. Saluja, R. Zou, J. C. Drach, L. B. Townsend, *J. Med. Chem.* **39** (1996) 881
6. R. Zou, K. R. Ayres, J. C. Drach, L. B. Townsend, *J. Med. Chem.* **39** (1996) 3477
7. A. S. Demir, H. Hamamci, O. Sesenoglu, R. Neslihanoglu, B. Asikoglu, D. Capanoglu, *Tetrahedron Lett.* **43** (2002) 6447
8. C. Delescluse, M. P. Piechock, N. Ledirac, R. H. Hines, R. Li, X. Gidrol, R. Rahmani, *Biochem. Pharmacol.* **61** (2001) 399
9. K. K. Monthilal, C. Karunakaran, A. Rajendran, R. Murugesan, *J. Inorg. Biochem.* **98** (2004) 322

10. C. S. P. Sastry, P. Y. Naidu, S. S. N. Murty, *Talanta* **44** (1997) 1211
11. E. J. Cardoso, A. F. Luna, J. P. Urizar, *Acta Tropica* **92** (2004) 237
12. M. Savlik, P. Polaskova, B. Szotakova, J. Lamka, L. Skalova, *Res. Vet. Sci.* **79** (2005) 139
13. R. G. Almeida, J. C. Florio, H. S. Spinosa, M. M. Bernardi, *Neurotoxicol. Teratol.* **24** (2002) 255
14. J. Gronvold, T. S. Svendsen, H. O. Kraglund, J. Bresciani, J. Monrad, *Vet. Parasitol.* **124** (2004) 91
15. A. Tavman, N. M. Agh-Atabay, S. Güner, F. Gücin, B. Dülger, *Transition Met. Chem.* **32** (2007) 172
16. P. G. Ramappa, K. G. Somasekharappa, *J. Inorg. Biochem.* **55** (1994) 13
17. A. Tavman, N. M. Agh-Atabay, A. Neshat, F. Gücin, B. Dülger, D. Hacıu, *Transition Met. Chem.* **31** (2006) 194
18. Q. Zhou, P. Yang, *Inorg. Chim. Acta* **359** (2006) 1200
19. W. W. Porterfield, *Inorganic Chemistry, A Unified Approach*, 2nd Ed., Academic Press, New York, 1993
20. a) A. Tavman, B. Ulküseven, *Main Group Met. Chem.* **24** (2001) 211; b) B. Ulküseven, A. Tavman, G. Otük, S. Birteksöz, *Folia Microbiol.* **47** (2002) 481
21. H. F. Ridley, G. W. Spickett, G. M. Timmis, *J. Heterocycl. Chem.* **2** (1965) 453
22. *NCCLS Performance Standards for Antimicrobial Disk Susceptibility Tests*, 6th Ed., Approved Standard, NCCLS Document M2-A6, NCCLS, Wayne, PA, 1997
23. *NCCLS Methods for Dilution Antimicrobial Susceptibility Tests for Bacteria That Grow Aerobically*, 5th Ed., Approved Standard, NCCLS Document M7-A5 NCCLS, Wayne, PA, 2000
24. T. A. Khan, S. Naseem, Y. Azim, S. Parveen, M. Shakir, *Transition Met. Chem.* **32** (2007) 706
25. W. J. Geary, *Coord. Chem. Rev.* **7** (1971) 81
26. S. Chandra, Sangeetika, S. D. Sharma, *Spectrochim. Acta* **A49** (2003) 755
27. S. Padhye, G. B. Kauffman, *Coord. Chem. Rev.* **63** (1985) 127
28. D. Y. Kong, Y. Y. Xie, *Polyhedron* **19** (2000) 1527
29. M. M. Abd-Elzaher, *Appl. Organomet. Chem.* **18** (2004) 149
30. A. B. P. Lever, *Inorganic Electronic Spectroscopy*, Elsevier, Amsterdam, 1984
31. D. Kanamori, Y. Yamada, A. Onoda, T. A. Okamura, S. Adachi, H. Yamamoto, N. Ueyama, *Inorg. Chim. Acta* **358** (2005) 331
32. N. Ueyama, N. Nishikawa, Y. Yamada, T. Okamura, A. Nakamura, *Inorg. Chim. Acta* **283** (1998) 91
33. V. M. Leovac, L. S. Jovanović, V. S. Cesljević, L. J. Bjelica, V. B. Arion, N. V. Gerbeleu, *Polyhedron* **13** (1994) 3005
34. K. Nakamoto, *Infrared and Raman Spectra of Inorganic and Coordination Compounds*, Part B, 5th Ed., Wiley, New York, 1997, p. 87
35. A. Tavman, *Spectrochim. Acta* **A63** (2006) 343
36. F. R. Prieto, J. C. Penedo, M. Mosquera, *J. Chem. Soc. Faraday Trans.* **94** (1998) 2775.



J. Serb. Chem. Soc. 74 (5) 549–554 (2009)
JSCS–3854

Verifying the PCP-rule by five-center bond indices

JELENA ĐURĐEVIĆ¹, IVAN GUTMAN^{1*#} and ROBERT PONEC^{2**}

¹Faculty of Science, University of Kragujevac, P.O. Box 60, 34000 Kragujevac, Serbia and

²Institute of Chemical Process Fundamentals, Czech Academy of Sciences,
Prague 6, Suchbátarova 165 02, Czech Republic

(Received 21 November 2008)

Abstract: According to the recently discovered PCP-rule, the (stabilizing) energy-effect of the cyclic conjugation in the 5-membered ring of acenaphthylene- and fluoranthene-type polycyclic conjugated hydrocarbons increases with the number of phenyl–cyclopentadienyl (PCP) fragments present in the molecule. It is now shown that the validity of the PCP-rule is also supported by the 5-center bond indices, an independent quantitative theoretical measure of cyclic conjugation in 5-membered rings.

Keywords: acenaphthylene-type hydrocarbons; fluoranthene-type hydrocarbons; PCP-rule; multicenter bond index; cyclic conjugation.

INTRODUCTION

The theory of benzenoid hydrocarbons^{1,2} is nowadays one of the best developed areas of theoretical organic chemistry. Motivated by recent progress in this field (see the papers^{3–7} and the references quoted therein), a systematic study^{8–10} of a class of polycyclic conjugated systems closely related to benzenoid hydrocarbons, the acenaphthylenes and fluoranthenes, was undertaken. These differ from “true” benzenoids by possessing a five-membered ring; for examples see Fig. 1. A more formal definition of acenaphthylenes and fluoranthenes can be found in the literature.⁸

The PCP-rule

According to classical theories of benzenoid and similar polycyclic conjugated molecules,^{1,2} there is no cyclic conjugation in the 5-membered ring of acenaphthylenes and fluoranthenes. Investigating the energy-effect of cyclic conjugation using the method described in detail in a review¹¹ and elsewhere,^{3,7} it was found that a weak cyclic conjugation exists in the 5-membered ring of acena-

* Corresponding author. E-mail: gutman@kg.ac.rs; **ponec@icpf.cas.cz

Serbian Chemical Society member.

doi: 10.2298/JSC0905549D



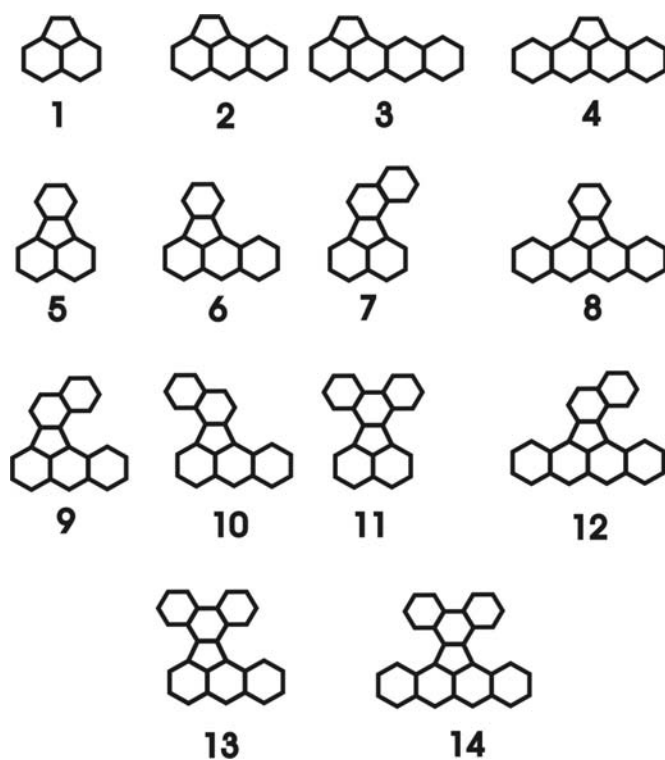


Fig. 1. Acenaphthylene (**1**) and some of its congeners (**2–4**), and fluoranthene (**5**) and some of its congeners (**6–14**). Data on the cyclic conjugation in the 5-membered ring of these compounds are given in Table I.

TABLE I. The number of PCP fragments ($\#PCP$), the five-center bond index ($5-CBI$) of the five-membered rings and the energy-effect (ef , in β -units) of the same rings of the acenaphthylenes and fluoranthenes depicted in Fig. 1

Compound	$\#PCP$	$5-CBI$	ef
1	0	0.5250	0.0026
2	1	0.6124	0.0206
3	1	0.6394	0.0255
4	2	0.7281	0.0390
5	0	0.2685	0.0031
6	1	0.3062	0.0054
7	1	0.3096	0.0043
8	2	0.3566	0.0105
9	2	0.3559	0.0079
10	2	0.3558	0.0080
11	2	0.3457	0.0056
12	3	0.4181	0.0159
13	3	0.3994	0.0105
14	4	0.4716	0.0211

phthylenes and fluoranthenes. In addition, it was established¹⁰ that this (weak) cyclic conjugation effect is amplified by the presence of 6-membered rings connected to the 5-membered ring by a single carbon–carbon bond. This effect was named the PCP-rule, where PCP is the abbreviation for “Phenyl-CycloPentadienyl”. According to the PCP-rule, the extent of the energy-effect due to cyclic conjugation in the 5-membered ring is proportional to the number of PCP fragments present in the respective acenaphthylene and fluoranthene. These PCP fragments are indicated for two selected examples in Fig. 2.

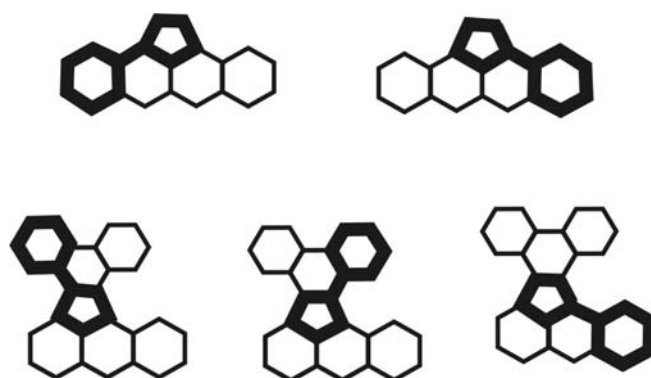


Fig. 2. The compounds **4** and **13** from Fig. 1 have two and three PCP fragments, respectively; these are indicated by thick lines.

A simple example illustrating the validity of the PCP-rule is provided by the two isomeric acenaphthylenes **3** and **4**. Whereas **3** has one PCP fragment, its isomer **4** has two PCP fragments. The energy-effects of their 5-membered rings are 0.0255 and 0.0390 β -units, respectively. Further examples are found in Table I. It should be noted that until now not a single violation of the PCP-rule has been observed.¹⁰

In view of the fact that the PCP-rule was established by studying the energy-effects of the 5-membered rings, it was thought purposeful to check it by other measures of cyclic conjugation. In this paper, the PCP-rule was tested by means of multicenter bond indices.

Multicenter bond indices

Multicenter bond indices are quantities specifically designed to detect and quantify the presence of delocalized multicenter bonding in molecules such as non-classical carbocations, electron deficient boranes, lithiated hydrocarbons, *etc.* The respective theory was developed in the 1990s^{12–18} and was then successfully applied to a variety of types of molecules.^{19–23} In view of the capability of these indices to describe non-classical three-center bonding, the idea of the multicenter bond index was recently generalized so as to be also applicable for the description of cyclically conjugated bonding extended over any number of

centers. In the general case of k -center bonding, the corresponding index was defined as the permutation-unique k -center term resulting from the partitioning of the total number (N) of electrons:

$$N = \frac{\text{Tr}(PS)^{\{k\}}}{2^{k-1}} = \sum_A \Delta_A^{(k)} + \sum_{A<B} \Delta_{AB}^{(k)} + \sum_{A<B<C} \Delta_{ABC}^{(k)} + \cdots + \sum_{A<B<C<\cdots<K} \Delta_{ABC\dots K}^{(k)}$$

where P is the charge/bond-order matrix and S the overlap matrix. In this work, the 5-center bonding index (5-CBI), pertaining to the five carbon atoms (labeled by A, B, C, D and E) of the 5-membered ring in the acenaphthylene and fluoranthene species, was employed. This index, characterizing the extent of the cyclic conjugation within the particular 5-membered ring, is defined as:

$$\begin{aligned} 5\text{-CBI} &= 2^4 \Delta_{ABCDE}^{(5)} = \\ &= \sum_{\mu \in A} \sum_{\nu \in B} \sum_{\lambda \in C} \sum_{\kappa \in D} \sum_{\xi \in E} \sum_i \Gamma_i [(PS)_{\mu\nu} (PS)_{\nu\lambda} (PS)_{\lambda\kappa} (PS)_{\kappa\xi} (PS)_{\xi\mu}] \end{aligned}$$

where $\mu, \nu, \lambda, \kappa, \xi$ refer to the basic functions and Γ is the permutation operator that takes into account all possible ($= 5!$) permutations of the atomic labels. For the sake of straightforward comparability with ef -values, which are calculated using a generalized version of the Coulson formula¹¹ at the level of the simple HMO theory, the calculation of 5-center bond indices was also performed at the same level. Within such an approach, the overlap matrix is a unit matrix and the formula reduces to:

$$\begin{aligned} 5\text{-CBI} &= 2^4 \Delta_{ABCDE}^{(5)} = \\ &= \sum_{\mu \in A} \sum_{\nu \in B} \sum_{\lambda \in C} \sum_{\kappa \in D} \sum_{\xi \in E} \sum_i \Gamma_i [P_{\mu\nu} P_{\nu\lambda} P_{\lambda\kappa} P_{\kappa\xi} P_{\xi\mu}] \end{aligned}$$

NUMERICAL WORK

The 5-CBI -values were computed for the 5-membered rings of all acenaphthylenes and fluoranthenes depicted in Fig. 1. These data, together with the (earlier studied¹⁰) energy-effects, are given in Table 1.

An inspection of the 5-CBI -data from Table I reveals that these perfectly agree with the PCP-rule. For understandable reasons, the acenaphthylenes have to be considered separately from the fluoranthenes. Within each of these two classes, when the counts of PCP fragments are equal, then the respective 5-CBI -values are nearly the same. When a molecule X has greater number of PCP fragments than another molecule Y , then, without a single exception, $5\text{-CBI}(X) > 5\text{-CBI}(Y)$. For instance, for the isomers **3** and **4** (possessing, respectively, one

and two PCP fragments), $5-CBI(\mathbf{3}) = 0.64$ and $5-CBI(\mathbf{4}) = 0.73$. Among the fluoranthenes shown in Fig. 1, the minimum and maximum $5-CBI$ have, respectively, fluoranthene ($\mathbf{5}$, no PCP fragment) and tetrabenzofluoranthene ($\mathbf{25}$, four PCP fragments); $5-CBI(\mathbf{5}) = 0.27$, $5-CBI(\mathbf{25}) = 0.47$. For more examples of this kind, see Table I.

CONCLUSIONS

The PCP-rule is a peculiar property of acenaphthylenes and fluoranthenes, having no counterpart in the classical theory of polycyclic conjugated molecules. It was discovered by studying the energy-effects of the 5-membered rings contained in these molecules.¹⁰ The obvious question that emerged at this point was whether the PCP-rule is an artifact of the graph-theory-based method used for computing the energy-effects or if the PCP-rule reflects some real feature of the π -electron distribution in the respective molecules. The analysis performed by employing a completely independent approach, based on multicenter bond indices, clearly indicates that the latter might be the case.

A reasonably good linear correlation between the five-center indices and the energy-effects of the five-membered rings exists, as seen in Fig. 3. Of course, the data-points for acenaphthylenes and fluoranthenes lie on two different lines. This implies that not only is the PCP-rule convincingly corroborated by multicenter bond indices, but also so is the molecular-structure dependence of the extent of cyclic conjugation, predicted by two different methods, in quantitative agreement.

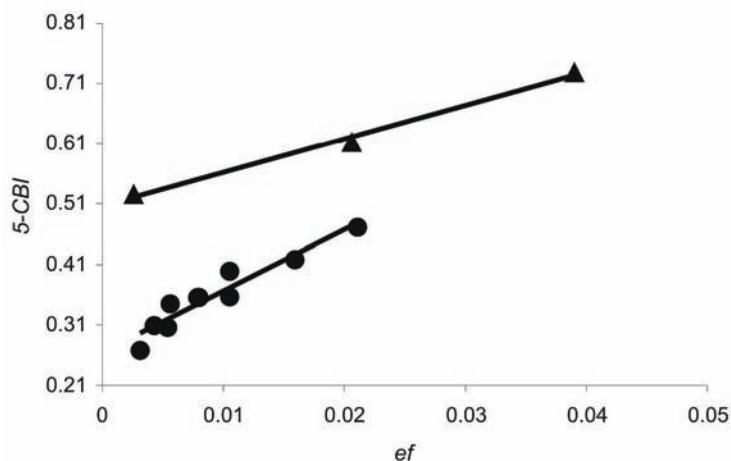


Fig. 3. The five-center bond indices ($5-CBI$) vs. the energy-effects (ef) for the acenaphthylenes (triangles) and fluoranthenes (circles) depicted in Fig. 1.

The quantum-chemical origin of the PCP-rule remains obscure, but the real existence of such a rule seems to be now additionally verified.

Acknowledgements. J. Đ. and I. G. thank the Serbian Ministry of Science and Technological Development for partial support of this work, through Grant no. 144015G. R. P. acknowledges the support of the Grant Agency of the Czech Academy of Sciences, Grant no. IAA 4072403.

ИЗВОД

ПРОВЕРА РСР-ПРАВИЛА ПОМОЋУ ПЕТОЦЕНТРИЧНИХ ИНДЕКСА ВЕЗЕ

ЈЕЛЕНА ЂУРЂЕВИЋ¹, ИВАН ГУТМАН¹ и ROBERT PONEC²

¹Природно–математички факултет Универзитета у Краљеву и ²Institute of Chemical Process Fundamentals, Czech Academy of Sciences, Prague 6, Suchbát, 165 02, Czech Republic

На основу недавно откривеног РСР-правила, (стабилизујући) енергетски ефекат цикличне конјугације у петочланом прстену полицикличних конјугованих угљоводоника аце-нафтиленског и флуорантенског типа расте са бројем фенил-циклопентаденилних (РСР) фрагмената садржаних у молекулу. У раду показујемо да је важење РСР-правила потврђено и помоћу петоцентричних индекса везе, који су једно независно теоријско квантитативно мерило цикличне коњугације у петочланим прстеновима.

(Примљено 21. новембра 2008)

REFERENCES

1. I. Gutman, S. J. Cyvin, *Introduction to the Theory of Benzenoid Hydrocarbons*, Springer-Verlag, Berlin, 1989
2. M. Randić, *Chem. Rev.* **103** (2003) 3449
3. I. Gutman, S. Stanković, J. Đurđević, B. Furtula, *J. Chem. Inf. Model.* **47** (2007) 776
4. I. Gutman, B. Furtula, R. Kovačević, *J. Serb. Chem. Soc.* **72** (2007) 663
5. S. Gojak, I. Gutman, S. Radenković, A. Vodopivec, *J. Serb. Chem. Soc.* **72** (2007) 673
6. S. Stanković, J. Đurđević, I. Gutman, R. Milentijević, *J. Serb. Chem. Soc.* **73** (2008) 547
7. I. Gutman, S. Stanković, *Monatsh. Chem.* **139** (2008) 1179
8. I. Gutman, J. Đurđević, *MATCH Commun. Math. Comput. Chem.* **60** (2008) 659
9. J. Đurđević, S. Radenković, I. Gutman, *J. Serb. Chem. Soc.* **73** (2008) 898
10. I. Gutman, J. Đurđević, A. T. Balaban, *Polyc. Arom. Comp.* **29** (2009) 3
11. I. Gutman, *Monatsh. Chem.* **136** (2005) 1055
12. M. Giambiagi, M. S. Giambiagi, K. C. Mundim, *Struct. Chem.* **1** (1990) 423
13. A. B. Sannigrahi, T. Kar, *Chem. Phys. Lett.* **173** (1990) 569
14. K. C. Mundim, M. Giambiagi, M. S. Giambiagi, *J. Phys. Chem.* **98** (1994) 6118
15. R. Ponec, F. Uhlík, *Croat. Chim. Acta* **69** (1996) 941
16. R. Ponec, I. Mayer, *J. Phys. Chem.* **A101** (1997) 1738
17. A. B. Sannigrahi, T. Kar, *J. Mol. Struct. (Theochem.)* **496** (2000) 1
18. R. Ponec, D. L. Cooper, *Int. J. Quantum Chem.* **97** (2004) 1002
19. R. Ponec, G. Yuzhakov, D. J. Tantillo, *J. Org. Chem.* **69** (2004) 2992
20. P. Bultinck, R. Ponec, S. van Damme, *J. Phys. Org. Chem.* **18** (2005) 706
21. R. Ponec, P. Bultinck, A. Gallegos, *J. Phys. Chem.* **A109** (2005) 6606
22. R. Ponec, P. Bultinck, P. Gutta, D. J. Tantillo, *J. Phys. Chem.* **A110** (2006) 3785
23. R. Ponec, S. Fias, S. Van Damme, P. Bultinck, I. Gutman, S. Stanković, *Coll. Czechoslovak Chem. Commun.* **74** (2009) 147.



J. Serb. Chem. Soc. 74 (5) 555–571 (2009)
JSCS–3855

Journal of
the Serbian
Chemical Society

JSCS@tmf.bg.ac.rs • www.shd.org.rs/JSCS

UDC 547.564.4:77+547.821+547.46+547.828+
547.586.71:535.338+535.513

Original scientific paper

Theoretical and experimental investigations on the structure and vibrational spectra of 6-amino-3-methyl-1-phenyl-1*H*-pyrazolo[3,4-*b*]pyridine-5-carboxylic acid and 6,7-dihydro-3-methyl-6-oxo-1-phenyl-1*H*-pyrazolo[3,4-*b*]pyridine-5-carbonitrile

KHALED BAHGAT^{1*}, NAZM AL-DEN JASEM² and TALAAT EL-EMARY³

¹Chemistry Department, Faculty of Petroleum and Mining Engineering, Suez Canal University, Suez, Egypt, ²Chemistry Department, Faculty of Sciences, Aleppo University, Syria and ³Chemistry Department, Faculty of Science, Assiut University, Assiut, Egypt

(Received 22 October 2008, revised 12 February 2009)

Abstract: The solid phase FT-IR and FT-Raman spectra of 6-amino-3-methyl-1-phenyl-1*H*-pyrazolo[3,4-*b*]pyridine-5-carboxylic acid (PYRPCA) and 6,7-dihydro-3-methyl-6-oxo-1-phenyl-1*H*-pyrazolo[3,4-*b*]pyridine-5-carbonitrile (PYRPCN) were recorded in the region 4000–400 cm⁻¹. The spectra were interpreted with the aid of normal coordinate analysis following full structure optimization and force field calculations based on the density functional theory (DFT) using standard B3LYP, BLYP and *ab initio* RHF methods with 6-31G* basis set and were scaled using a recommended set of scaling factors yielding fairly good agreement between the observed and calculated frequencies. Based on the present good quality, the scaled quantum mechanical (SQM) force field, a reliable description of the fundamentals of PYRPCA and PYRPCN, was provided. The calculations predicated a predominance of different tautomers in PYRPCA and keto-enol tautomers in PYRPCN. For PYRPCA, the most stable conformer is stabilized by intramolecular hydrogen bonding. The characteristic of the hydrogen bonding is its strengthening effect on the conjugation of the NH₂ and COOH groups with the pyridine ring.

Keywords: DFT calculations; vibrational spectra; 6-amino-3-methyl-1-phenyl-1*H*-pyrazolo[3,4-*b*]pyridine-5-carboxylic acid; 6,7-dihydro-3-methyl-6-oxo-1-phenyl-1*H*-pyrazolo[3,4-*b*]pyridine-5-carbonitrile.

INTRODUCTION

In the past two decades, quantum chemical computational methods have proven themselves to be essential tools for interpreting and predicting vibrational spectra.^{1,2} A significant advance in this area was made by combining empirical and *ab initio* information in the scaled quantum mechanical (SQM) force field me-

*Corresponding author. E-mail: khabahgat1@hotmail.com
doi: 10.2298/JSC0905555B



thod.³⁻⁷ In the SQM method, the computed harmonic force field is improved usually by a few scale factors, obtained by fitting theoretical vibrational frequencies to experimental data. These scale factors were generally found to be well transferable between chemically related molecules, nibbling to obtain reliable vibrational information for a large variety of organic compounds.⁸⁻¹² For organic molecules containing a hydrogen bonded system, the scaled B3LYP/6-31G* force field, using unscaled factors recommended by Rauhat and Pulay for large scale studies,⁸ also provided a proper description of the vibrational properties of these molecules. However, few publications are devoted to the chemistry of pyrazolo pyridines derivatives.¹³ The UV absorption spectra for several bis-pyrazolopyridine derivatives were provided using the TDDFT method.¹⁴

6-Amino-3-methyl-1-phenyl-1*H*-pyrazolo[3,4-*b*]pyridine-5-carboxylic acid (PYRPCA) and 6,7-dihydro-3-methyl-6-oxo-1-phenyl-1*H*-pyrazolo[3,4-*b*]pyridine-5-carbonitrile (PYRPCN) are interesting representatives of pyrazolo pyridine derivatives. Due to conjugation with the π system of the pyridine ring and a possible intermolecular hydrogen bond formation, the carboxylic group in PYRPCA may play an important role in pyrazolo-pyridine tautomerism. Also, 6,7-dihydro-3-methyl-6-oxo-1-phenyl-1*H*-pyrazolo[3,4-*b*]pyridine-5-carbonitrile (PYRPCN) carrying an NH at the peri position to a carbonyl group is a characteristic representative of keto-enol forms with a strong HB.

The aim of the present study was to determine the structure (tautomerism and hydrogen bonding) and subsistent effect on the vibrational spectra of 6-amino-3-methyl-1-phenyl-1*H*-pyrazolo[3,4-*b*]pyridine-5-carboxylic acid (PYRPCA) and 6,7-dihydro-3-methyl-6-oxo-1-phenyl-1*H*-pyrazolo[3,4-*b*]pyridine-5-carbonitrile (PYRPCN) by the concentrated application of quantum chemical calculations and vibrational spectroscopy. Based on experimental FT-IR and FT-Raman data, a complete vibrational analysis of the molecules was performed using the Pulay DFT-based SQM method.⁴ The ground state geometries were optimized using DFT with B3LYP and BLYP and *ab initio* restricted Hartree-Fock methods with the 6-31G* basis set, and comparing the effect of simpler and more elaborate versions of scaling, while paying attention to ensuring correct band assignment. The calculated infrared and Raman spectra of the title compounds were simulated utilizing the computed dipole derivatives for IR intensities and polarizability derivatives for Raman intensities.

EXPERIMENTAL

6-Amino-3-methyl-1-phenyl-1*H*-pyrazolo[3,4-*b*]pyridine-5-carboxylic acid and 6,7-dihydro-3-methyl-6-oxo-1-phenyl-1*H*-pyrazolo[3,4-*b*]pyridine-5-carbonitrile were obtained as previously described in the literature.^{15,16}

The infrared spectra were recorded with a Nicolet Magna 750 FT-IR spectrometer equipped with a room temperature DTGS detector. The spectra of the solid (in the 4000–400 cm^{-1} spectral region) were recorded in the form of KBr pellets at a 2 cm^{-1} spectral resolution accumulating 128 scans.

The Raman spectra were measured with a Nicolet 950 FT-Raman spectrometer equipped with a liquid nitrogen cooled Ge detector. An Nd:YAG laser (1064 nm) was used for excitation at 30–150 mW output power at a spectral resolution of 4 cm⁻¹.

Computational details

The molecular geometry optimization, energy and vibrational frequency calculations were performed with the GAUSSIAN 94W software package,¹⁷ using the B3LYP functionals BLYP and RHF,^{18,19} combined with the standard 6-31G* basis set. The cartesian representation of the theoretical force constants were computed at the optimized geometry by assuming C1 point group symmetry. Scaling of the force field was performed according to the SQM procedure,^{4,8} using selective scaling in the natural internal coordinate representation.^{5,20} Transformations of the force field and subsequent normal coordinate analysis, including the least square refinement of the scaling factors, calculation of potential energy distribution (PED) and the prediction of IR and Raman intensities, were realized on a PC with the MOLVIB program (version 7.0 – G77) written by Sundius.²¹⁻²³ For the plots of the simulated IR and Raman spectra, pure Lorentzian band shapes were used with a bandwidth (FWHM) of 6 cm⁻¹. The symmetry of the molecules was also helpful in making the vibrational assignments. The symmetries of the vibrational modes were realized using the standard procedure.²⁴ The symmetry analysis for the vibrational modes of the title molecules are presented in some detail in order to describe the basis for the assignments.

RESULTS AND DISCUSSION

Tautomerization and conformation

The molecular structures of PYRPCA and PYRPCN are shown in Figs. 1 and 2, respectively. The bond lengths and bond angles determined at the DFT level of the theory for the title compounds are listed in Table I. The global minimum energy obtained by DFT structure optimization for the title compound is presented in Table II. The geometrical optimization studies of PYRPCA and PYRPCN revealed that the molecules belong to the C1 symmetry point group, in which the phenyl ring make a dihedral angle of 26.23° with the adjacent pyrazole ring. The conformational variation of PYRPCA compound involve four tautomers/conformers, due to the different substitution in position 8 and 7 of the pyridine ring (numbering as in Fig. 1), and conformational variation, evolving from H-proton transfer and the relative orientation of the amino and carbonyl groups. PYRPCN involves three tautomers, in which conformational variation evolves from keto–enol tautomerization, and constitutes an intriguing set of compounds that form strong intra-molecular hydrogen bonds. The energies for the possible tautomers/conformers of the title compounds were calculated at the 6-31G* basis sets and they are listed in Table II. The energy obtained for **Ia** and **Ib** tautomers of the studied compounds at B3LYP, BLYP and RHF at 6-31G* bases set were found to be the global minimum. The large stability of the conformers **Ia** results from a shortening of the O14··H11 (1.935 Å) contact with respect to the **IIa** conformer (2.547 Å), as well as to its non-hydrogen-bonded counterpart.

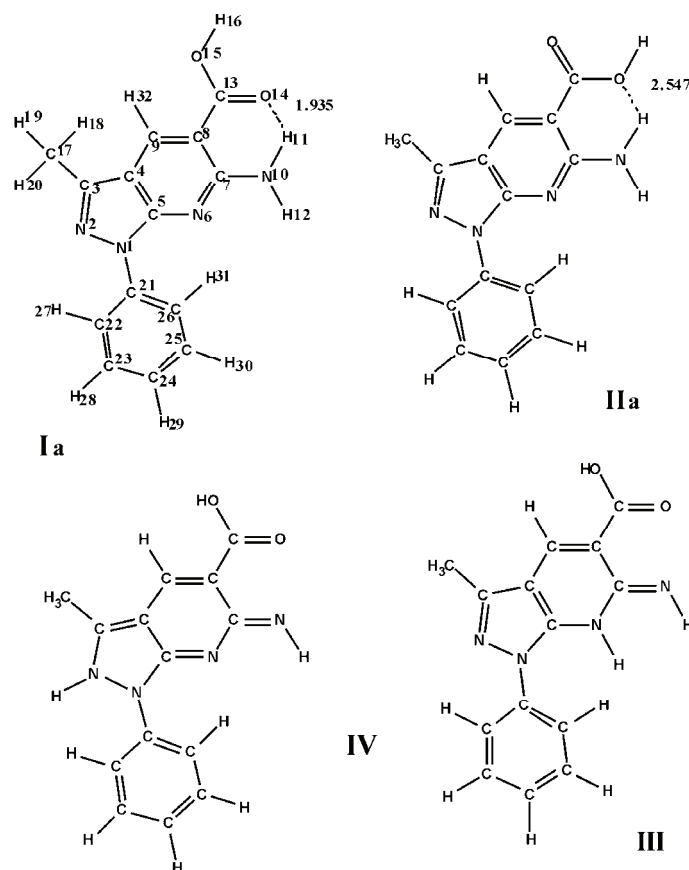


Fig. 1. The conformers considered and the numbering of the atoms in the PYRPCA molecule.

Geometric structure and hydrogen bonding

Structural analysis revealed the presence of intramolecular hydrogen bond interactions in PYRPCA and intermolecular hydrogen bond in PYRPCN. The $\text{CO}\cdots\text{NH}$ hydrogen bond in the **Ia** tautomer of PYRPCA and the $\text{N-H}\cdots\text{O}$ hydrogen bond in the **Ib** tautomer of PYRPCN are very similar in their characteristics to analogous compounds,^{25–27} in which NH_2 , NH and C=O groups participate in several inter-molecular and intra-molecular hydrogen bonds.^{28–31} The strength of the interactions can be related to the length of the hydrogen bond. The shorter $\text{O}\cdots\text{H}$ contact is in agreement with the large stability of **Ia** with respect to the non-hydrogen-bonded counterpart (*cf.* Figs. 1 and 2). The strength of hydrogen bond is also supported by the geometrical characteristics, most significant of which are the large elongation of C13-O14 and N10-H11 (in PYRPCA) and the large tilt of the NH_2 group towards the carbonyl group and rotation by 90° of the COOH group as compared to the other non-hydrogen-bonded isomers. Moreover,

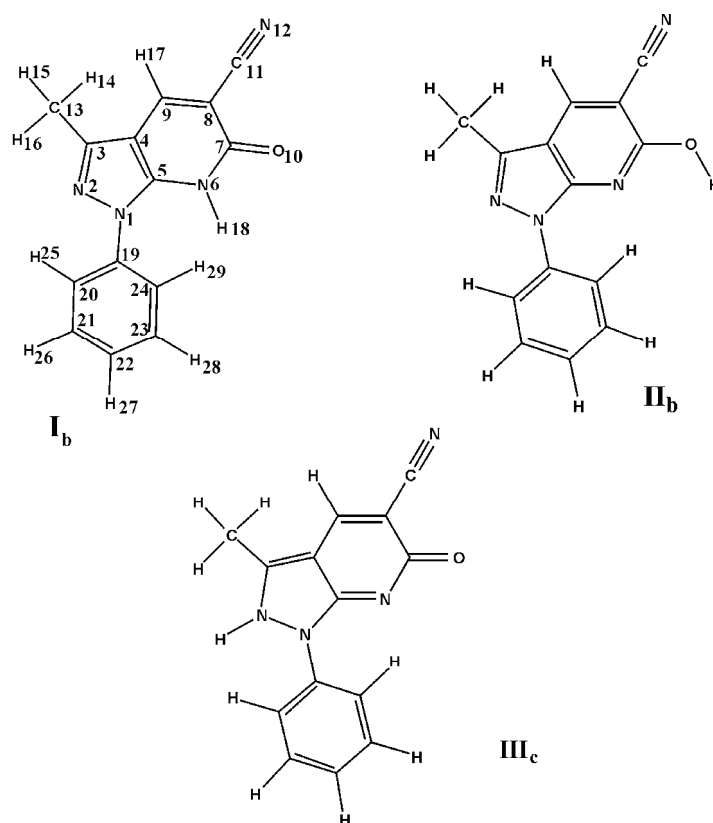


Fig. 2. The conformers considered and the numbering of the atoms of the PYRPCN molecule.

the computed C13–O14 and N10–H11 bond lengths in PYRPCA are too large compared with similar compounds.²⁵ Also, the computed C8–C13 and C7–N10 bond distances seem to be somewhat short. These geometrical parameters are sensitive to hydrogen bonding.²⁶ The hydrogen bonding interaction in **Ia** has a strong promoting effect on the conjugation of the NH₂ and COOH groups with the pyridine ring. A strengthening of the double bond character of C7–N10 and C8–C13 is indicated by a shortening of these bonds by 0.12 and 0.03 Å, respectively (*cf.* Table I). The intra-molecular hydrogen bond in PYRPCN affects the N–H and C=O bond lengths; thus in the case of the **Ib** tautomer, this lengthening amounts to 0.09 Å for the N–H and 0.04 Å for the C=O bonds, compared with similar compounds.²⁷ These changes are in agreement with the resonance character of this tautomeric system.

Vibrational spectra

The PYRPCA and PYRPCN molecules are not planar, with the phenyl ring making a dihedral angle of 26.230° with the adjacent pyrazole ring. As a result of

TABLE I. Optimized geometrical parameters of PYRPCA and PYRPCN (values for PYRPCN in parentheses); for the numbering of the atoms, see Figs. 1 and 2

Bond	Bond length, Å			Bond	Bond angle, deg.		
	B3LYP	BLYP	RHF		B3LYP	BLYP	RHF
N1-C2	1.388 (1.391)	1.408 (1.413)	1.374 (1.373)	N1-C2-C3	107.667 (106.420)	107.170 (106.040)	108.340 (106.990)
N2-C3	1.313 (1.332)	1.330 (1.330)	1.280 (1.290)	N2-C3-C4	110.437 (110.980)	110.720 (111.460)	110.060 (110.560)
C3-C4	1.433 (1.434)	1.440 (1.440)	1.430 (1.430)	C3-C4-C5	105.170 (104.240)	105.480 (104.350)	104.920 (103.750)
C4-C5	1.420 (1.380)	1.430 (1.410)	1.400 (1.370)	C4-C5-N6	126.014 (122.740)	126.150 (121.900)	125.760 (122.670)
C5-N6	1.333 (1.360)	1.340 (1.370)	1.320 (1.350)	C5-N6-C7	116.095 (122.750)	115.870 (122.900)	116.640 (122.290)
N6-C7	1.344 (1.410)	1.350 (1.430)	1.320 (1.390)	N6-C7-C8	122.965 (114.220)	123.150 (114.130)	122.780 (114.710)
C7-C8	1.449 (1.435)	1.460 (1.480)	1.440 (1.470)	C7-C8-C9	118.577 (122.400)	118.460 (122.430)	118.250 (122.110)
C8-C9	1.396 (1.380)	1.340 (1.390)	1.380 (1.350)	N10-C7-N6	116.332 (119.760)	116.210 (110.970)	115.820 (119.710)
N10-C7	1.350	1.360	1.330	C8-C7-N10	120.704	120.530	121.280
N10-H11	1.012	1.020	0.990	C7-N10-H11	119.439	118.930	121.050
N10-H12	1.008	1.010	0.990	C7-N10-H12	118.180	118.270	117.900
C13-C8	1.466	1.470	1.460	C7-C8-C13	120.678	120.560	121.310
C13-O14	1.227	1.240	1.190	C8-C13-O14	126.243	126.243	126.180
C13-O15	1.359	1.370	1.330	C8-C13-O15	113.491	113.470	113.380
O15-H16	0.974	0.980	0.950	C13-O15-H16	105.349	104.420	107.450
O14-H11	1.935	1.930	2.006	N2-C3-C17	121.008	120.490	121.690
C17-C3	1.496	1.500	1.490	N2-N1-C21	118.621	118.560	118.470
C17-H18	1.093	1.010	1.080	C24-C25-C26	121.027	121.040	121.100
C17-H19	1.097	1.010	1.080	N2-N1-C21-C22	26.32	26.41	26.89
C17-H20	1.097	1.010	1.080	N10-C7-N6-C5	179.84	179.980	180.00
C21-N1	1.421	1.430	1.410	O14-C13-C8-C9	179.48	179.960	179.980
C22-C21	1.403	1.410	1.390	O15-C13-C8-C7	179.97	179.960	179.970
C23-C22	1.392	1.400	1.380	N6-C7-O10	(119.710)	(119.400)	(119.880)
C24-C23	1.396	1.400	1.380	C7-C8-C11	(109.85)	(110.880)	(110.180)
C25-C24	1.395	1.400	1.380	N2-N1-C19-C20	(37.880)	(36.290)	(38.910)
C26-C25	1.381	1.400	1.380	N2-N1-C19-C24	(141.757)	(143.240)	(143.870)

the C1 symmetry, the 90 and 81 fundamentals for PYRPCA and PYRPCN, respectively, are active in both the infrared absorption and Raman scattering. The FT-IR and FT-Raman spectra of PYRPCA and PYRPCN molecules are shown in Figs. 3–6, respectively. The absence of definite bands in the OH stretching region of the experimental IR and Raman spectra of PYRPCN suggests that no enol tautomer is present in the solid phase of the PYRPCN molecule. The absence of this

TABLE II. Total energies (in hartrees) of PYRPCA obtained from B3LYP/6-31G* calculations

Conformers	PYRPCA	PYRPCN
I	-910.206137 ^a	-833.7311
II	-910.166388	-833.6541
III	-910.150738	-833.7132
IV	-910.111532	

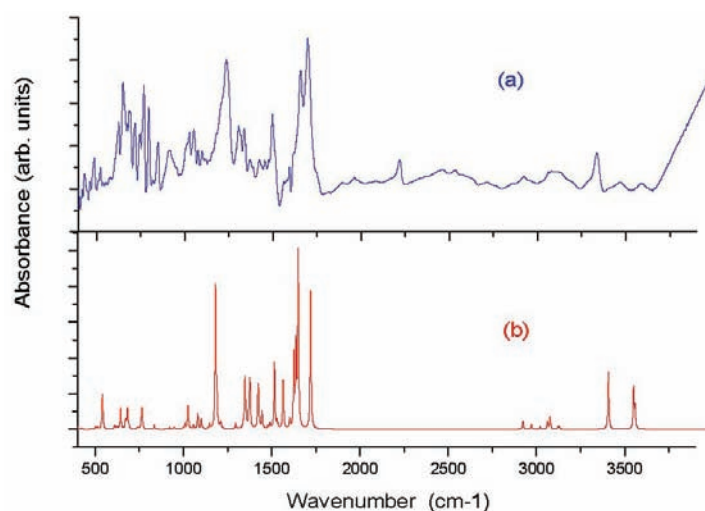
^aGlobal minimum energy

Fig. 3. FT-IR spectra of PYRPCA; a) observed, b) calculated.

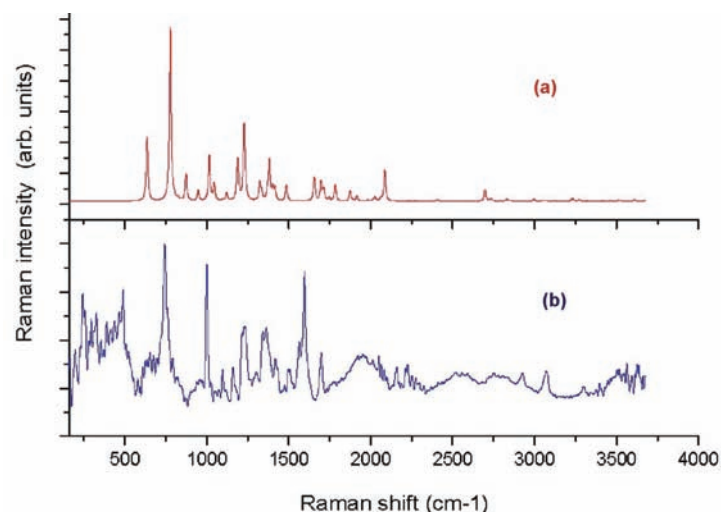


Fig. 4. FT-Raman spectra of PYRPCA; a) calculated, b) observed.

band is a general spectral feature of enolized β -diketones, attributed to the electron configuration of the chelate ring.²⁸ The results of the present vibrational analysis, *viz.*, calculated unscaled vibrational frequencies, IR and Raman intensities, SQM frequencies; potential energy distribution (PED) and assignment of the fundamentals, are shown in Table V-SM (Supplementary material). The well-known good performance of the density functional theory for the estimation of the vibrational spectra of organic compounds can be observed also in case of the **Ia** and **Ib** conformer. The interpretation of the experimental spectra was based on the scaled computed B3LYP/6-31G* force field utilizing additional information from computed (unscaled) IR intensities and Raman activities. The choice of the B3LYP force field was reasoned by the found good agreement between the B3LYP results for the HB interaction and geometrical parameters of the **Ia** and **Ib** conformers. In fact, a rough assignment can already be performed based on the unscaled computed results. However, for reliable information on the vibrational properties (e.g., good quality force field), the use of selective scaling is necessary.

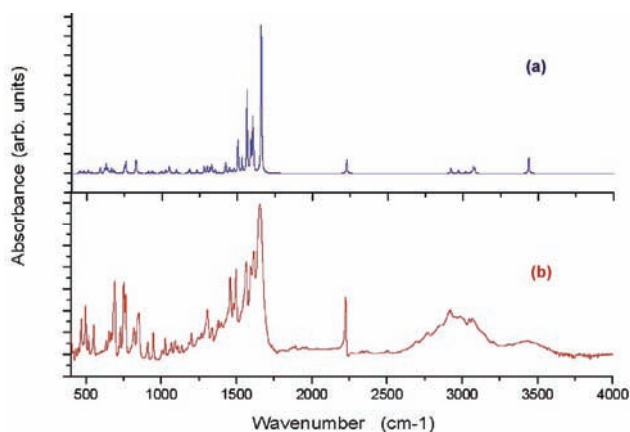


Fig. 5. FT-IR spectra of PYRPCN; a) calculated, b) observed.

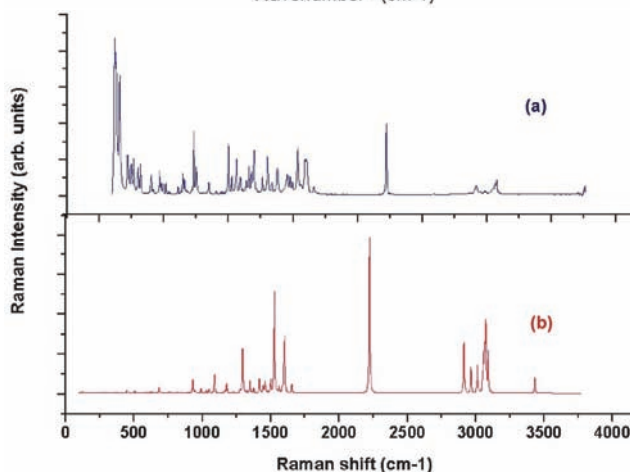


Fig. 6. FT-Raman spectra of PYRPCN; a) observed, b) calculated.

SQM analysis, assignment

The effect of scaling was studied using the DFT force fields of the title compounds. Several calculations were performed with different kinds of scaling. Calculations A performed with the unscaled (raw) DFT force field transformed to the natural internal coordinates; calculation B, labeled C_0 , was performed with selective scaling according to the SQM scheme, using 9 transferable scale factors from the recommended set⁴ without refinement. In calculation of C_{ref} , the number of distinct scale factors was increased to 15 (as shown in the last columns of Tables III and IV) and 14 of these were refined in a least-squares procedure to achieve a better frequency fit. Special attention was paid to the vibrations of the OH, NH₂, NH and C=O groups, whether the errors of the B3LYP/6-31G* level for hydrogen bonding were not sufficiently corrected by the original scale factors. This SQM treatment resulted in a weighted mean deviation of 81.81 cm⁻¹ for PYRPCA and 73.21 cm⁻¹ for PYRPCN. The largest deviations between the experimental and SQM frequencies were observed for the vibration of the NH₂, OH, NH and CO groups. The following were registered:

- OH stretch, an overestimation of *ca.* 114 cm⁻¹;
- NH stretch, an overestimation of *ca.* 158 cm⁻¹;
- CN stretch, an overestimation of *ca.* 121 cm⁻¹;
- NH₂ stretch, an overestimation of *ca.* 152 cm⁻¹;
- C=O stretch, an overestimation of 80 cm⁻¹ by the scaled B3LYP/6-31G* force field.

TABLE III. Definition of the local symmetry coordinates for 6-amino-3-methyl-1-phenyl-1*H*-pyrazolo[3,4-*b*]pyridine-5-carboxylic acid and the values of the corresponding scale factors used to correct the B3LYP/6-31G* (C_0 , C_{ref}) force fields

No(i)	Symbol	Definition	Scale factors used		
			Notat	C_0	C_{ref}
1-6	CHar	$R_1, R_2, R_3, R_4, R_5, R_6$	S1-S6	0.920	0.931
7	CH ₃ ss	$(R_7+R_8+R_9)/\sqrt{3}$	S7	0.920	0.920
8	CH ₃ ips	$(2R_7-R_8-R_9)/\sqrt{6}$	S8	0.920	0.920
9	CH ₃ ops	$(R_8-R_9)/\sqrt{2}$	S9	0.920	0.920
10	CCH ₃	T_{10}	S10	0.922	0.922
11-15	CN	$q_{11}, q_{12}, q_{13}, q_{14}, q_{15}$	S11-S15	0.922	0.922
16-26	CCar	$R_{16}, R_{17}, R_{18}, R_{19}, R_{20}, R_{21}, R_{22}, R_{23}, R_{24}, R_{25}, R_{26}$	S16-S26	0.922	0.984
27	NN	P_{27}	S27	0.922	0.922
28	CNH ₂	P_{28}	S28	0.922	0.922
29-30	NH ₂	P_{29}, P_{30}	S29-S30	0.922	0.965
31	CCO ₂	P_{31}	S31	0.922	0.984
32-33	CO ₂	P_{32}, P_{33}	S32-S33	0.922	0.896
34	OH	P_{34}	S34	0.920	0.920
35-40	bCH _{ar}	$(\alpha_{35}-\alpha_{36})/\sqrt{2}, (\alpha_{37}-\alpha_{38})/\sqrt{2}, (\alpha_{39}-\alpha_{40})/\sqrt{2}$ $(\alpha_{41}-\alpha_{42})/\sqrt{2}, (\alpha_{43}-\alpha_{44})/\sqrt{2}, (\alpha_{45}-\alpha_{46})/\sqrt{2}$	S35-S40	0.950	0.950

TABLE III. Continued

No(i)	Symbol	Definition	Scale factors used		
			Notat	C ₀	C _{ref}
41	CH ₃ sb	$(-\alpha_{47}-\alpha_{48}-\alpha_{49}+\beta_{50}+\beta_{51}+\beta_{52})/\sqrt{6}$	S41	0.915	0.915
42	CH ₃ ipb	$(-\beta_{50}-\beta_{51}+2\beta_{52})/\sqrt{6}$	S42	0.915	0.915
43	CH ₃ opb	$(-\beta_{50}-\beta_{51})/\sqrt{2}$	S43	0.915	0.915
44	CCH ₃	$(\alpha_{53}-\alpha_{54})/\sqrt{2}$	S44	0.950	0.950
45	bR1	$\beta_{55}+a(\beta_{56}+\beta_{58})+b(\beta_{57}+\beta_{59})$	S45	0.990	0.990
46	bR1	$(a-b)(\beta_{56}-\beta_{58})+(1-a)(\beta_{57}+\beta_{59})$	S46	0.990	0.990
47	R2trigd	$(\alpha_{60}-\alpha_{61}+\alpha_{62}-\alpha_{63}+\alpha_{64}-\alpha_{65})/\sqrt{6}$	S47	0.990	0.990
48	R2sym	$(-\alpha_{60}-\alpha_{61}+2\alpha_{62}-\alpha_{63}-\alpha_{64}+2\alpha_{65})/\sqrt{12}$	S48	0.990	0.990
49	R2asym	$(\alpha_{60}-\alpha_{61}+2\alpha_{63}+\alpha_{64})/2$	S49	0.990	0.990
50	bCNH ₂	$(\delta_{66}-\delta_{67})/\sqrt{2}$	S50	0.950	0.950
51	bNH ₂	$(\delta_{68}-\delta_{69})/\sqrt{2}$	S51	0.915	0.915
52	bNH ₂	$(2\delta_{70}-\delta_{68}-\delta_{69})/\sqrt{6}$	S52	0.915	0.915
53	bCCO ₂	$(\delta_{71}-\delta_{72})/\sqrt{2}$	S53	0.99	0.99
54	bCO ₂	$(\delta_{73}-\delta_{74})/\sqrt{2}$	S54	0.990	0.876
55	bCO ₂	$(2\sigma_{75}-\sigma_{73}-\sigma_{74})/\sqrt{6}$	S55	0.990	0.876
56	bOH	δ_{76}	S56	0.990	0.990
57-58	bCN1	$(\theta_{77}-\theta_{78})/\sqrt{2}, (\theta_{79}-\theta_{80})/\sqrt{2}$	S57-S58	0.990	0.990
59	R3trigd	$(\alpha_{81}-\alpha_{82}+\alpha_{83}-\alpha_{84}+\alpha_{85}-\alpha_{86})/\sqrt{6}$	S59	0.990	0.990
60	R3sym	$(-\alpha_{81}-\alpha_{82}+2\alpha_{83}-\alpha_{84}-\alpha_{85}+2\alpha_{86})/\sqrt{12}$	S60	0.990	0.990
61	R3asym	$(\alpha_{81}-\alpha_{82}+2\alpha_{84}+\alpha_{85})/2$	S61	0.990	0.990
62-67	gCH _{ar}	$\omega_{87}, \omega_{88}, \omega_{89}, \omega_{90}, \omega_{91}, \omega_{92}$	S62-S67	0.976	0.976
68-69	gCC _{ar}	ω_{93}, ω_{94}	S68-S69	0.976	0.976
70	gCCO ₂	ω_{95}	S70	0.976	0.976
71-72	gCN1	ω_{96}, ω_{97}	S71-S72	0.976	0.976
73	gCNH ₂	ω_{98}	S73	0.976	0.976
74	gNH ₂	ω_{99}	S74	0.806	0.806
75	gCCH ₃	ω_{100}	S75	0.976	0.984
76	gCO ₂	ω_{101}	S76	0.976	0.976
77	tR1	$\tau_{102}+b(\tau_{103}+\tau_{105})+a(\tau_{104}-\tau_{106})$	S77	0.935	0.935
78	tR1	$(a-b)(\tau_{103}-\tau_{105})+(1-a)(\tau_{104}-\tau_{106})$	S78	0.935	0.935
79	tR2trigd	$(\tau_{107}+\tau_{108}+\tau_{109}+\tau_{110}+\tau_{111}+\tau_{112})/\sqrt{6}$	S79	0.935	0.935
80	tR2sym	$(\tau_{107}+\tau_{108}+\tau_{110}+\tau_{111})/\sqrt{2}$	S80	0.935	0.935
81	tR2asym	$(-\tau_{107}+\tau_{108}+2\tau_{109}-\tau_{110}-\tau_{111}+2\tau_{112})/\sqrt{12}$	S81	0.935	0.935
82					
83	tR3trigd	$(\tau_{113}+\tau_{114}+\tau_{116}+\tau_{117})/\sqrt{2}$	S82	0.935	0.935
84	tR3sym	$(\tau_{113}+\tau_{114}+\tau_{116}+\tau_{117})/\sqrt{2}$	S83	0.935	0.935
85	tR3asym	$(-\tau_{113}+\tau_{114}+2\tau_{115}-\tau_{116}-\tau_{117}+2\tau_{118})/\sqrt{12}$	S84	0.935	0.935
86					
87	tCH ₃	τ_{119}	S85	0.831	0.831
88	tCCO ₂	τ_{120}	S86	0.831	0.678
89	tCNH ₂	τ_{121}	S87	0.913	0.910
90	tCN1	τ_{122}	S88	0.831	0.831
	tCO ₂	τ_{123}	S89	0.831	0.831
	Butterfly	τ_{124}	S90	0.913	0.913

In the second step of the SQM analysis, the scale factors for selected vibrations: C=O, NH₂, OH stretch, COH bend, CO wag, OH and ring torsion, were released and optimized using the experimental data. Comparing the experimental and the newly obtained scaled frequencies, some additional systematic deviations could be observed which were smoothed before due to the coupling between the internal coordinates. These were: an overestimation for C=O, NH₂, and CC–O bond. Satisfactory agreement was obtained for C=O and NH stretching in PYRPCN. The final SQM force field (see the column headed C_{ref} in Tables IV and V-SM) reproduced the experimental spectra with a weight mean deviation of 13.9 cm⁻¹ for PYRPCA and 10.12 cm⁻¹ for PYRPCN between the experimental and the scale frequencies. The frequencies of ν_1 , ν_2 , ν_3 and ν_{12} in PYRPCA were excluded from this comparison because of the obvious large effect of intermolecular hydrogen bonding in the solid phase.

TABLE IV. Definition of the local symmetry coordinates for 6,7-dihydro-3-methyl-6-oxo-1-phenyl-1*H*-pyrazolo[3,4-*b*]pyridine-5-carbonitrile (PYRPCN) and the values of the corresponding scale factors used to correct the B3LYP/6-31G* (C₀, C_{ref}) force fields

No(i)	Symbol	Definition	Scale factors used		
			Notat	C ₀	C _{ref}
1	N1H	R ₁	s ₁	0.920	0.914
2–7	CH _{ar}	R ₂ , r ₃ , r ₄ , r ₅ , r ₆ , r ₇	s ₂ → s ₇	0.920	0.914
8	CH _{3ss}	(r ₈ + r ₉ + r ₁₀)/√6	s ₈	0.920	0.914
9	CH _{3ips}	(2r ₈ – r ₉ – r ₁₀)/√6	s ₉	0.920	0.914
10	CH _{3ops}	(r ₉ – r ₁₀)/√2	s ₁₀	0.922	0.922
11	CCH ₃	T ₁₁	s ₁₁	0.922	0.922
12–16	CN	Q ₁₂ , Q ₁₃ , Q ₁₄ , Q ₁₅ , Q ₁₆	s ₁₂ → s ₁₆	0.922	0.926
17–27	CC _{ar}	R ₁₇ , R ₁₈ , R ₁₉ , R ₂₀ , R ₂₁ , R ₂₂ , R ₂₃ , R ₂₄ , R ₂₅ , R ₂₆ , R ₂₇	s ₁₇ → s ₂₇	0.922	0.922
28	NN	P ₂₈	s ₂₈	0.920	0.920
29	C=O	P ₂₉	s ₂₉	0.922	0.830
30	CC(N)	P ₃₀	s ₃₀	0.922	0.922
31	C≡N	P ₃₁	s ₃₁	0.922	0.897
32–37	bCH _{ar}	(α ₃₂ – α ₃₃)/√2, (α ₃₄ – α ₃₅)/√2, (α ₃₆ – α ₄₇)/√2	s ₃₂ → s ₃₇	0.950	0.950
38	CH _{3sb}	(α ₃₈ – α ₃₉)/√2, (α ₄₀ – α ₄₁)/√2, (α ₄₂ – α ₄₃)/√2	s ₃₈	0.950	0.950
39	CH _{3ipb}	(–α ₄₄ – α ₄₅ – α ₄₆ + β ₄₇ + β ₄₈ + β ₄₉)/√6	s ₃₉	0.915	0.915
40	CH _{3opb}	(–β ₄₇ – β ₄₈ + 2β ₄₉)/√6	s ₄₀	0.915	0.915
41	CH _{3ipr}	(β ₄₇ – β ₄₈)/√2	s ₄₁	0.915	0.915
42	CH _{3opr}	(2α ₄₄ – α ₄₅ – α ₄₆)/√6	s ₄₂	0.915	0.915
43	bR1	(α ₅₀ – α ₅₁)/√2	s ₄₃	0.915	0.915
44	bR1	β ₅₂ + a(β ₅₃ + β ₅₅) + b(β ₅₄ + β ₅₆)	s ₄₄	0.990	0.990
45	R2trigd	(a – b)(β ₅₃ – β ₅₅) + (1 – a)(β ₅₄ – β ₅₆)	s ₄₅	0.990	0.990
46	R2sym	(α ₅₇ – α ₅₈ + α ₅₉ – α ₆₀ + α ₆₁ – α ₆₂)/√6	s ₄₆	0.990	0.990
47	R2asym	(–α ₅₇ – α ₅₈ + 2α ₅₉ – α ₆₀ – α ₆₁ + 2α ₆₂)/√12	s ₄₇	0.990	0.990
48	bC=O	(α ₅₇ – α ₅₈ + α ₆₀ – α ₆₁)/2	s ₄₈	0.990	0.990
49	bN1H	(δ ₆₃ – δ ₆₄)/√2	s ₄₉	0.950	0.913
50	bCC(N)	(δ ₆₅ – δ ₆₆)/√2	s ₅₀	0.950	0.915

TABLE IV. Continued

No(i)	Symbol	Definition	Scale factors used		
			Notat	C ₀	C _{ref}
51	bC≡N _{in}	$(\delta_{66} - \delta_{68})/\sqrt{2}$	S ₅₁	0.915	0.950
52–53	bC≡N _{op}	δ_{69}	S ₅₂ → S ₅₃	0.915	0.913
54	bCN1	δ_{70}	S ₅₄	0.915	0.913
55	R3trigd	$(\theta_{71} - \theta_{72})/\sqrt{2}, (\theta_{73} - \theta_{74})/\sqrt{2}$	S ₅₅	0.915	0.913
56	R3sym	$(\alpha_{75} - \alpha_{76} + \alpha_{77} - \alpha_{78} + \alpha_{79} - \alpha_{80})/\sqrt{6}$	S ₅₆	0.990	0.990
57–62	R3asym	$(-\alpha_{75} - \alpha_{76} + 2\alpha_{77} - \alpha_{78} - \alpha_{79} + 2\alpha_{80})/\sqrt{12}$	S ₅₇ → S ₆₂	0.990	0.990
63–64	gCH _{ar}	$(\alpha_{75} - \alpha_{76} + \alpha_{78} - \alpha_{79})/2$	S ₆₃ → S ₆₄	0.990	0.990
65	gCC _{ar}	$\omega_{81}, \omega_{82}, \omega_{83}, \omega_{84}, \omega_{85}, \omega_{86}$	S ₆₅	0.990	0.934
66–67	gC=O	ω_{87}, ω_{88}	S ₆₆ → S ₆₇	0.976	0.934
68	gCN1	ω_{89}	S ₆₈	0.976	0.976
69	gCC(N)	ω_{90}, ω_{91}	S ₆₉	0.976	0.976
70	gN1H	ω_{92}	S ₇₀	0.976	0.934
71	tR1	ω_{93}	S ₇₁	0.976	0.976
72	tR1	$\tau_{95} + b(\tau_{96} + \tau_{98}) + a(\tau_{97} - \tau_{99})$	S ₇₂	0.831	0.831
73	tR2trigd	$(a - b)(\tau_{96} - \tau_{98}) + (1 - a)(\tau_{97} - \tau_{99})$	S ₇₃	0.831	0.831
74	tR2sym	$(\tau_{100} + \tau_{101} + \tau_{102} + \tau_{103} + \tau_{104} + \tau_{105})/\sqrt{6}$	S ₇₄	0.831	0.831
75	tR2asym	$(\tau_{100} + \tau_{101} + \tau_{103} + \tau_{104})/2$	S ₇₅	0.831	0.831
76	tR3trigd	$(-\tau_{100} - \tau_{103} + 2\tau_{102} - \tau_{103} - \tau_{104} + 2\tau_{105})/\sqrt{12}$	S ₇₆	0.831	0.831
77	tR3sym	$(\tau_{106} + \tau_{107} + \tau_{108} + \tau_{109} + \tau_{110} + \tau_{111})/\sqrt{6}$	S ₇₇	0.831	0.831
78	tR3asym	$(\tau_{106} + \tau_{107} + \tau_{109} + \tau_{110})/2$	S ₇₈	0.831	0.831
79	tCH ₃	$(-\tau_{106} - \tau_{107} + 2\tau_{108} - \tau_{109} - \tau_{110} + 2\tau_{111})/\sqrt{12}$	S ₇₉	0.831	0.831
80	tC19N	τ_{112}	S ₈₀	0.831	0.831
81	Butterfly	τ_{113}	S ₈₁	0.831	0.935
		τ_{114}		0.935	0.935

COOH vibrations

Hydrogen bonding alters the frequencies of the stretching and bending vibrations. The O–H stretching bands move to lower frequencies, usually with increased intensity and band broadening in hydrogen bonded species. In the present study, the O–H stretching frequency was observed at 3407 cm⁻¹.²⁸ However, the wave number calculated by the B3LYP method showed a strong negative deviation of 214 cm⁻¹. The C–O stretching is a characteristic frequency of carboxylic acid.²⁹ The strong band appearing at 1697 cm⁻¹ in the FT-IR spectrum was assigned as the C=O stretching vibration. The theoretical value of 1721 cm⁻¹ computed by the B3LYP method showed a negative deviation of 24 cm⁻¹ because of mixing with the pyridine ring vibrations.^{30,32} The O–H in-plane bending occurred between 1440 and 1395 cm⁻¹ and the out-of-plane bending vibration at between 970 and 875 cm⁻¹.³³ The medium band at 1419 cm⁻¹ in FT-IR spectrum was assigned as the O–H in-plane bending vibration and frequency at 935 cm⁻¹ to the O–H out-of-plane bending vibration for the present molecule. The theoretically computed value of 1382 cm⁻¹ is in very good agreement for the O–H in-plane bending vibration. However, the calculated value of OH out-of-pla-

ne bending deviates positively by about 200 cm^{-1} . This shift in the O–H out-of-plane bending vibration reflects on the strength of the hydrogen bond. The band observed at 1186 cm^{-1} in FT-Raman spectrum of PYRPCA corresponds to the C–COOH stretching vibration. The calculated result at 1182 cm^{-1} is in excellent agreement with the experimental data.

C≡N vibrations

The assignment of the highly characteristic nitrile stretching mode ($\nu(\text{C}\equiv\text{N})$) to the band at 2224 cm^{-1} is quite obvious in all calculations. The degenerate pair of linear bending vibrations of the C–C≡N moiety is split into in-plane and out-of-plane components, both strongly mixed with several other in-plane and out-of-plane vibrations, respectively. They contribute to several normal modes in the $600\text{--}100\text{ cm}^{-1}$ range (see Table V-SM). In the final force field, the in-plane linear bend has a smaller force constant (0.319 N/cm) than the out-of-plane counterpart (0.399 N/cm), which may be due to a stronger interaction of the latter with the p-electrons of the pyridine ring.

Amino group vibrations

The frequencies of the amino group appear at around $3500\text{--}3300\text{ cm}^{-1}$ for the N–H stretching, $1700\text{--}1600\text{ cm}^{-1}$ for the scissoring and $1150\text{--}900\text{ cm}^{-1}$ for the rocking deformations.³⁴ In the present study, the NH_2 asymmetric and symmetric stretching modes move to lower frequencies, usually with increased intensity and band broadening in the hydrogen bonded species. The FT-IR bands at 3407 and 3301 cm^{-1} in the infrared spectrum and at 3413 and 3311 cm^{-1} in the Raman spectrum of PYRPCA were assigned to NH_2 asymmetric and symmetric stretching, respectively. The bands observed at 1597 cm^{-1} in the infrared and Raman are assigned undoubtedly to the scissoring modes of the NH_2 group. According to PED, this band is strongly mixed with the NH_2 rocking mode. According to NCA calculations, the medium and weak IR bands at 1027 and 796 cm^{-1} are assigned to NH_2 rocking and NH_2 out-of-plane bending, respectively.

Methyl group vibrations

For the assignments of CH_3 group frequencies, basically nine fundamentals can be associated to each CH_3 group, namely: CH_3 ss, symmetrical stretch; CH_3 ips, in-plane stretch (*i.e.*, in-plane hydrogen stretching modes); CH_3 ipb, in-plane-bending (*i.e.*, hydrogen deformation modes); CH_3 sb, symmetric bending; CH_3 ipr, in-plane rocking; CH_3 opr, out-of-plane rocking and CH_3 t, twisting hydrogen bending modes, as well as, CH_3 ops, out-of-plane stretch and CH_3 opb, out-of-plane bending modes of the CH_3 group. For PYRPCA, the CH_3 ss frequency was established at 2921 cm^{-1} in the IR spectrum of both compounds and CH_3 ips was found at 3045 and 3042 cm^{-1} in the IR and Raman, respectively. These bands were also observed at 3022 and 3017 cm^{-1} in the IR and Raman

spectrum, respectively, of PYRPYCN. These assignments are also supported by the literature.³⁵ The two in-plane methyl hydrogen deformation modes are also well established. The symmetrical methyl deformation was observed at 1354 and 1356 cm^{-1} in the infrared and Raman spectrum of PYRPCA, and the in-plane-bending methyl deformation mode at 1455 cm^{-1} in the Raman spectrum. These bands were observed at 1378 and 1381 cm^{-1} in the infrared and Raman spectrum of PYRPCN and at 1446 cm^{-1} for the methyl in-plane-bending. The bands at 3027 and 1432 cm^{-1} in the infrared spectrum of PYRPCA were attributed to CH_3 ops and CH_3 opb, respectively. These bands were observed at 3047 and 1455 cm^{-1} in the infrared spectrum of PYRPCN. The methyl deformation modes mainly coupled with the in-plane bending vibrations. The bands obtained at 1020 and 651 cm^{-1} in IR and Raman spectrum of PYRPCA and at 1028 and 654 cm^{-1} in the IR and Raman spectrum of PYRPCN were assigned to CH_3 in-plane and out-of-plane rocking modes. The band at 399 cm^{-1} in the IR spectrum of PYRPCA and at 404 cm^{-1} in the IR spectrum of PYRPCN is attributed to the methyl twisting mode.

Pyrazole–pyridine ring vibrations

Many ring modes are affected by substitutions to pyrazole and pyridine rings. The pyridine ring absorb strongly in the region 1630–1300 cm^{-1} .³⁶ In the present study, for the PYRPCA molecule, the peaks absorbing at 1614, 1562, 1530, 1497 and 1372 cm^{-1} in the IR spectrum and at 1623, 1563, 1525, 1493 and 1362 cm^{-1} in the Raman spectrum (*cf.* Table V-SM) were assigned to ring stretching vibrations. For PYRPCN, peaks absorbing at 1616, 1595, 1536, 1481 and 1308 cm^{-1} in the IR spectrum and at 1605, 1592, 1535, 1479 and 1304 cm^{-1} in the Raman spectrum were assigned to the pyridine ring. The pyrazole ring has several bands of variable intensities in the range of 1530–1013 cm^{-1} due to ring stretching vibrations.³⁷ In the present study, the IR peaks observed at 1429, 1342, 1237 and 1060 cm^{-1} and the Raman bands at 1419, 1342, 1232 and 1057 cm^{-1} were assigned to ring stretching vibrations. Pyrazole ring deformations were observed at 1016, 694, 515 and 487 cm^{-1} and the pyridine ring deformation vibrations at 900, 674, 515 and 487 cm^{-1} . These bands are also observed at the same wave number in the IR and Raman spectra of the PYRPCN molecule. For most of the remaining ring vibrations, the overall agreement was satisfactory. Small changes in frequencies observed for these modes are due to changes in the force constant/reduced mass ratio, resulting mainly due to the extent of mixing between the rings and substituent group vibrations.³⁸

CONCLUSIONS

Presently, the DFT-based SQM approach provides the most reliable information on the vibrational properties of large-size molecules. This method, using the Pulay standard scale factors, performed well for pyrazolo-pyridine derivatives.

Based on the SQM force field, complete vibrational analyses of the title compounds were performed, resulting in the assignment of all the fundamentals. The overall good quality of the SQM force field was confirmed by the achieved root mean square deviation of 13.9 and 10.12 cm^{-1} between the experimental and scale frequencies for PYRPCA and PYRPCN, respectively. The assignment of most of the fundamentals provided in the present study is unambiguous taking advantage of selective scaling (correcting effectively the different systematic errors of the computed force field) and the fairly good information on the IR and Raman intensities from the density functional theory. It is remarkable that all the vibrations affected by the strong hydrogen bonding were described satisfactorily by the scaled DFT force field with modification of the original scale factors of C=O, NH, C≡N and NH₂ stretching and bending. From the view of an extension of the Pulay DFT-based SQM method for the strongly hydrogen-bonded systems, the above results are very promising. Vibrations of the OH and CO and NH₂ and NH groups reflect the effect of the strong inter-molecular hydrogen bonding. In addition, the intermolecular hydrogen bonding interaction strengthens the conjugation of the NH₂ and COOH groups with the pyrazolo-pyridine rings.

SUPPLEMENTARY MATERIAL

TABLE V-SM: Comparison of the observed and calculated frequencies (in cm^{-1}) of the fundamental vibrations of 6-amino-3-methyl-1-phenyl-1*H*-pyrazolo[3,4-*b*]pyridine-5-carboxylic acid (PYRPCA) and 6,7-dihydro-3-methyl-6-oxo-1-phenyl-1*H*-pyrazolo[3,4-*b*]pyridine-5-carbonitrile (PYRPCN) obtained by DFT force fields by B3LYP/6-31G*, is available electronically from <http://www.shd.org.rs/JSCS> or from the corresponding author on request.

ИЗВОД

ТЕОРИЈСКА И ЕКСПЕРИМЕНТАЛНА ИСТРАЖИВАЊА СТРУКТУРЕ И ВИБРАЦИОНИХ СПЕКТРА 6-АМИНО-3-МЕТИЛ-1-ФЕНИЛ-1*H*-ПИРАЗОЛО[3,4-*b*]ПИРИДИН-5-КАРБОКСИЛНЕ КИСЕЛИНЕ И 6,7-ДИХИДРО-3-МЕТИЛ-6-ОКСО-1-ФЕНИЛ-1*H*-ПИРАЗОЛО[3,4-*b*]ПИРИДИН-5-КАРБОНИТРИЛА

KHALED BAHGAT¹, NAZM AL-DEN JASEM² и TALAAT EL-EMARY³

¹Chemistry Department, Faculty of Petroleum and Mining Engineering, Suez Canal University, Suez, Egypt,

²Chemistry Department, Faculty of Sciences, Aleppo University, Syria и ³Chemistry Department, Faculty of Science, Assiut University, Assiut, Egypt

FT-IR и FT-рамански спектри чврсте фазе 6-амино-3-метил-1-фенил-1*H*-пиразоло[3,4-*b*]пиридин-5-карбоксилне киселине (PYRPCA) и 6,7-дихидро-3-метил-6-оксо-1-фенил-1*H*-пиразоло[3,4-*b*]пиридин-5-карбонитрила (PYRPCN) снимљени су у области 4000–400 cm^{-1} . Спектри су тумачени помоћу нормалне координатне анализе, праћене потпуном оптимизацијом структуре и прорачуном поља сила, који су засновани на функционалној теорији густине (DFT) уз коришћење стандардних метода B3LYP, BLYP и *ab initio* RHF, заснованих на 6-31G* поставци, уз одређивање размере помоћу предложеног скупа размерних фактора, чиме се добило задовољавајуће слагање између уочених и израчунатих учестаности. На основу овога, постављено је прилагођено квантно-механичко поље сила (SQM) као поуздан темељни опис PYRPCA и PYRPCN. Израчунавања су предвидела преовлађивање различитих таутомера за PYRPCA

и кето-енолних таутомера за PYRPCN. Формирање међумолекулских водоничних веза доводи до најстабилније конформације PYRPCA. Карактеристика овог водоничног повезивања јесте ефекат јачања у односу на коњугацију NH₂ и COOH група са пиридинским прстеном.

(Примљено 22. октобра 2008, ревидирано 12. фебруара 2009)

REFERENCES

1. B. A. Hess Jr., J. Schaad, P. Carsky, R. Zahradnik, *Chem. Rev.* **86** (1986) 709
2. P. Pulay, X. Zhou, G. Fogarasi, in NATOASI Series, Vol.C406, R. Fausto, Ed., Kluwer, Dordrecht, 1993, p. p. 99–112
3. C. E. Blom, C. Altona, *Mol. Phys.* **31** (1976) 1377
4. P. Pulay, G. Fogarasi, G. Pongor, J. E. Boggs, A. Vargha, *J. Am. Chem. Soc.* **105** (1983) 7037
5. G. Fogarasi, P. Pulay, in *Vibrational Spectra and Structure*, Vol. 14, J. R. Durig, Ed., Elsevier, Amsterdam, 1985, p. 125
6. G. Fogarasi, *Spectrochim. Acta* **52A** (1997) 1211
7. G. Pongor, P. Pulay, G. Fogarasi, J. E. Boggs, *J. Am. Chem. Soc.* **106** (1984) 2765
8. G. Rauhut, P. Pulay, *J. Phys. Chem.* **99** (1995) 3093
9. G. Rauhut, P. Pulay, *J. Am. Chem. Soc.* **117** (1995) 4167
10. P. M. Kozlowski, G. Rauhut, P. Pulay, *J. Chem. Phys.* **103** (1995) 5650
11. A. Kovacs, K. B. Borisenko, G. Pongor, *Chem. Phys. Lett.* **280** (1997) 343
12. I. Macsari, V. Izvekov, A. Kovacs, *Chem. Phys. Lett.* **269** (1997) 343
13. B. M. Lynch, M. A. Teo, H. C. Pedrotti, *Can. J. Chem.* **66** (1988) 420
14. M. Makowska-Janusik, I. V. Kityk, *Spectrochim. Acta A* **65** (2006) 511
15. A. M. Hussein, T. I. El-Emary, *J. Chem. Res., Synop.* **1** (1998) 241
16. J. Haufel, E. Breitmaier, *Angew. Chem. Int. Ed.* **13** (1974) 604
17. M. J. Frisch, G. W. Trucks, H. B. Schlegel, P. M. Johnson, M. A. Robb, J. R. Cheeseman, T. A. Keith, G. A. Peterson, J. A. Montgomery, M. A. Al-Laham, U. G. Zakrzewski, J. V. Ortiz, J. B. Foresman, C. Y. Reng, P. Y. Ayala, M. W. Wong, J. L. Andres, E. S. Replogle, R. Gomperts, R. L. Martin, D. J. Fox, J. S. Binkley, D. J. Defrees, J. Baker, J. P. Stewart, M. Head-Gordon, C. Gonzalez, A. Pople, gaussian94w (revision B. 3), Gaussian, Inc., Pittsburgh, PA, 1995
18. A. D. Becke, *J. Chem. Phys.* **98** (1993) 5648
19. C. Lee, W. Yang, R. G. Parr, *Phys. Rev. B* **37** (1998) 785
20. G. Fogarasi, X. Zhou, P. W. Taylor, P. Pulay, *J. Am. Chem. Soc.* **114** (1992) 8191
21. T. Sundius, *J. Mol. Struct.* **218** (1990) 321
22. T. Sundius, *Vib. Spectrosc.* **29** (2002) 89
23. Molvib (V. 7.0), Calculation of Harmonic Force Fields and Vibrational Modes of Molecules, QCPE Program No. 807, 2002
24. F. A. Cotton, *Chemical Application of Group Theory*, Wiley Interscience, New York, 1971
25. A. J. Dobson, R. E. Gerkin, *Acta Crystallogr. C* **53** (1997) 1427
26. K. B. Borisenko, C. W. Bock, I. Hargittai, *J. Phys. Chem.* **98** (1994) 1442
27. N. Z. Tugusheva, L. M. Alekseeva, A. S. Shashkov, V. V. Chernyshev, V. G. Granik, *Russ. Chem. Bull., Int. Ed.* **55** (2006) 1475
28. G. Varsanyi, *Assignments for Vibrational Spectra of 700 Benzene Derivatives*, Vols. 1 and 2, Adam Hilger, London, 1974

29. V. K. Rastogi, M. P. Rajpoot, S. N. Sharma, *Indian J. Phys.* **58B** (1984) 311
30. V. Chis, *Chem. Phys.* **300** (2004) 1
31. G. C. Pimentel, A. L. McClellan, *The Hydrogen Bond*, W. H. Freeman, San Francisco, CA, 1960
32. A. Szab, A. Kovács, *J. Mol. Struct.* **510** (1999) 215
33. A. Kovács, V. Izvekov, G. Keresztury, G. Pongor, *Chem. Phys.* **238** (1998) 231
34. G. Socrates, *Infrared and Raman Characteristic Group Frequencies, Tables and Charts*, 3rd ed., Wiley, Chichester, 2001
35. V. Krishnakumar, V. Balachandran, *Spectrochim. Acta A* **61** (2005) 2510
36. A. Topaçli, S. Bayari, *Spectrochim. Acta A* **57** (2001) 1385
37. M. Majoube, *J. Raman Spectrosc.* **20** (1989) 2434
38. F. Billes, H. Endrédi, G. Jalsovszky, *THEOCHEM* **465** (1999) 157.



SUPPLEMENTARY MATERIAL TO
Theoretical and experimental investigations on the structure and vibrational spectra of 6-amino-3-methyl-1-phenyl-1*H*-pyrazolo[3,4-*b*]pyridine-5-carboxylic acid and 6,7-dihydro-3-methyl-6-oxo-1-phenyl-1*H*-pyrazolo[3,4-*b*]pyridine-5-carbonitrile

KHALED BAHGAT^{1*}, NAZM AL-DEN JASEM² and TALAAT EL-EMARY³

¹Chemistry Department, Faculty of Petroleum and Mining Engineering, Suez Canal University, Suez, Egypt, ²Chemistry Department, Faculty of Sciences, Aleppo University, Syria and ³Chemistry Department, Faculty of Science, Assiut University, Assiut, Egypt

J. Serb. Chem. Soc. **74** (5) 555–571 (2009)

*Corresponding author. E-mail: khabahgat1@hotmail.com



TABLE V-SM. Comparison of the observed and calculated frequencies (in cm^{-1}) of the fundamental vibrations of 6-amino-3-methyl-1-phenyl-1*H*-pyrazolo[3,4-*b*]pyridine-5-carboxylic acid (PYRPCA) and 6,7-dihydro-3-methyl-6-oxo-1-phenyl-1*H*-pyrazolo[3,4-*b*] pyridine-5-carbonitrile (PYRPCN) obtained by DFT force fields by B3LYP/6-31G^{*}

No. <i>i</i>	IR	Raman	No scaling	Scaling ^a	Ai, IR ^b	Ii, Raman	PED %	IR	Raman	No scaling	Scaling ^a	Ai, IR ^b	Ii, Raman	PED %
1	3407	3413	3711	3559	62.78	203.60	OH(98)	3435	–	3593	3436	56.38	50.46	N1H(100)
2	3337	3339	3702	3551	123.89	83.69	NHas(92)	3088	3079	3237	3095	0.64	120.76	CH _{ar} (99)
3	3301	3311	3552	3408	175.57	164.02	NHs(92)	3073	3065	3218	3077	15.36	203.77	CH _{ar} (99)
4	3141	–	3263	3130	8.07	60.67	CH _{ar} (90)	–	–	3211	3071	3.597	69.70	CH _{ar} (99)
5	3114	–	3254	3122	6.81	62.34	CH _{ar} (99)	–	–	3208	3068	19.17	68.21	CH _{ar} (99)
6	–	–	3231	3100	0.45	107.67	CH _{ar} (99)	–	–	3200	3060	4.71	106.00	CH _{ar} (99)
7	3078	3072	3208	3077	38.41	215.86	CH _{ar} (99)	–	–	3193	3053	2.31	26.55	CH _{ar} (100)
8	–	–	3191	3062	24.55	139.59	CH _{ar} (99)	3047	3047	3154	3016	5.90	82.58	CH3ops(72), CH3asym(23)
9	–	–	3182	3053	0.71	56.59	CH _{ar} (99)	3022	3017	3105	2969	11.97	81.58	CH3ips(75), CH3ops(25)
10	3045	3042	3149	3044	7.39	80.79	CH3ips(95)	2920	2921	3052	2918	18.59	150.16	CH3ss(95)
11	3027	3031	3098	3030	15.64	92.02	CH3ops(100)	2226	2224	2347	2227	48.21	476.72	CN'(87), CC*(12)
12	2921	2926	3047	2923	26.08	206.86	CH3ss(94)	1655	1665	1792	1658	527.63	26.32	CO(66), CC _{ar} (11)
13	1697	1699	1777	1721	416.13	190.17	CO(65), CC _{ar} (8), bCO(10)	1616	1605	1663	1606	81.38	153.91	CC _{ar} (47), CO(19), CN(13)
14	1654	1648	1677	1650	527.77	525.65	CC _{ar} (46), bCH _{ar} (16), CN(12)	1595	1592	1657	1601	171.96	81.97	CC _{ar} (49), bCH _{ar} (20), CN(14)
15	1614	1633	1660	1638	236.71	4.15	CC _{ar} (62), bCH _{ar} (20)	–	–	1645	1589	103.48	12.71	CC _{ar} (60), bCH _{ar} (22)
16	–	–	1652	1626	220.66	6.70	CC _{ar} (77), bCH _{ar} (17)	1567	1565	1613	1564	288.66	19.63	CN(35), CC _{ar} (34), bN1H(8)
17	1597	1596	1646	1602	29.19	80.07	bNHs(46), CN(H2)(24), CC _{ar} (16)	1536	1535	1587	1531	55.14	303.41	CC _{ar} (41), CO(31), bCH _{ar} (13)

TABLE V-SM. Continued

No. <i>i</i>	IR	Raman	No scaling	Scaling ^a	Ai, IR ^b	Ii, Raman	PED %	IR	Raman	No scaling	Scaling ^a	Ai, IR ^b	Ii, Raman	PED %
18	1562	1563	1600	1565	144.34	30.31	CN(37), CCar(25), bNH(14)	1500	1494	1547	1504	114.90	39.29	bCH _{ar} (57), CC _{ar} (26), CN(13)
19	–	1525	1582	1531	23.46	135.59	CN(59), CCH ₃ (19), R1b(11)	1481	1479	1530	1477	15.37	6.56	CN(33), CC _{ar} (17), CH ₃ opb(12), CCH ₃ (10)
20	1516	1509	1548	1516	200.26	50.46	bCH(54), CC _{ar} (20), CN(15)	1461	–	1510	1462	7.97	34.40	bCH _{ar} (57), CC _{ar} (35)
21	1497	1493	1525	1491	16.15	2.66	CCar(45), bCH(19), bNH(15)	1455	–	1507	1449	12.70	19.76	CH ₃ opb(36), CC _{ar} (19), CH ₃ ipb(16), CCH ₃ (13)
22	1461	1471	1509	1478	8.64	22.48	bCH(35), CC _{ar} (34)	1446	–	1503	1445	13.35	4.26	CH ₃ ipb(72), CH ₃ opb(28)
23	–	1455	1509	1446	37.63	43.02	CH ₃ ipb(80)	1429	–	1474	1422	36.36	44.26	CN(25), CH ₃ opb(21), CC _{ar} (21), R1b(11)
24	1432	1432	1504	1444	18.57	93.28	CH ₃ opb(100)	1378	1381	1438	1378	4.13	15.23	CH ₃ sb(86)
25	–	–	1462	1425	117.18	220.96	CC _{ar} (45), CN(19), CN(H ₂)(12)	–	–	1406	1353	11.37	39.88	CN(32), bN1H(29), CH _{ar} (18), CC _{ar} (14)
26	1429	1419	1458	1421	53.76	27.61	CN(49), CC _{ar} (21), CN(H ₂)(11)	1339	1339	1369	1330	28.93	4.76	bCH _{ar} (63), CC _{ar} (16)
27	1382	1386	1432	1377	131.43	52.87	bOH(59), CC _{ar} (26), CN(17)	1308	1304	1364	1319	18.23	3.58	CC _{ar} (51), bCH _{ar} (26)
28	1372	1362	1410	1372	68.53	22.71	CN(51), CC _{ar} (24)	–	–	1345	1299	23.23	141.67	CC _{ar} (68), bCH _{ar} (21)
29	1354	1356	1390	1354	47.14	23.73	CH ₃ sb(65), CN(14)	1270	1264	1322	1280	22.63	8.66	bCH _{ar} (31), CC _{ar} (30), bN1H(23)



TABLE V-SM. Continued

No. <i>i</i>	IR	Raman	No scaling	Scaling ^a	Ai, IR ^b	Ii, Raman	PED %	IR	Raman	No scaling	Scaling ^a	Ai, IR ^b	Ii, Raman	PED %
30	1342	1342	1373	1348	144.83	119.64	CC _{ar} (72), bCH(23)	1241	–	1278	1232	11.44	5.85	bN1H(27), CC _{ar} (17), CN(12), CC*(11)
31	1338	1339	1371	1338	12.43	33.27	bCH _{ar} (30), CN(15), CC _{ar} (13), bOH(11)	1186	1199	1220	1182	15.31	29.36	bCH _{ar} (43), CN(19), CC _{ar} (19)
32	–	–	1354	1331	0.58	37.21	bCH _{ar} (53), CC _{ar} (19), bCN1(11)	–	1179	1207	1172	1.43	6.47	bCH _{ar} (70), CC _{ar} (16)
33	1306	1303	1324	1296	16.77	49.22	bCH _{ar} (41), CC _{ar} (25), CN(H ₂)(10)	1161	1156	1195	1162	0.10	2.13	bCH _{ar} (83), CC _{ar} (17)
34	1237	1232	1239	1211	20.18	71.22	CN(28), bCH _{ar} (25), CC _{ar} (19)	1094	1091	1188	1095	7.18	45.86	CN(36), bCO(14), CC _{ar} (13), R2trigd(13)
35	–	1216	1215	1190	83.96	59.49	bCH _{ar} (67), CC _{ar} (14)	–	–	1125	1092	8.06	22.31	bCH _{ar} (51), CC _{ar} (32), NN(11)
36	–	1186	1208	1182	426.59	34.98	CC*(45), bCH(19), CO(12)	1058	1064	1098	1053	7.51	11.54	NN(36), CN(18), CC _{ar} (16), bCH _{ar} (15)
37	–	1172	1193	1166	0.97	9.41	bCH _{ar} (90)	–	1051	1079	1046	21.83	0.88	CC _{ar} (30), bCH _{ar} (18), CN(11), CC*(11), NN(10)
38	–	1159	1177	1147	14.14	47.37	CN(20), bNH(17), NN(17), bCH _{ar} (16)	1028	1028	1075	1033	1.83	9.43	CH ₃ ipr(47), CH ₃ ipb(26), tR1(10), CH ₃ opb(9)
39	1103	1097	1123	1101	28.78	31.11	bCH _{ar} (54), CC _{ar} (30)	–	–	1052	1023	12.79	1.09	CC _{ar} (47), R3trig(20), bCH _{ar} (19)

TABLE V-SM. Continued

No. <i>i</i>	IR	Raman	No scaling	Scaling ^a	A _i , IR ^b	I _i , Raman	PED %	IR	Raman	No scaling	Scaling ^a	A _i , IR ^b	I _i , Raman	PED %
40	1078	1073	1110	1081	46.73	16.16	R2trigd(31), bCH _{ar} (13), CC _{ar} (13)	1008	1001	1031	995	5.29	9.79	CC _{ar} (47), R3trigd(20), bCH _{ar} (19)
42	1049	1050	1074	1047	1.16	74.36	CC _{ar} (50), bCH _{ar} (28)	–	–	1001	982	0.18	0.31	gCH _{ar} (97)
43	–	1020	1064	1032	2.69	2.69	CH3ipr(45), CH3opb(43)	948	961	973	950	0.63	7.54	gCH _{ar} (96)
44	1027	–	1050	1026	70.03	12.92	NH ₂ ipr (36), CO(24), CC _{ar} (19)	–	945	959	934	9.24	42.09	gCH _{ar} (94)
45	1016	–	1033	1008	16.15	8.21	R3trigd(58), CC _{ar} (41)	911	907	932	908	5.35	1.93	gCH _{ar} (80)
46	1000	100	1018	996	0.62	94.90	CN(47), CH ₃ ipb(25), bCN1(13)	–	–	924	900	1.48	3.08	gCH _{ar} (26), CC _{ar} (16), R1b(12), R2trig(12), CCH ₃ (10)
47	–	–	997	991	1.23	12.51	gCH _{ar} (98)	854	848	857	829	27.73	3.41	gCH _{ar} (54), CC _{ar} (24)
48	–	971	977	970	0.02	0.97	gCH _{ar} (93)	821	816	854	826	29.44	1.31	gCH _{ar} (74), CC _{ar} (10)
49	959	955	957	948	6.55	0.28	gCH _{ar} (93)	764	753	778	759	38.98	5.69	gCO(62), gCC*(19), gN1H(11)
50	916	–	930	922	6.04	1.03	gCH _{ar} (86), gCN1(7)	752	733	769	750	24.68	1.46	gCH _{ar} (76), gC12N(16)
51	–	900	919	903	1.33	1.03	R2trigd(19), CC _{ar} (18), CCH ₃ (14), R1asym(13)	729	–	740	714	2.20	1.08	CC _{ar} (37), gCH _{ar} (21), R2trig(11), CN(10)
52	849	847	860	850	0.01	0.57	gCH _{ar} (100)	692	676	735	689	1.97	18.63	gCC _{ar} (42), tR1(20), gCCH ₃ (17), tR2asym(10)



TABLE V-SM. Continued

No. <i>i</i>	IR	Raman	No scaling	Scaling ^a	A _i , IR ^b	I _i , Raman	PED %	IR	Raman	No scaling	Scaling ^a	A _i , IR ^b	I _i , Raman	PED %
53	820	824	853	835	12.44	4.62	CC _{ar} (29), R2asym(15), CN(8), CC*(7)	680	–	712	680	11.81	1.91	R3sym(40),R1b(18), CN(14),CC _{ar} (12),bC C*(10)
54	796	792	799	766	42.15	3.01	gNH ₂ (52), gCC*(24), gNH ₂ (14)	668	662	694	663	19.23	1.87	gCH _{ar} (30),gC12N(26) ,CC _{ar} (12)
55	769	759	774	763	38.28	0.75	gCH _{ar} (75), gCN1(19)	654	649	671	644	4.37	3.63	CH ₃ opr(33),gCH _{ar} (27) ,gC12N(18)
56	746	743	764	744	2.74	0.14	bR1(43), gCC _{ar} (12), tR2sym(11), tR2asym(10)	633	629	658	637	14.45	1.81	bCO(38), gCH _{ar} (23), gC12N(18), bCC*(12), gN1H(10)
57	720	717	753	740	4.16	0.91	R2asym(57), CN(17), tCCO ₂ (11)	–	–	649	628	29.76	4.65	gN1H(54), gCC*(18), gCCH ₃ (10)
58	694	696	720	690	11.52	35.99	bCO ₂ (22), R2trigd(13), CC _{ar} (11), CO ₂ (10)	–	608	628	618	15.26	3.31	R3asym(56), gN1H(34)
59	686	676	707	683	58.87	1.06	gCH _{ar} (60), gCN1(37)	551	541	623	589	20.24	4.01	gCCH ₃ (30), tR1(26), gC12N(23), gN1H(19)
60	–	–	705	674	16.12	2.64	R3sym(34), R1trigd(13), CN(13), bCH _{ar} (11)	–	–	556	532	3.84	1.41	bC12N(22), gCH _{ar} (20), bCCH ₃ (13), tR3asym(10)
61	674	–	684	671	19.08	5.87	gCO ₂ (53), tR2asy(15), gCC*(10)	517	516	530	509	11.67	6.68	bCN'op(51), gCC*(20), gCO(18)

TABLE V-SM. Continued

No. <i>i</i>	IR	Raman	No scaling	Scaling ^a	<i>A_i</i> , IR ^b	<i>I_i</i> , Raman	<i>PED</i> %	IR	Raman	No scaling	Scaling ^a	<i>A_i</i> , IR ^b	<i>I_i</i> , Raman	<i>PED</i> %
62	–	–	657	644	61.94	1.19	bCO ₂ (27), bCNH ₂ (15), CCH ₃ (15), bCC*(11)	498	495	503	482	8.90	1.33	gC12N(24), tR3asym(20), bCCH3(11), gCH _{ar} (10)
63	651	651	653	633	2.60	0.19	CH ₃ opr(48), tCNH ₂ (17), tR1asym(15)	469	468	483	465	3.55	0.71	gC12N(21), bCO(13), tR3asym(13), gCH _{ar} (10)
64	626	623	644	625	2.65	1.26	tCNH ₂ (28), gCCH ₃ (18), tR1(16), gCN1(15)	448	–	466	452	7.37	8.25	bCN'inp(31), R2asym(21), bCC*(8)
65	–	608	631	623	5.02	5.38	R3asym(66), bCN1(10)	403	418	425	395	1.17	0.52	gC12N(26), gCC*(22), gCCH ₃ (20)
66	–	–	624	611	12.21	1.22	bCO ₂ (35), R2sym(18), bCN1(13)	388	–	418	383	1.81	0.81	bCO(43), R2sym(22), bCN'inp(10)
67	553	522	588	541	106.19	6.29	t2R(85)	–	404	402	380	2.89	1.81	tR3asym(47), gCH _{ar} (39)
68	524	506	526	514	5.38	2.81	gCN1(41), tR3asym(28), gCH _{ar} (15)	370	–	394	376	7.08	1.66	gCC _{ar} (44), bCO(33), tR3asy(22)
69	515	486	510	503	7.40	2.37	R2asym(25), bCCH ₃ (18), bCN1(11)	–	320	317	304	1.60	2.26	bC12N(37), CN(34), bCO(10)
70	487	435	485	477	1.04	2.03	R2asym(38), bCN1(18), bCO ₂ (11)	–	302	299	289	0.35	3.41	CN(36), bC12N(25), R2sym(19)



TABLE V-SM. Continued

No. <i>i</i>	IR	Raman	No scaling	Scaling ^a	<i>A_i</i> , IR ^b	<i>I_i</i> , Raman	<i>PED</i> %	IR	Raman	No scaling	Scaling ^a	<i>A_i</i> , IR ^b	<i>I_i</i> , Raman	<i>PED</i> %
71	431	423	439	424	0.03	7.91	bCO ₂ (25), bCNH ₂ (23), bCN1(11), CC*(10)	–	267	267	257	1.54	2.06	gCC*(39), gCC _{ar} (23), bCN'op(22)
72	421	415	431	423	3.56	2.28	gCC*(35), gNH ₂ (20), tR2sym(20)	–	248	239	225	1.55	2.34	tR3asym(37), bCCH ₃ (25), gCH _{ar} (13)
73	–	390	417	403	0.04	4.41	tR3sym(61), gCH _{ar} (19), tR3asym(19)	–	220	205	199	0.73	0.57	bCCH ₃ (53), tR3asym(23)
74	399	371	410	399	5.84	0.36	tCH ₃ (83)	–	159	204	192	1.21	0.48	gN1H(49), gCCH ₃ (30), t2R(16)
75	–	326	387	380	3.38	1.33	bCNH ₂ (29), R2sym(16), CN(11)	–	133	134	129	2.77	4.73	bCC*(43), bCN'inp(35)
76	–	–	338	332	7.78	1.59	bCN1(30), CN(15), bCNH ₂ (12), bCC*(10)	–	121	121	114	2.72	0.33	tCH ₃ (30), gCC*(15), gN1H(13), gC12N(11)
77	–	294	310	306	17.28	1.39	gCC*(29), gCC _{ar} (20), gCNH ₂ (15)	–	–	109	101	4.06	0.92	tCH ₃ (56), gN1H(18), gCC*(12)
78	–	280	287	282	1.77	3.82	bCN1(41), bCCH ₃ (17), CN(15)	–	–	92	86	0.18	0.25	gN1H(25), tR2asym(21), gC12N(20)
79	–	–	280	276	141.43	0.41	gCNH ₂ (48), tCNH ₂ (11), tR2sym(11)	–	–	76	72	1.35	5.60	bC12N(36), gC12N(22), tR2asym(14)

TABLE V-SM. Continued

No. <i>i</i>	IR	Raman	No scaling	Scaling ^a	<i>A_i</i> , IR ^b	<i>I_i</i> , Raman	<i>PED</i> %	IR	Raman	No scaling	Scaling ^a	<i>A_i</i> , IR ^b	<i>I_i</i> , Raman	<i>PED</i> %
80	–	221	239	234	0.52	4.66	bCC*(28), bCCH ₃ (21), R2sym(11), CN(11)	–	–	51	47	0.28	2.45	tC12N(58), gC12N(14), bC12N(12)
81	–	197	232	226	3.10	0.51	tR3asym(49), gCCH ₃ (18), gCH _{ar} (13)	–	–	41	39	0.34	8.38	tC12N(40), gC12N(26)
82	–	165	205	199	48.48	4.62	gCNH ₂ (48), tR3asym(19), gCC*(11)							
83	–	131	178	175	0.36	0.51	bCCH ₃ (34), bCC*(25), bCN1(17)							
84	–	–	132	128	0.01	4.62	gCC*(24), gCCH ₃ (15), gCC _{ar} (13)							
85	–	–	119	110	1.33	6.31	gCN1(21), tR3asym(16), tR2sym(11)							
86	–	–	104	103	0.37	0.76	bCN1(61), bCC*(15)							
87	–	–	88	86	0.36	0.66	gCN1(27), gCNH ₂ (25), tR2asym(22)							
88	–	–	68	63	5.46	1.26	gCNH ₂ (48), tCCO ₂ (44)							
89	–	–	39	38	1.56	0.35	tR2asym(22), gCNH ₂ (21), tR2sym(19), gCN1(15)							
90	–	–	8	8	0.15	2.83	tCN1(52), gCN1(15), gCNH ₂ (13), gCH _{ar} (11)							

Abbreviations used: R, ring; ss, symmetric stretching; as, antisymmetric stretching; ips, in-plane stretching; ops, out-of-plane stretching; b, bending; ipb, in-plane bending; opb, out-of-plane bending; ipr, in-plane rock; opr, out-of-plane rock; asy, asymmetric; sym, symmetric; symd, symmetric deformation; asymd, antisymmetric deformation; g, wagging; t, torsion; trig, trigonal; trigd, trigonal deformation; ^aFor optimized values of the scale factors applied, see Tables III and IV; ^bRelative absorption intensities normalised with the highest peak absorbance





J. Serb. Chem. Soc. 74 (5) 573–579 (2009)
JSCS–3856

A study of the electrochemical behaviour of methomyl on a gold electrode in a neutral electrolyte

ANDJELKA V. TOMAŠEVIĆ¹, MILKA L. AVRAMOVIĆ^{2*#}, SLOBODAN D. PETROVIĆ^{3,4#}, MIĆA B. JOVANOVIĆ³ and DUŠAN Ž. MIJIN^{3#}

¹Center for Pesticides and Environment Protection, Banatska 31b, Belgrade-Zemun,

²ICTM – Institute of Electrochemistry, University of Belgrade, Njegoševa 12, Belgrade,

³Faculty of Technology and Metallurgy, University of Belgrade, Karnegijeva 4, Belgrade and ⁴Hemofarm, Pharmaceutical and Chemical Industry, Vršac, Serbia

(Received 9 December 2008, revised 16 January 2009)

Abstract: A gold electrode was used for the qualitative and quantitative electrochemical determination of analytical methomyl in a neutral electrolyte (0.050 M NaHCO₃) using cyclic linear sweep voltammetry. In the potential range from –800 mV vs. SCE to 1000 mV vs. SCE the analytical methomyl was quantitatively determined in the concentration range 4.0–16 mg L⁻¹. In the potential range from –1300 mV vs. SCE to 1300 mV vs. SCE, methomyl was qualitatively determined by two anodic and four cathodic reactions. Cycling the potential in this range for 150 min caused the degradation of the molecule, which was confirmed by HPLC analysis. On the other hand, technical methomyl exhibited an inhibition of the gold electrode surface due to the impurities.

Keywords: insecticide; methomyl; gold electrode; cyclic voltammetry.

INTRODUCTION

Methomyl (Fig. 1) is a broad-spectrum thiocarbamate insecticide, which was introduced in 1966.¹ It is also used as an acaricide to control ticks and spiders, for foliar treatment of vegetable, fruit and field crops, cotton, commercial ornamentals, and in and around poultry houses and dairies. Furthermore, it is used as a fly bait.² Methomyl is effective in two ways: a) as a “contact insecticide” because it kills the target insects upon direct contact and b) as a “systemic insecticide” because of its capability to cause overall “systemic” poisoning of the target insects, after it is absorbed and transported throughout pests that feed on the treated plants. It is capable of being absorbed by plants without being “phyto-toxic” or harmful to the plant. It is a very toxic and hazardous compound and an

* Corresponding author. E-mail: milka@tmf.bg.ac.rs

Serbian Chemical Society member.

doi: 10.2298/JSC0905573T

environmental pollutant of concern because of its high solubility in water (57.9 g/L at 25 °C).³

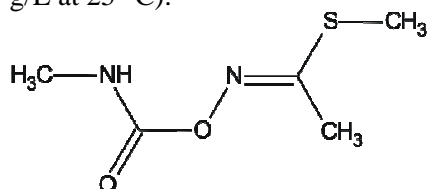


Fig. 1. Structure of methomyl; IUPAC name: *S*-methyl-*N*-(methylcarbamoyloxy) thioacetimidate.

Different thiocarbamate herbicides were the subject of electrochemical studies using different electrodes.^{4–9} Methomyl and aldicarb were detected by fast scan differential voltammetry with a hanging Hg drop electrode.⁴ Later, the electrochemical behaviour of methomyl was studied using d.c. and a.c. polarography, differential pulse polarography and cyclic voltammetry in ethanol–water mixtures. It was found that methomyl undergoes irreversible four-electron reductions.⁵ Mogyoródy^{6–8} published the results of studies of the electrochemical degradation of several thiocarbamates in NaCl solution using a Pt electrode. Pulsed amperometric detection at a gold electrode was used for the separation of eight pesticides in reversed-phase liquid chromatography, including methomyl.⁹ Current–potential curves were obtained by cyclic voltammetry at a gold, rotating-disc electrode in 50 % (v/v) acetonitrile in acetate buffer.

In studies of the degradation of organic compounds¹⁰ and the electrochemical behaviour of physiologically active compounds,^{11–13} a study the electrochemical behaviour of methomyl was included. Analytical and technical methomyl were used in order to develop an electrochemical method for the qualitative and quantitative determination of methomyl. Methomyl was examined at a gold electrode in a neutral electrolyte using cyclic linear sweep voltammetry. HPLC was used for analysing the bulk electrolyte during the electrochemical reactions.

EXPERIMENTAL

Analytical methomyl (99.8 %, analytical standard) and technical methomyl (98 %) were obtained from DuPont. Before each experiment, a fresh solution of methomyl in 0.050 M NaHCO₃ (methomyl concentration = 16 mg L⁻¹) was prepared. The solution was added directly into the cell and than purged with nitrogen during each experiment.

The NaHCO₃ used as the supporting electrolyte was of analytical grade (Merck). The solutions were prepared with 18 MΩ water. Standard equipment and a three electrode electrochemical cell were used for the cyclic voltammetry measurements, as previously described in detail.^{12–13} Polycrystalline gold (surface area 0.50 cm²), which served as the working electrode, was polished with diamond paste and cleaned with a mixture of 18 MΩ water and sulphuric acid. A platinum wire was employed as the counter electrode and a saturated calomel electrode (SCE) as the reference electrode. All the potentials are given vs. SCE. The electrode surface was controlled by cyclic voltammetry before each experiment. Prior to the control of the electrode surface and before the addition of methomyl, the electrolyte was purged with nitrogen. All the experiments were performed at room temperature.

The characteristics of the HPLC instrument were as follows: HPLC Instrument GBC, pump LC 1120, UV-Vis detector LC 1205, operating at 234 nm, manual injector RHEODYNE 7725i, column ZORBAX Eclipse XDB-C8 (4.6 mm×150 mm, 5 μ m), mobile phase acetonitrile–water (25:75, flow rate 1.0 cm³ min⁻¹).

RESULTS AND DISCUSSION

The reactivity of methomyl (analytical and technical) was investigated on a gold electrode in 0.050 M NaHCO₃ by cyclic voltammetry. On a gold electrode, in the potential range from -800 mV vs. SCE to 1000 mV vs. SCE, the analytical methomyl exhibited one anodic and two cathodic reactions and the observed anodic reaction was later used for its quantitative determination. In the potential range from -1300 mV vs. SCE to 1300 mV vs. SCE, methomyl exhibited two anodic and four cathodic reactions (Fig. 2). The potential was cycled in this range for 150 min in order to follow any possible changes of these anodic and cathodic reactions with time. It is obvious from Fig. 2 that the anodic peak at 1200 mV vs. SCE increased with time from 0.46 mA cm⁻² (first cycle) to 0.80 mA cm⁻² at the end of the cycling. The anodic peak, which appeared at the beginning of oxide formation at the gold electrode, at 600 mV vs. SCE was slightly higher and shifted 30 mV to more negative potential values at the end of the cycling. The four cathodic peaks remained unchanged during the cycling.

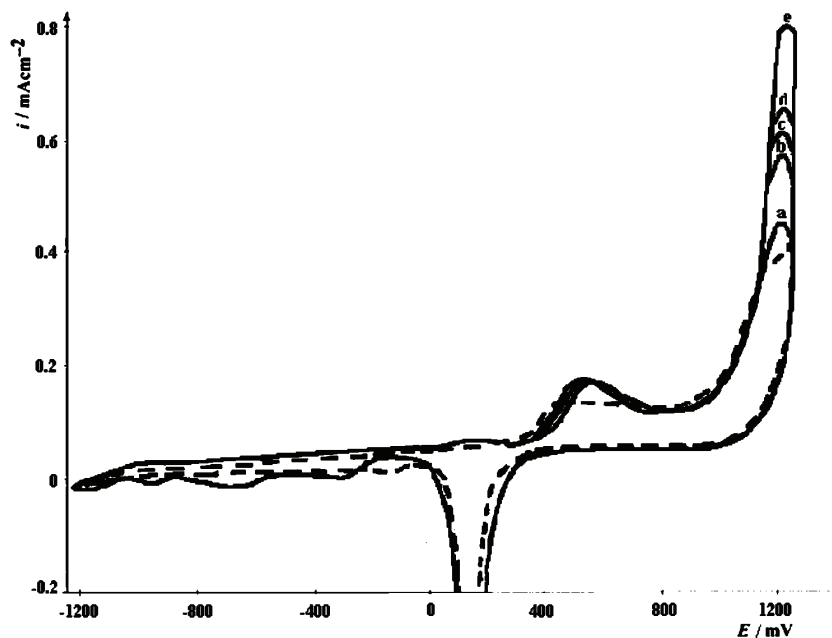


Fig. 2. Cyclic voltammogram of an Au electrode in 0.050 M NaHCO₃ (dashed line) and in the presence of the methomyl solution (concentration 16 mg L⁻¹) in 0.050 M NaHCO₃ (full line; a, 0; b, 30; c, 60; d, 90; e, 150 min of continuous cycling); sweep rate: 50 mV s⁻¹.

The observed reactions presented in Fig. 2 indicate the degradation of the methomyl molecule in 0.050 M NaHCO₃. In order to check this assumption, HPLC analysis was performed before the electrochemical experiment and after 30, 60, 90 and 150 min of potential cycling under the conditions presented in Fig. 2. The results of the HPLC analysis are presented in Figs. 3 and 4. Fig. 3 shows the change in the methomyl concentration given as normalized concentrations (c/c_0 , where c is the methomyl concentration at time t and c_0 is the initial methomyl concentration) vs. time, while Fig. 4 represents the HPLC chromatogram. As can be seen, the starting molecule, which represents the analytical product, contained only small amounts of impurities. The HPLC analysis showed a small decrease in the methomyl concentration after the electrochemical reactions (less than 6 %).

As mentioned previously, pulsed amperometric detection at a gold electrode was used for the separation of eight pesticides, including methomyl, in reversed-phase liquid chromatography, and the anodic reaction at the beginning of oxide

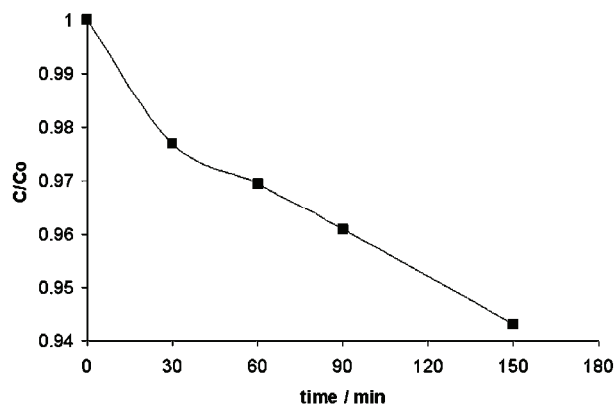


Fig. 3. Change in the methomyl concentration during potential cycling.

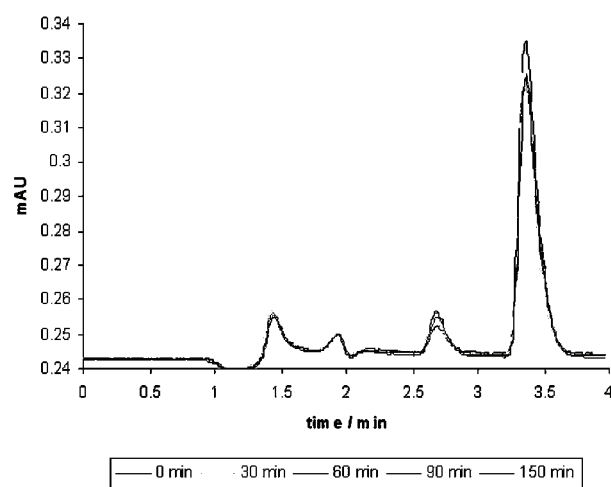


Fig. 4. HPLC chromatogram of the methomyl solution during potential cycling.

formation was used for the quantitative determination.⁹ The limit of detection for methomyl was found to be below $80 \mu\text{g cm}^{-3}$ (80 mg L^{-1}).

On the gold electrode, in the potential range from -800 to 1000 mV vs. SCE , the anodic reaction which commences at the beginning of oxide formation was used for the quantitative determination of the analytical methomyl. This range of the potential was selected in order to avoid apparent methomyl degradation at 1200 mV and two cathodic reactions in the potential range from -800 to -1300 mV .

The voltammogram presented in Fig. 5 shows that each investigated methomyl concentration gives only one very clear, wide and reproducible anodic peak in the concentration range $4\text{--}16 \text{ mg L}^{-1}$, which followed a linear relationship corresponding to the equation:

$$i_{\text{pa}} / \text{mA cm}^{-2} = 183.8 \pm 2.9 \times 10^{-3} + 3.9 \pm 0.2 \times 10^{-3} c / \text{mg cm}^{-3} \quad (1)$$

$$r = 0.9953$$

This type of the equation was successfully applied for the quantitative determination of different small concentrations of macrolide antibiotics on a gold^{14,15} and on a glassy carbon electrode.^{15–17}

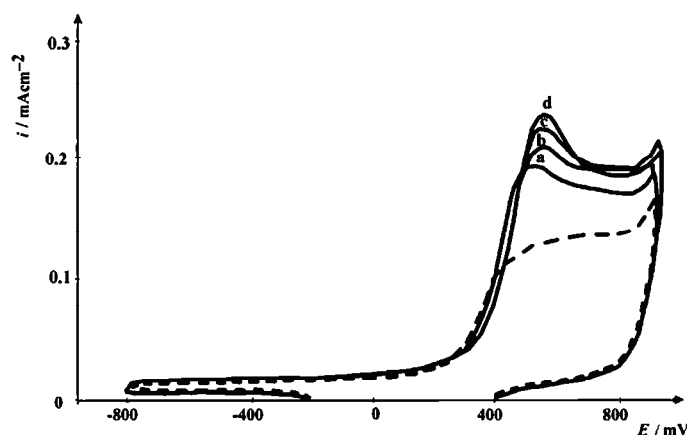


Fig. 5. Cyclic voltammogram of an Au electrode in 0.050 M NaHCO_3 (dashed line) and in the presence of the methomyl solution ($4\text{--}16 \text{ mg L}^{-1}$) in 0.050 M NaHCO_3 (full line; a, 4; b, 8; c, 12; d, 16 mg L^{-1}); sweep rate: 50 mV s^{-1} .

The obtained relationship can be used for the quantitative determination of analytical methomyl at lower concentrations in comparison to the literature value.⁹ The selected concentration range was based on the methomyl concentrations used in a previous study,¹⁰ in which the reaction of methomyl photodegradation was followed by UV spectroscopy. The standard error of the correlation was found to be 2.37×10^{-3} , while the standard deviation and the error of the measurements were 2.13×10^{-3} and $6.15 \times 10^{-4} \text{ mA cm}^{-2}$, respectively. This relationship is also given in Fig. 6.

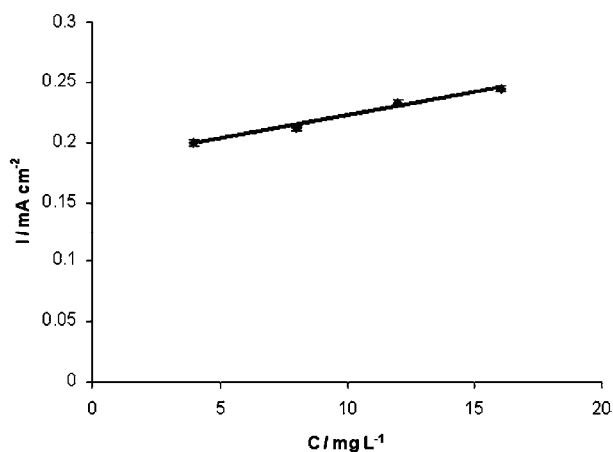


Fig. 6. Dependency of the peak current value of the oxidation peak of the analytical methomyl at 600 mV vs. SCE in 0.050 M NaHCO₃ at a scan rate of 50 mV s⁻¹, from the data presented in Fig. 5, as a function of the concentration in the range of 4–16 mg L⁻¹.

On the other hand, when technical methomyl was subjected to the same experimental conditions, an inhibition was observed due to the presence of impurities.

CONCLUSIONS

A gold electrode was successfully employed for the qualitative and quantitative electrochemical determination of analytical methomyl in a neutral electrolyte (0.050 M NaHCO₃) using cyclic linear sweep voltammetry. In the potential range from –800 to 1000 mV vs. SCE, the analytical methomyl was quantitatively determined in the concentration range 4–16 mg L⁻¹. In the potential range from –1300 to 1300 mV vs. SCE, methomyl exhibited two anodic and four cathodic reactions and its electrochemical treatment for 150 min showed the disappearance of the molecule. HPLC analysis of the bulk of electrolyte showed a decrease of the methomyl concentration because of the electrochemical reactions which had occurred. The same experiments could not be performed with the technical methomyl due to the inhibition effect of impurities present in such a product.

Acknowledgments. The authors are grateful to the Ministry of Science and Technological Development for the financial support (project 142063).

ИЗВОД

ПРОУЧАВАЊЕ ЕЛЕКТРОХЕМИЈСКОГ ПОНАШАЊА МЕТОМИЛА НА ЕЛЕКТРОДИ ОД ЗЛАТА У НЕУТРАЛНОМ ЕЛЕКТРОЛИТУ

АНЂЕЛКА В. ТОМАШЕВИЋ¹, МИЛКА Л. АВРАМОВ ИВИЋ², СЛОБОДАН Д. ПЕТРОВИЋ^{3,4}, МИЋА Б. ЈОВАНОВИЋ³ и ДУШАН Ж. МИЛИН³

¹Центар за пестициде и заштитну животне средине, Банајска 316, Београд-Земун, ²ИХТМ – Центар за електрохемију, Њеѓошева 12, Београд, ³Технолошко–металуршки факултет, Карнегијева 4, Београд и

⁴Хемофарм група, Фармацеутска и хемијска индустрија, Вршац

У раду су дати резултати испитивања електрохемијског понашања активности метомила (аналитичког и техничког производа) на електроди од злата у неутралном електролиту (0,050 М NaHCO₃). HPLC је коришћена за анализу електролита у току електрохемијске ре-

акције. Максимална вредност висине струјног врха oksidacije čistog metomila на 600 mV према ЗКЕ у 0,050 M NaHCO₃ на 50 mV s⁻¹ је линеарна функција његове концентрације у опсегу 4–16 mg L⁻¹ што је омогућило развијање методе за његово квантитативно одређивање. Аналитички метомил је квалитативно одређен детекцијом репродуктивне четири анодне и једне катодне реакције у опсегу потенцијала од –1300 до 1300 mV према ЗКЕ. Потенцијал је циклизиран 150 min у наведеном опсегу и анализа анодних и катодних реакција на почетку, у току и на крају циклизирања потенцијала је указала на деградацију молекула метомила. Током циклизирања потенцијала, HPLC анализа електролита је показала смањење концентрација метомила као последицу његове деградације. Технички метомил није погодан за испитивање под наведеним условима јер присутне нечистоће инхибирају површину електроде.

(Примљено 9. децембра 2008, ревидирано 16. јануара 2009)

REFERENCES

1. W. J. Hayes, *Handbook of Pesticide Toxicology, Classes of Pesticides*, Vol. 3, E. R. Laws, Ed., Academic Press Inc., NY, 1990
2. R. E. Gosselin, R. P. Smith, H. C. Hodge, *Clinical toxicology of commercial products*, 5th Ed., MD Williams and Wilkins, Baltimore, PA, 1984
3. C. D. S. Tomlin, *The Pesticide Manual*, 13th ed., BCPC Publications, Alton, 2003, p. 650
4. V. Stara, M. Kopanica, *Coll. Czech. Chem. Comm.* **49** (1984) 1282
5. M. Subbalakshamma, M. Sreedhar, N. V. Jyothi, J. Damodar, S. J. Reddy, *Trans. SAEST* **34** (1999) 35; *CAN* 131: 239094
6. F. Mogyorody, *J. Appl. Electrochem.* **36** (2006) 635
7. F. Mogyorody, *J. Appl. Electrochem.* **36** (2006) 765
8. F. Mogyorody, *J. Appl. Electrochem.* **36** (2006) 773
9. A. Ngoviwatchai, D. C. Johnson, *Anal. Chim. Acta* **215** (1988) 1
10. A. Tomašević, G. Bošković, D. Mijin, E. Kiss, *React. Kin. Catal. Lett.* **91** (2007) 53
11. M. L. Avramov Ivić, S. D. Petrović, D. Ž. Mijin, *J. Serb. Chem. Soc.* **72** (2007) 1424
12. M. L. Avramov Ivić, S. D. Petrović, F. Vonmoos, D. Ž. Mijin, P. M. Živković, K. M. Drljević, *Electrochem. Comm.* **9** (2007) 1643
13. M. L. Avramov Ivić, S. D. Petrović, D. Ž. Mijin, F. Vanmoos, D. Ž. Orlović, D. Ž. Marjanović, V. V. Radović, *Electrochim. Acta* **54** (2008) 649
14. M. L. Avramov Ivić, S. D. Petrović, D. Ž. Mijin, P. M. Živković, I. M. Kosović, K. M. Drljević, M. B. Jovanović, *Electrochim. Acta* **51** (2006) 2407
15. R. Greaf, R. Peat, R. L. Peter, D. Pletcher, J. Robinson, *Instrumental Methods in Electrochemistry*, Ellis Horwood, Chichester, 1985, p. 178
16. B. Nigović, *Analyt. Sci.* **20** (2004) 640
17. B. Nigović, B. Simunić, *J. Pharm. Biomed. Anal.* **32** (2003) 97.



J. Serb. Chem. Soc. 74 (5) 581–593 (2009)
JSCS–3857

Electro-oxidation of ascorbic acid catalyzed on cobalt hydroxide-modified glassy carbon electrode

GHASEM KARIM-NEZHAD^{1*}, MOHAMMAD HASANZADEH¹,
LOTFALI SAGHATFOROUSH¹, NASRIN SHADJOU¹,
BALAL KHALILZADEH² and SOHRAB ERSHAD³

¹Department of Chemistry, Faculty of Science, Payame Noor University, P.O. Box 58168-45164, Khoy, ²Department of Chemistry, Faculty of Science, Arak University, Arak and ³Department of Chemistry, Faculty of Science, Payame Noor University, Marand, Iran

(Received 15 July, revised 8 December 2008)

Abstract: The electrochemical behavior of ascorbic acid on a cobalt hydroxide modified glassy carbon (CHM–GC) electrode in alkaline solution was investigated. The process of the involved oxidation and its kinetics were established using the cyclic voltammetry, chronoamperometry techniques, as well as by steady state polarization measurements. The results revealed that cobalt hydroxide promotes the rate of oxidation by increasing the peak current; hence ascorbic acid is oxidized at lower potentials, which is thermodynamically more favorable. The cyclic voltammograms and chronoamperometry indicate a catalytic EC mechanism is operative with the electrogeneration of Co(IV) as the electrochemical process. Also, the process is diffusion-controlled and the current–time responses follow Cottrellian behavior. This result was confirmed by steady state measurements. The rate constants of the catalytic oxidation of ascorbic acid and the electron-transfer coefficient are reported.

Keywords: ascorbic acid; electrocatalysis; modified electrode; alkaline media; cyclic voltammetry; chronoamperometry.

INTRODUCTION

The electrochemical modification of electrodes with a suitable reagent has been widely used for analytical applications. The resulting electrodes were designed to provide the desired selective sites towards the analytes. Electrochemically modified electrodes have played an important role in the studies of electrocatalysis,^{1–4} electron transfer kinetics,^{5,6} membrane barriers,^{7,8} electro-organic synthesis,⁹ etc. One of the most important electrode modification techniques involves the formation of an electrocatalytic system on to the electrode sur-

* Corresponding author. E-mail: g.knezhad@gmail.com
doi: 10.2298/JSC0905581K

face in which redox species are capable of undergoing a rapid and reversible electrode reaction are incorporated. These electrodes reduce the overpotential required for either oxidation or reduction of compounds. Many mixed valent compounds, such as oxides, complexes, or alloys of copper,^{10–12} cobalt^{13–15} and ruthenium^{16–18} exhibit electrocatalytic properties.

Ascorbic acid (AA) is a powerful antioxidant naturally present in many foods, especially fruits and vegetables, and plays an important role in the prevention of infectious diseases. Apart from its vitamin activity, ascorbic acid is frequently used in the food industry as an antioxidant to prevent undesirable changes in color, taste and odor. Due to its biological and technological importance, it is of great interest in the food field to have rapid and sensitive methods for its routine and reliable determination.

The direct electrochemical oxidation of ascorbic acid is possible but requires high overpotentials, the equilibrium potential of the couple is -0.185 V vs. SCE¹⁹ but its oxidation at bare glassy carbon or platinum electrodes requires potentials of 0.40 and 0.60 V vs. SCE, respectively. These high overpotentials result in electrode fouling, poor reproducibility, low selectivity and poor sensitivity and thus this technique is rarely employed analytically. The poor reproducibility of direct electrochemical oxidation of ascorbic acid has led to interest in the use of mediators and modified electrodes to catalyze the electrochemical oxidation of ascorbic acid.

Recently, a cobalt hydroxide modified glassy carbon (CHM–GC) electrode was used for the electrocatalytic oxidation of carbohydrates²⁰ and hydrazine.²¹ The present study is an attempt aimed at inspecting the kinetics and mechanisms of electrochemical processes on application of modified electrodes. The findings of this study show the results of the anodic oxidation of ascorbic acid on a glassy carbon surface on which catalytically active cobalt hydroxide had been deposited. The studies were performed in 100 mM sodium hydroxide solution.

EXPERIMENTAL

All employed chemicals were of analytical grade from Merck (Darmstadt, Germany) and used without further purification. All solutions were prepared with doubly distilled water. The electrochemical measurements were performed in a conventional three-electrode cell powered by an electrochemical system comprising an Autolab system with PGSTAT12 boards (Eco Chemie, Utrecht, The Netherlands). The system was run on a PC using GPES 4.9 software. A saturated calomel electrode (SCE) was the reference electrode. All potentials were measured with respect to the SCE, which was positioned as close to the working electrode as possible by means of a luggin capillary. Films of cobalt hydroxide were formed on the GC electrode with surface area 0.125 cm² by the method previously reported by Casella.²² The modified electrodes were prepared by cycling the potential of the working electrode in the range of -250 to 750 mV vs. SCE at a scan rate of 100 mV s⁻¹ for 70 cycles. The surface concentration of cobalt hydroxide which was controlled by the number of cycles applied to the deposition process was electrochemically evaluated in 100 mM NaOH solution. Prior to the modification,

the GC electrode was polished with a 0.05 μm alumina suspension on a polishing micro-cloth and rinsed thoroughly with doubly distilled water. Working standard solutions were obtained by appropriate dilution of the stock standard solution in an appropriate volume of 100 mM sodium hydroxide solution (which was also used as the supporting electrolyte), and then stored in the dark at 4 $^{\circ}\text{C}$. All experiments were performed at ambient temperature 22 ± 3 $^{\circ}\text{C}$.

RESULTS AND DISCUSSION

Cyclic voltammetry

Seventy-five consecutive cyclic voltammograms (CV) of a GC electrode in the presence of 100 mM Na_2CO_3 + 40 mM NaK tartrate + 4.0 mM CoCl_2 at pH 11.6, recorded at a potential sweep rate of 100 mV s^{-1} , are presented in Fig. 1A. The voltammograms are similar to those reported in literature.^{22,23} A cyclic voltammogram of the CHM-GC electrode in 100 mM NaOH solution in the range of -200 to 690 mV, recorded at a potential sweep rate of 100 mV s^{-1} , is shown in Fig. 1B. It consists of anodic peaks located at 225 and 550 mV vs. SCE, which were attributed to Co(II)/Co(III) and Co(III)/Co(IV) redox transitions associated with different cobalt oxide species on the electrode surface^{24,25}. The cathodic

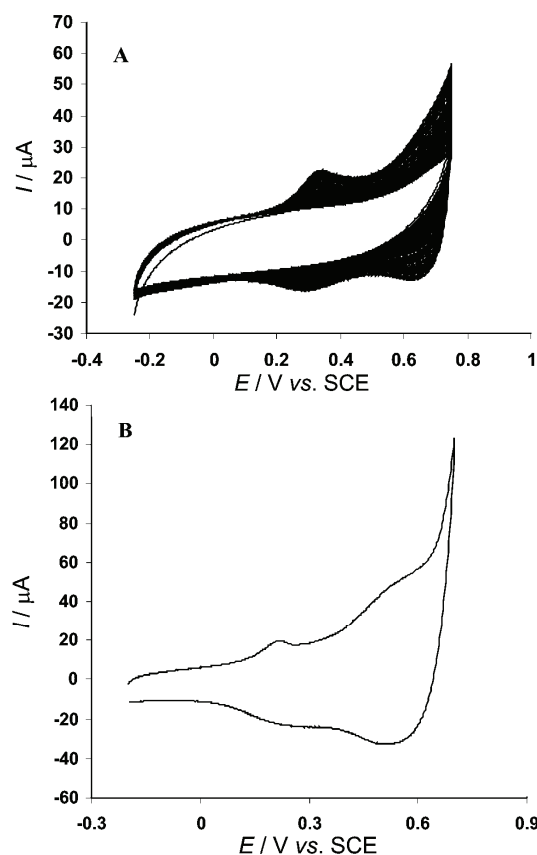


Fig. 1. Cyclic voltammograms for 4.0 mM CoCl_2 + 40 mM NaK tartrate + 100 mM Na_2CO_3 using a GC electrode. The potential was scanned continuously at 100 mV s^{-1} between -250 and 750 mV (A); cyclic voltammogram of CHM-GC in 100 mM NaOH solution in the range of -200 to 690 mV at a sweep rate 100 mV s^{-1} (B).

peaks at 186 and 522 mV correspond to the reduction of various cobalt oxide species formed during the positive sweep.

Typical CVs of a CHM-GC electrode in 100 mM NaOH solution at various potential sweep rates from 2.0–150 mV s^{-1} are presented in Fig. 2A. The peak currents were proportional to the sweep rates in the range 2.0–75 mV s^{-1} , as

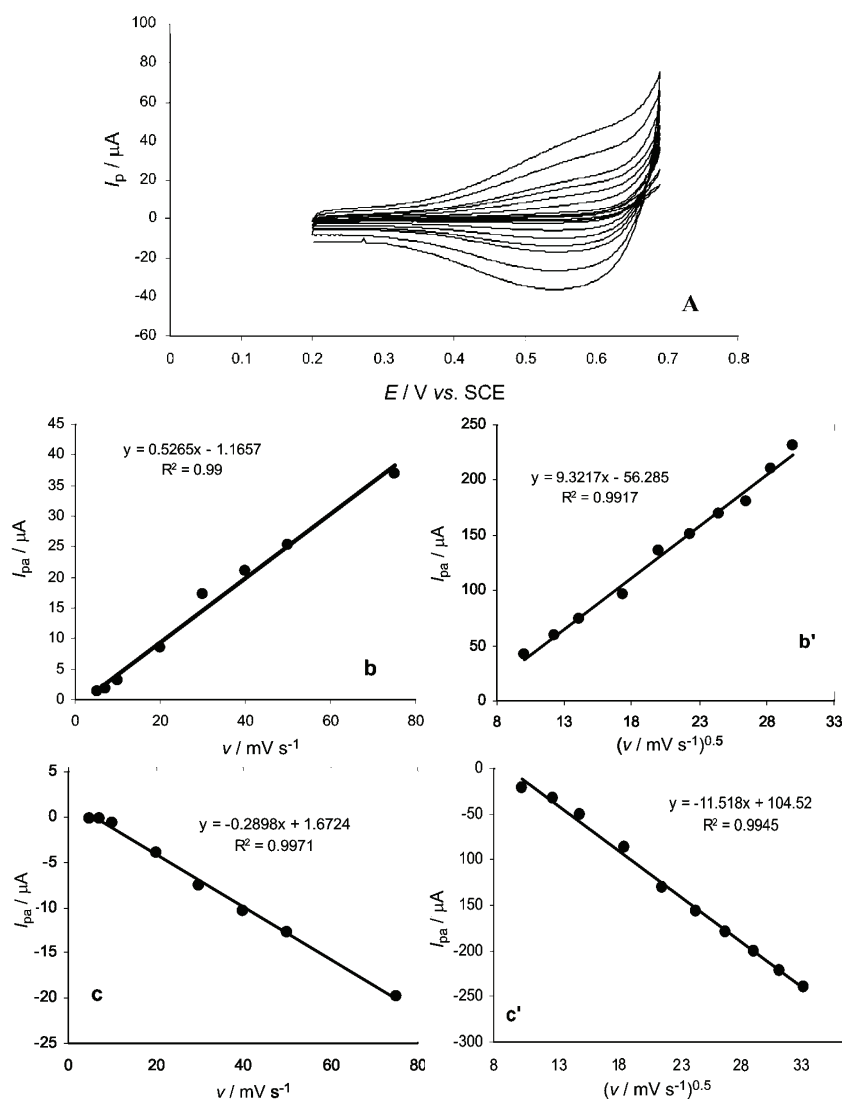


Fig. 2. Typical cyclic voltammograms of a CHM-GC electrode in 100 mM NaOH at potential sweep rates of 2, 5, 7, 10, 20, 30, 40, 50, 75, 100, 150 mV s^{-1} (A); the dependence of the anodic (b) and cathodic (c) peak currents on the sweep rate at lower values (2.0–75 mV s^{-1}) and the proportionality between the anodic (b') and cathodic (c') peak currents and the square root of sweep rate at higher values (100–900 mV s^{-1}).

shown in Figs. 2b and 2c, indicating the electrochemical activity of the surface redox couple. From the slope of both lines and using:

$$I_p = \left(\frac{n^2 F^2}{4RT} \right) \nu A \Gamma^* \quad (1)$$

where Γ^* is the surface coverage of the redox species and ν the potential sweep rate²⁶, and taking the average of both the cathodic and anodic results, Γ^* values of around $1.98 \times 10^9 \text{ mol cm}^{-2}$ were derived. In all the range of sweep rates, this dependency is of square root form, as shown in Figs. 2b' and 2c', signifying the dominance of diffusion controlled processes.

The CVs of a freshly prepared CHM-GC in 100 mM NaOH solution in the presence of ascorbic acid at various potential sweep rates in the range 2–300 mV s^{-1} are shown in Fig. 3A. As the scan rate increases, the anodic peak potentials shift to positive and the cathodic peak potentials are converted to a slightly negative

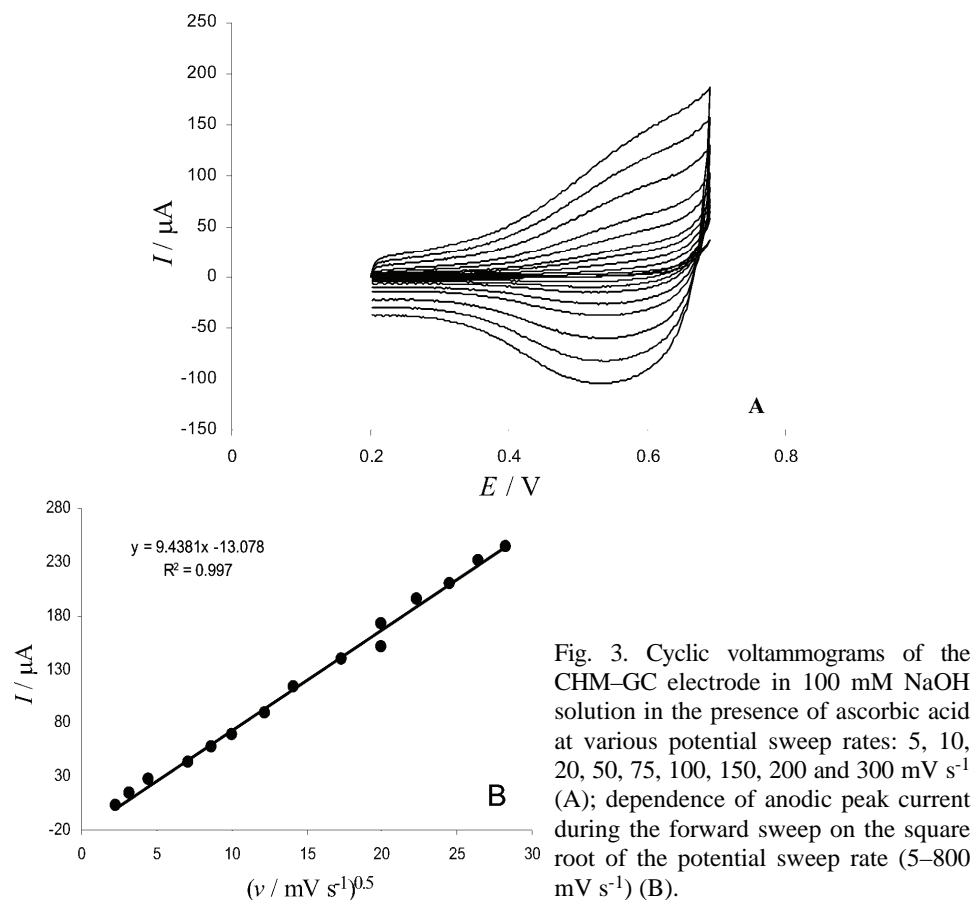


Fig. 3. Cyclic voltammograms of the CHM-GC electrode in 100 mM NaOH solution in the presence of ascorbic acid at various potential sweep rates: 5, 10, 20, 50, 75, 100, 150, 200 and 300 mV s^{-1} (A); dependence of anodic peak current during the forward sweep on the square root of the potential sweep rate (5–800 mV s^{-1}) (B).

direction. Figure 3B indicates the plot of the anodic peak current against the square root of the scan rate. As can be seen, the anodic peak current is linearly proportional to $v^{1/2}$, showing the dominance of a diffusion-controlled process.

Upon increasing the ascorbic acid concentration, its irreversible oxidation developed in the region of the electrochemical formation of Co(IV), as can be seen from Fig. 4. Thus, it is likely that electro-generated Co(IV) species is the active moiety, which efficiently accelerates the oxidation of ascorbic acid. Any increase in the concentration of ascorbic acids causes a proportional and almost linear enhancement of the anodic wave. It is worth emphasizing that the anodic formation of Co(IV) seems to be an irreversible process. Also, plotting the current function (peak current divided by the square root of the potential sweep rate) against the square root of the potential sweep rate (Fig. 5) revealed a negative slope, confirming the electrocatalytic nature of the process.

Based on the reported results, the following mechanism can be proposed for the mediated oxidation of ascorbic acid on the modified surface. The correspond-

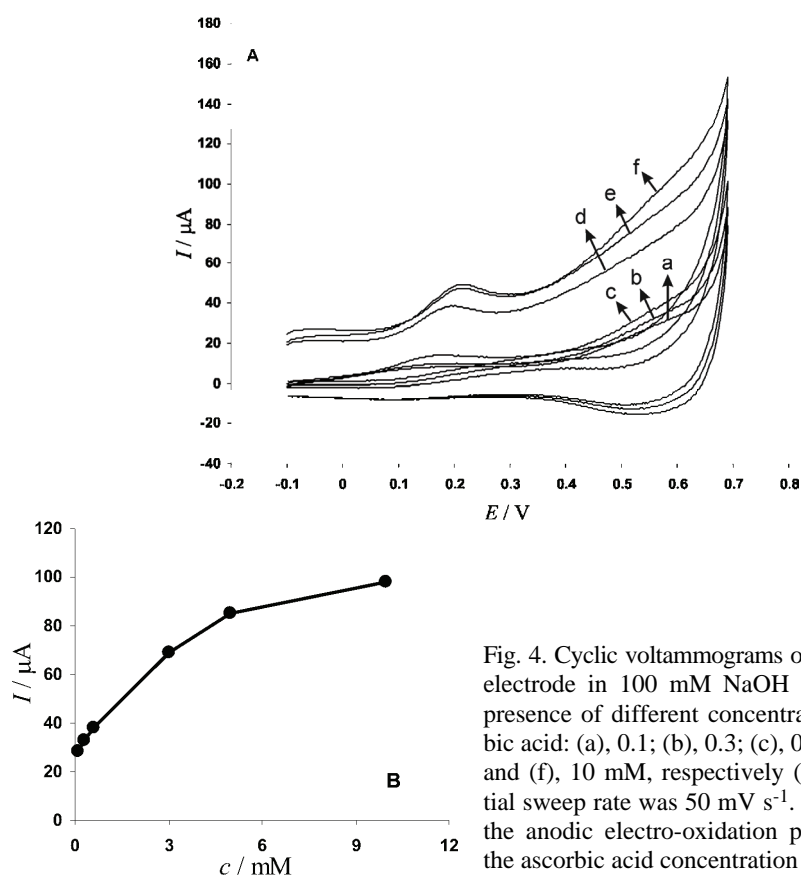
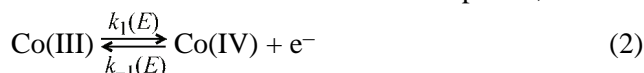


Fig. 4. Cyclic voltammograms of the CHM-GC electrode in 100 mM NaOH solution in the presence of different concentrations of ascorbic acid: (a), 0.1; (b), 0.3; (c), 0.6; (d), 3; (e), 5 and (f), 10 mM, respectively (A). The potential sweep rate was 50 mV s^{-1} . Dependency of the anodic electro-oxidation peak current on the ascorbic acid concentration (B).

ing kinetics is also formulated. The redox transition of the cobalt species,



where the intermediate is further oxidized to the product through a similar electro-oxidation process:

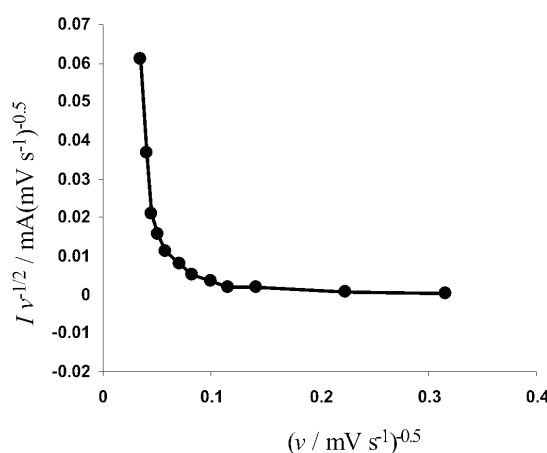


Fig. 5. $Iv^{-1/2}$ vs. $v^{0.5}$ for 100 mM NaOH solution in the presence of 0.20 mM ascorbic acid.

Chronoamperometry

Chronoamperograms were recorded by setting the working electrode potential to the desired values and measuring the catalytic rate constant on the CHM-GC electrode surface. The chronoamperograms for the CHM-GC electrode in the absence (curve a) and presence (curves b–f) of ascorbic acid over the concentration range of 0.20–10 mM are shown in Fig. 6A. The applied potential step was 586 mV. Plotting the net current vs. the minus square root of time gives a straight line (Fig. 6B). This indicates that a diffusion-controlled process is dominant for electro-oxidation of ascorbic acid, as was demonstrated previously using cyclic voltammetry (Fig. 3).

The rate constants of the reactions of ascorbic acid and the ensuing intermediates with the redox sites of the CHM-GC electrode can be derived from the chronoamperograms according to:²⁷

$$\frac{I_{\text{catal}}}{I_d} = \lambda^{1/2} \left[\pi^{1/2} \text{erf}(\lambda^{1/2}) + \frac{\exp(-\lambda)}{\lambda^{1/2}} \right] \quad (5)$$

where I_{catal} is the catalytic current in the presence of ascorbic acid, I_d the limiting current in the absence of ascorbic acid and $\lambda = kct$ (where k , c and t are the catalytic rate constant, the bulk concentration of ascorbic acid and the elapsed

time, respectively) is the argument of the error function. For $\lambda > 1.5$, $\text{erf}(\lambda^{1/2})$ almost equals unity and Eq. (5) reduces to:²⁵

$$\frac{I_{\text{catal}}}{I_d} = \lambda^{1/2} \pi^{1/2} = \pi^{1/2} (kct)^{1/2} \quad (6)$$

From the slope of the I_{catal}/I_d vs. $t^{1/2}$ plot, as shown in Fig. 6C, the value of k was estimated as $2.36 \times 10^6 \text{ cm}^3 \text{ mol}^{-1} \text{ s}^{-1}$. It should be pointed out that k is either k_2 or k_3 (see reactions (3) and (4)), whichever is smaller.

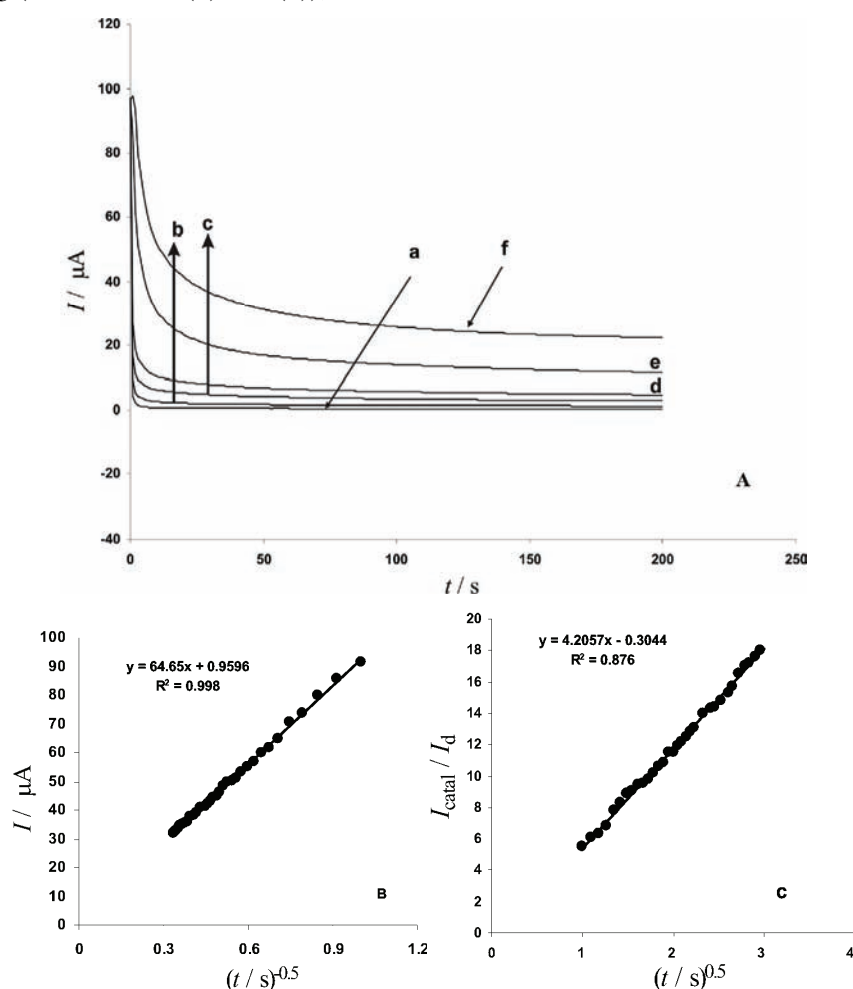


Fig. 6. Chronoamperograms of the CHM–GC electrode in the absence (a) and the presence of (b), 0.20; (c), 0.60; (d), 1.0; (e), 5.0 and (f), 10 mM ascorbic acid in 100 mM NaOH solution (A). The potential step was 586 mV; dependency of the transient current on $t^{0.5}$ (B). Dependence of I_{catal}/I_d on $t^{0.5}$ derived from the data of the chronoamperograms of (a) and (e) in the main panel (C).

*Steady state polarization*²⁸

The rate laws for the reactions (2) and (3) have the forms:

$$v_1 = k_1 \Gamma \theta_{\text{III}} - k_{-1} \Gamma \theta_{\text{IV}} \quad (7)$$

$$v_2 = k_2 \Gamma \theta_{\text{IV}} c \quad (8)$$

where Γ is the total number of adsorption sites per unit area of the electrode surface, the θ represents the fractional surface coverage of different cobalt valence states and c is the bulk concentration of ascorbic acid. With only the 3 and 4 valence states of cobalt prevailing, then:

$$\theta_{\text{III}} + \theta_{\text{IV}} = 1 \quad (9)$$

and the rates of changes of their surface coverage, as well as that of the intermediate compounds are:

$$\frac{d\theta_{\text{III}}}{dt} = -\frac{d\theta_{\text{IV}}}{dt} = -k_1 \theta_{\text{III}} + k_{-1} \theta_{\text{IV}} + k_2 \theta_{\text{IV}} c + k_3 \theta_{\text{IV}} c_i \quad (10)$$

$$\frac{dc_i}{dt} = k_2 \theta_{\text{IV}} c - k_3 \theta_{\text{IV}} c_i \quad (11)$$

where c_i is the concentration of the intermediate.

Assuming that the steady state dominates:

$$\frac{d\theta_{\text{III}}}{dt} = -\frac{d\theta_{\text{IV}}}{dt} = 0 \quad (12)$$

$$\frac{dc_i}{dt} = 0 \quad (13)$$

the values of the coverage are given by:

$$\theta_{\text{III}} = \left(\frac{k_{-1} + 2k_2 c}{k_1 + k_{-1} + 2k_2 c} \right) \quad (14)$$

$$\theta_{\text{IV}} = \left(\frac{k_1}{k_1 + k_{-1} + 2k_2 c} \right) \quad (15)$$

and subsequently:

$$v_1 = \left(\frac{2k_1 \Gamma k_2 c}{k_1 + k_{-1} + 2k_2 c} \right) \quad (16)$$

Based on this rate equation, the Faradic current will be:

$$i_f = \left(\frac{2FAk_1 \Gamma k_2 c}{k_1 + k_{-1} + 2k_2 c} \right) \quad (17)$$

where A is the surface area of the electrode and the rate constants k_1 and k_{-1} are obviously potential-dependent and are of the forms:

$$k_1(E) = k_1^0 \exp\left[\frac{\alpha nFE}{RT}\right] \quad (18)$$

$$k_{-1}(E) = k_{-1}^0 \exp\left[\frac{(\alpha - 1)nFE}{RT}\right] \quad (19)$$

where k_1^0 and k_{-1}^0 are the chemical rate constants measured at E vs. SCE = 0, α is the anodic transfer coefficient and the other parameters have their usual meaning. Equation (17) is well suited for the calculation of rate constants and is the validity test of the kinetics and mechanism of the oxidation process.

The pseudo-steady state polarization curves of the electro-oxidation of ascorbic acid on the CHM-GC electrode at a number of ascorbic acid concentrations are presented in Fig. 7. The oxidation process was found to begin at nearly 520 mV vs. SCE and reach a plateau at 590 mV vs. SCE, while oxygen evolution commenced at still higher potentials. In the course of reaction, the coverage of Co(IV) increases and reaches a saturation (steady state) level and the oxidation current follows accordingly. According to Eq. (17), plots of the inverse of current against the inverse ascorbic acid concentration should be linear:

$$i_f^{-1} = (FAk_1\Gamma)^{-1} + \left[\frac{k_1 + k_{-1}}{2FAk_1k_2\Gamma}\right]c^{-1} \quad (20)$$

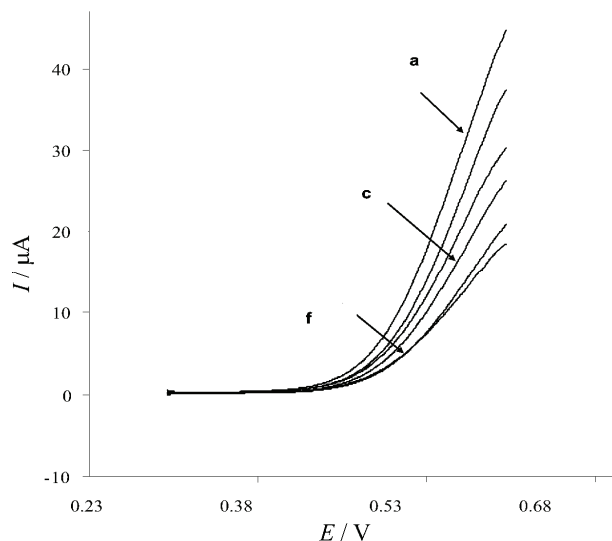


Fig. 7. Typical pseudo-steady state polarization curves of the CHM-GC electrode obtained in (a), 10; (b), 5.0; (c), 3.0; (d), 1.0; (e), 0.40 and 0.10 (f) mM ascorbic acid.

The i_f^{-1} vs. c_m^{-1} dependencies are presented in Fig. 8A, from which it can be seen that straight lines at various potentials were obtained. Both the intercepts

and slopes of the straight lines appearing in this figure were potential dependent. The slopes were plotted against $\exp(-nFE/RT)$ with $n = 1$ and the obtained graph is presented in Fig. 8B. Using this graph together with Eq. (20), it was found that the rate constant of reaction 3, $k_2\Gamma$, and the ratio of k_{-1}^0/k_1^0 are 4.13×10^{-11} and $2.01 \times 10^{10} \text{ cm s}^{-1}$, respectively. The variation of the intercepts of the lines in Fig. 8A with the applied potential on a semi-log scale is presented in Fig. 8C. Using this graph and Eq. (20), the magnitudes of $k_1^0\Gamma$, $2.26 \times 10^{-16} \text{ mol s}^{-1} \text{ cm}^{-2}$, and the anodic transfer coefficient, 0.64, were obtained. From the above findings, the value of $k_{-1}^0\Gamma$ was calculated to be $4.54 \times 10^{-6} \text{ mol s}^{-1} \text{ cm}^{-2}$.

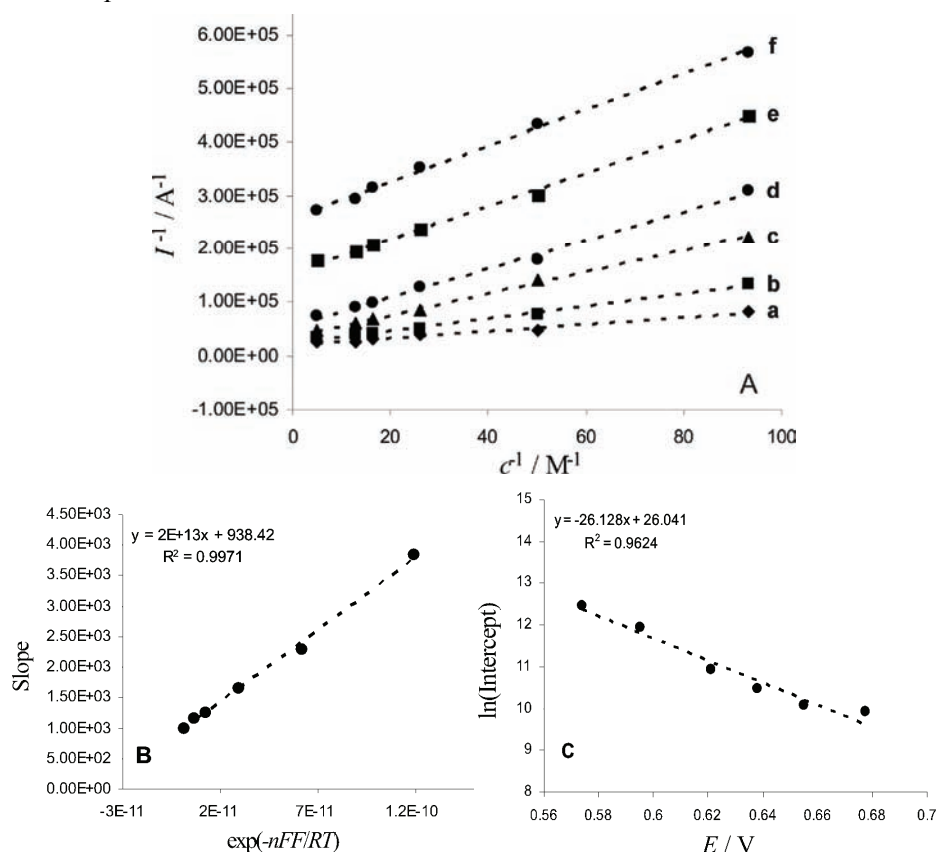


Fig. 8. Plot of i^{-1} (from the polarization curves in Fig. 6) against C_m^{-1} at various potentials: 574, 559, 616, 638, 659 and 680 mV vs. SCE, curves a–f, respectively (A); plot of the slopes of the curves in (a) vs. $\exp(-nFE/RT)$ (B); plot of the \ln (intercepts) of the curves in (a) vs. the applied potential (C).

The results obtained for ascorbic acid on a cobalt hydroxide modified glassy carbon electrode are compared in Table I with those previously reported for

cyclohexanol on a copper electrode.²⁸ It can be seen that the catalytic properties are comparable.

TABLE I. Comparison of the catalytic properties of Co(IV) on the cobalt hydroxide-modified electrode with the catalytic properties of Cu(III) species on a copper electrode

Property	Electrode	
	Copper	Cobalt hydroxide modified glassy carbon electrode
Mediator	Cu(III)	Co(IV)
Compound	Cyclohexanol	Ascorbic acid
$k_2\Gamma / \text{cm s}^{-1}$	8.74×10^{-12}	4.13×10^{-11}
k_{-1}^0/k_1^0	2.10×10^7	2.01×10^{10}
$k_{-1}^0\Gamma / \text{mol s}^{-1} \text{cm}^{-2}$	1.91×10^{-13}	2.26×10^{-16}
$k_{-1}^0\Gamma / \text{mol s}^{-1} \text{cm}^{-2}$	4.01×10^{-5}	4.54×10^{-6}

CONCLUSIONS

A cobalt hydroxide film was formed electrochemically in a regime of cyclic voltammetry on a glassy carbon electrode and checked for the electro-oxidation of ascorbic acid in alkaline media. The modified electrode showed electrocatalytic activity for the oxidation of ascorbic acid at around 565 mV *vs.* SCE. Using the cyclic voltammetry and chronoamperometry techniques and also steady-state polarization measurements, the kinetic parameters, such as charge transfer coefficient (α) and the catalytic reaction rate constant (k) for oxidation of ascorbic acid were determined. Moreover, the cobalt hydroxide glassy carbon electrode can be used for the determination of real samples. The kinetics of the reaction based on the reported mechanism was developed and the magnitudes of the rate constants and anodic transfer coefficient of the electro-oxidation reaction were obtained.

ИЗВОД

КАТАЛИЗА ЕЛЕКТРОХЕМИЈСКЕ ОКСИДАЦИЈЕ АСКОРБИНСКЕ КИСЕЛИНЕ НА СТАКЛАСТОМ УГЉЕНИКУ МОДИФИКОВАНОМ КОБАЛТ-ХИДРОКСИДОМ

GHASEM KARIM-NEZHAD¹, MOHAMMAD HASANZADEH¹, LOTFALI SAGHATFOROUSH¹, NASRIN SHADJOU¹, BALAL KHALILZADEH² и SOHRAB ERSHAD³

¹Department of Chemistry, Faculty of Science, Payame Noor University, P.O. Box 58168-45164, Khoy,

²Department of Chemistry, Faculty of Science, Arak University, Arak u ³Department of Chemistry, Faculty of Science, Payame Noor University, Marand, Iran

Испитивано је електрохемијско понашање аскорбинске киселине у алкалној средини на електроди од стакластог угљеника модификованој кобалт-хидроксидом. Кинетика реакције је одређена коришћењем цикличне волтаметрије, хроноамперометрије и стационарних поларизационих мерења. Резултати показују да кобалт-хидроксид убрзава реакцију оксидације тако да се она одиграва на нижим потенцијалима. Циклична волтаметрија и хроноамперометрија су показале да се реакција одиграва по ЕС механизму са генерисањем Co(IV) врсте као електрохемијским ступњем. Процес је дифузионо контролисан и зависност струје од времена прати Котрелову једначину. Овај резултат је такође потврђен стационарним полариза-

ционим мерењем. Одређене су вредности константе брзине каталитичке оксидације аскорбинске киселине и коефицијента прелаза.

(Примљено 15. јула, ревидирано 8. децембра 2008)

REFERENCES

1. Y. Xie, S. Dong, *Electroanalysis* **6** (1994) 119
2. B. Nalini, S. S. Narayanan, *Anal. Chim. Acta* **405** (2000) 93
3. D. Leech, J. Wang, M. R. Shysmith, *Analyst* **115** (1990) 1447
4. S. Dong, G. J. Che, *J. Electroanal. Chem.* **309** (1991) 103
5. F. M. Hawdridge, I. Taniguchi, *Comm. Inorg. Chem.* **17** (1995) 163
6. A. S. Praximos, H. Günther, D. J. M. Schoneddings, H. Simon, *Bioelectrochem. Bioenerg.* **25** (1991) 425
7. A. Nelson, *Anal. Proc.* **28** (1991) 64
8. J. Wang, T. Golden, *Anal. Chem.* **61** (1989) 1397
9. K. K. Shiu, O. Y. Chan, S. K. Pang, *Anal. Chem.* **67** (1995) 2828
10. V. E. M. Filho, A. L. B. Marques, J. J. Zhang, G. O. Chierice, *Electroanalysis* **11** (1999) 1130
11. N. Chebotareva, T. J. Nyokong, *Appl. Electrochem.* **27** (1997) 975
12. Y. Lei, F. C. Anson, *Inorg. Chem.* **34** (1995) 1083
13. Q. Xiaohe, R. P. Baldwin, *J. Electrochem. Soc.* **143** (1996) 1283
14. J. Wang, P. V. A. Pamidi, C. Parrade, D. S. Park, J. Pingerron, *Electroanalysis* **9** (1997) 908
15. S. A. Wring, J. P. Hard, B. J. Birch, *Anal. Chim. Acta* **229** (1990) 63
16. M. E. G. Lyons, C. A. Fitzgerald, *Analyst* **119** (1994) 855
17. B. Nalini, S. S. Narayanan, *Electroanalysis* **10** (1998) 779
18. E. G. Cookeas, C. E. Efstathiou, *Analyst* **125** (2000) 1147
19. R. M. C. Dawson, D. C. Elliott, W. H. Elliott, K. M. Jones, *Data for Biochemical Research*, Oxford Science Publications, Clarendon Press, Oxford, 1986
20. G. Karim-Nezhad, M. Hasanzadeh, L. Saghatforoush, N. Shadjou, S. Earshad, B. Khalilzadeh, *J. Brazilian Chem. Soc.* **20** (2009) 141
21. M. Hasanzadeh, G. Karim-Nezhad, N. Shadjou, B. Khalilzadeh, L. Saghatforoush, S. Earshad, I. Kazeman, *Chinese J. Chem.*, in press
22. I. G. Casella, *J. Electroanal. Chem.* **520** (2002) 119
23. M. Jafarian, M. G. Mahjani, H. Heli, F. Gobal, H. Khajehsharifi, M. H. Hamed, *Electrochim. Acta* **48** (2003) 3423
24. C. Barbero, G. A. Planes, M. C. Miras, *Electrochem. Commun.* **3** (2001) 113
25. S. Bruckenstein, M. Shay, *Electrochimica Acta* **30** (1985) 851
26. A. J. Bard, L. R. Faulkner, *Electrochemical Methods*, Ch. 12, Wiley, New York, 2001
27. A. J. Bard, L. R. Faulkner, *Electrochemical Methods*, Wiley, New York, 2001, p. 503
28. M. Hasanzadeh, G. Karim-Nezhad, M. G. Mahjani, M. Jafarian, N. Shadjou, B. Khalilzadeh, L. A. Saghatforoush, *Catal. Commun.* **10** (2008) 295.



J. Serb. Chem. Soc. 74 (5) 595–605 (2009)
JSCS–3858

Characteristics of Cu–Al₂O₃ composites of various starting particle size obtained by high-energy milling

VIŠESLAVA RAJKOVIĆ*, DUŠAN BOŽIĆ and MILAN T. JOVANOVIĆ

Institute of Nuclear Sciences "Vinča", P.O. Box 522, 11001 Belgrade, Serbia

(Received 9 December 2008)

Abstract: The powder Cu–Al₂O₃ composites were produced by high-energy milling. Various combinations of particle size and mixtures and approximately constant amount of Al₂O₃ were used as the starting materials. These powders were separately milled in air for up to 20 h in a planetary ball mill. The copper matrix was reinforced by internal oxidation and mechanical alloying. During the milling, internal oxidation of pre-alloyed Cu-2 mass %-Al powder generated 3.7 mass % Al₂O₃ nano-sized particles finely dispersed in the copper matrix. The effect of different size of the starting copper and Al₂O₃ powder particles on the lattice parameter, lattice distortion and grain size, as well as on the size, morphology and microstructure of the Cu–Al₂O₃ composite powder particles was studied.

Keywords: Cu–Al₂O₃ composite powders; high-energy milling; size of the starting powder particles.

INTRODUCTION

The copper-based matrix obtained by powder metallurgy (PM) techniques and reinforced applying the process of mechanical alloying has been extensively studied in recent years.^{1–4} The application of mechanical alloying as a method for obtaining a uniform distribution of dispersoids in a copper matrix accompanied with a fine-grained microstructure greatly improves the properties of such copper-based composites. The particle size of both the matrix alloy and the strengthening powders determines to a large extent many of the final properties of the produced PM compacts.

In this study, the copper matrix was reinforced with Al₂O₃ particles by internal oxidation and mechanical alloying. The effects of both the copper and Al₂O₃ particles size on the lattice distortion and grain size, as parameters with a considerable effect on the process of the sintering of copper-based composites,⁴ were the subject of this investigation. At the same time, the influence of these

* Corresponding author. E-mail: visnja@vinca.rs
doi: 10.2298/JSC0905595R

parameters on the evolution of the morphology and the microstructure of the Cu-based composite powder particles was also studied.

EXPERIMENTAL

Inert gas-atomized, pre-alloyed copper powder containing 2 mass %-Al and different mixtures of electrolytic copper powders and Al₂O₃ particles served as the starting materials for this investigation. The characteristics of the pre-alloyed copper powder and the powder mixtures used in this study are given in Table I. The starting powders are characterized by the same or different copper and Al₂O₃ powder particle size. These powders were separately milled in air for up to 20 h in a planetary ball mill. The weight ratio of the powder to steel balls was 1:35.

TABLE I. Size of the starting copper and Al₂O₃ powder particles

Material	Size of pre-alloyed copper particles and size of copper particles, μm	Size of Al ₂ O ₃ particles, μm	Designation
Pre-alloyed Cu-2 mass %-Al	30	0.010	Cu-2Al
Cu-4 mass %-Al ₂ O ₃	30	0.75	Cu-4Al ₂ O ₃
Cu*-4 mass %-Al ₂ O ₃	15	0.75	Cu*-4Al ₂ O ₃

*After internal oxidation⁸

The milled powders were characterized by X-ray diffraction analysis (XRD) using a Siemens D-500 X-ray powder diffractometer with CuK_α Ni-filtered radiation. The lattice parameters were determined using the least square root method. The average lattice distortion, *i.e.*, the relative deviation of the lattice parameters from their main value ($\Delta d/d$)⁵ and the grain size (*D*) were determined from the broadening (β) of the first four diffraction lines (111, 200, 220 and 311) using the approach developed by Williamson and Hall:⁶

$$\beta \cos \theta = \frac{k\lambda}{D} + \frac{k\Delta d}{d} \sin \theta \quad (1)$$

where the shape factor $k = 0.9$ and the radiation wave length, $\lambda = 0.15405$ nm.

The microstructure of the treated powders was characterized by light microscopy using a Zeiss Axiovert 25 microscope and scanning electron microscopy (SEM) using a Philips XL30 instrument. Samples for light microscopy were mounted in an acrylic resin. Polishing was performed using the standard procedure and a mixture of 5 g FeCl₃ and 50 ml HCl in 100 ml distilled water was used for etching.

RESULTS AND DISCUSSION

Change of powder particles parameters

During milling of the pre-alloyed Cu-2Al powder, the lattice parameter decreased with milling time, whereas the lattice parameters of the other starting powder mixtures slightly increased (Fig. 1). The decrease in the Cu-2Al lattice parameter results from the oxidation of the aluminum during internal oxidation, which precipitates from pre-alloyed copper forming a fine dispersion of Al₂O₃. The decrease in the lattice parameter was rapid during the first 10 h of milling but become slower with prolonged milling. This indicates that the most of alu-

minum precipitates from the copper matrix at the beginning of the milling process due to facilitation of the oxidation process through the severe deformation of the copper matrix in this period of milling. The difference in the lattice parameter of the pre-alloyed Cu–2Al powders before ($a_{\text{Cu-2Al}} = 0.3624$ nm) and after 20 h of milling ($a_{\text{Cu-2Al}} = 0.36167$ nm) is 0.20 %. This difference is similar to the difference (0.24 %) in the theoretical lattice parameters of the pre-alloyed powder ($a_{\text{Cu-2Al}} = 0.36210$ nm) and the copper powder ($a_{\text{Cu}} = 0.36150$ nm), indicating that after 20 h of milling almost all the aluminum had been precipitated from the copper matrix. Assuming that the complete amount of aluminum was oxidized, it was calculated that 3.7 mass % of Al₂O₃ was generated by internal oxidation of 2 mass % Al in the copper matrix. This result shows that the amount of the strengthening particles was kept nearly constant in pre-alloyed copper and the powder mixtures, being around 4 mass % Al₂O₃. On the other hand, the slight increase of the lattice parameters of the mixtures containing Al₂O₃ particles might be the result of contamination of the copper matrix with steel balls debris during milling.⁷

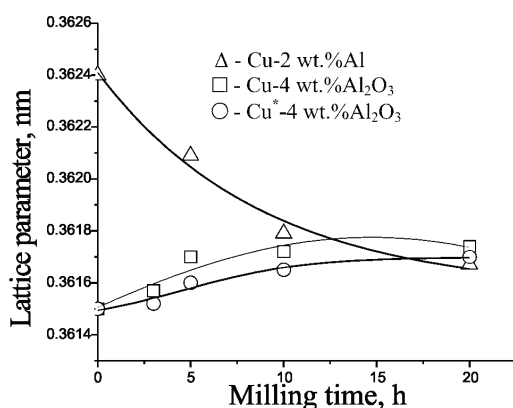


Fig. 1. Lattice parameter vs. milling time for pre-alloyed copper powder and copper Al₂O₃ powder mixtures.

The full width at half maximum (FWHM) height measured from X-ray the diffraction patterns of the examined powders showed a progressive line broadening with milling time (Figs. 2a–2c). From Figs. 2a and 2b, it may be seen that the FWHM of the pre-alloyed Cu–2Al powder strengthened with 0.01 μm Al₂O₃ particles (Fig. 2a) were higher than those of a mixture of Cu–4Al₂O₃ with an average Al₂O₃ particle size of 0.75 μm (Fig. 2b; the size of the copper powder ≈ 30 μm). The FWHM of the Cu*–4Al₂O₃ mixture (Fig. 2c; size of copper powder ≈ 15 μm) were significantly higher than the FWHM of Cu–4Al₂O₃. The higher FWHM of the Cu*–4Al₂O₃ sample implies that the starting size of copper powder particles had a great influence on the FWHM during the milling process. The separate diagram (Figs. 3a and 3b) shows that the values of the FWHM of Cu*–4 Al₂O₃ were slightly higher than those of Cu–2Al. These results suggest

that the influence of the smaller starting copper powder particles (15 μm) on the FWHM prevails over the effect of the Al_2O_3 particles size.

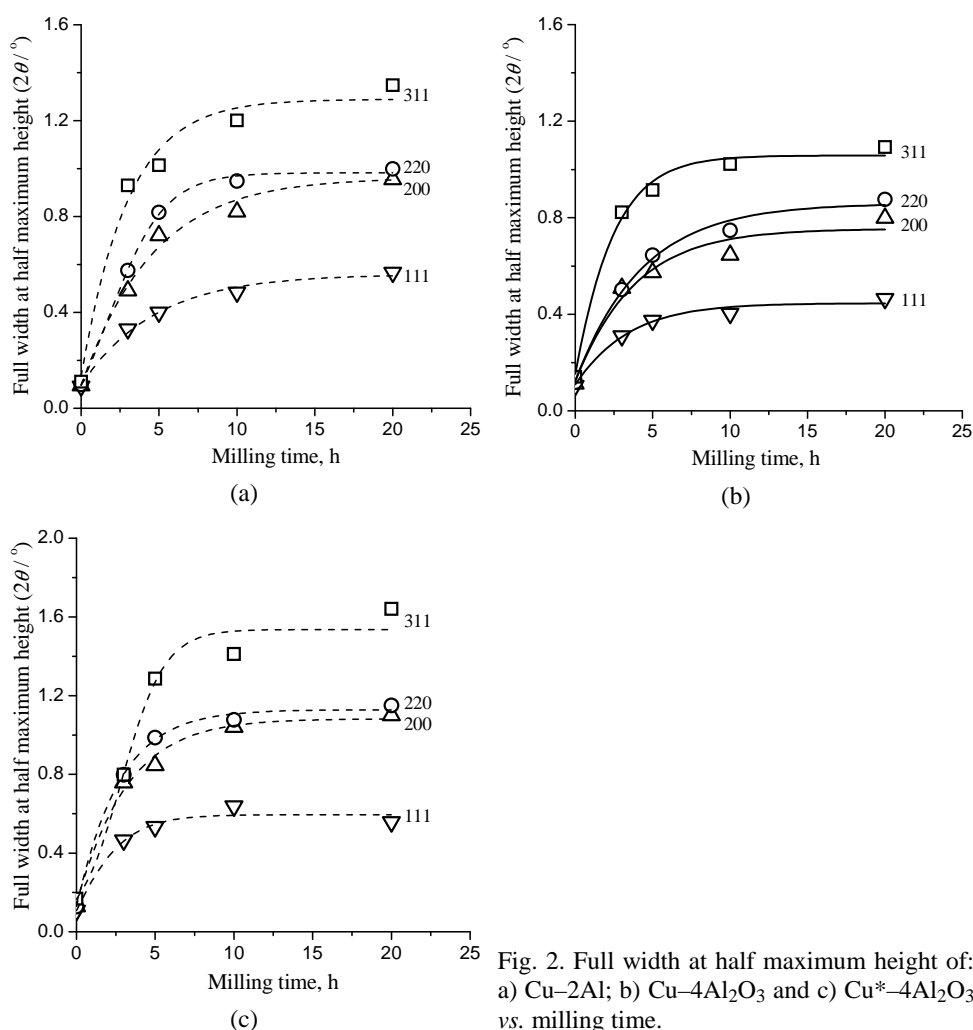


Fig. 2. Full width at half maximum height of: a) Cu-2Al; b) Cu-4Al₂O₃ and c) Cu*-4Al₂O₃ vs. milling time.

The progress in the broadening of the FWHM with milling time is a result of a severe lattice distortion and grain size refinement.⁹ Lattice distortion and grain size are important parameters of milled powders since they have a significant effect on both compacting the powders during the sintering process and the properties of the finely dispersed strengthened copper matrix. Lattice distortion normally increases with milling time. However, there are exceptions to this behavior and some literature results claim that the lattice distortion may decrease during milling.⁹ The results of this study show that the lattice distortion increased with time of milling (Fig. 4), being the highest in the powder mixture Cu-2Al

strengthened with very small Al₂O₃ particles, whereas the lowest lattice distortion was observed in the powder mixture Cu*–4Al₂O₃. According to the results in Fig. 4, it is obvious that the lattice distortion decreased with decreasing particle size of the starting copper powders. The presence of smaller Al₂O₃ strengthening particles increased the lattice distortion, *i.e.*, very small (0.01 μm) Al₂O₃ particles caused higher lattice distortion than the coarse (0.75 μm) particles. These changes of lattice distortion are probably due to polygonized dislocation structures of the highly deformed small particles during high-energy milling.¹⁰ The smallest distortions in the Cu*–4Al₂O₃ powders suggest that the dislocations formed during milling of small copper powder particles due to the very low amount of stored elastic energy are arranged in configurations that reduce the strain energy. However, in the case of such small-sized powders, a contributing factor to the low strain energy due to partial amorphization of the powders¹⁰ cannot be excluded, in spite of the fact that the diffraction peaks remained sharp up to 20 h of milling, as in the present case.

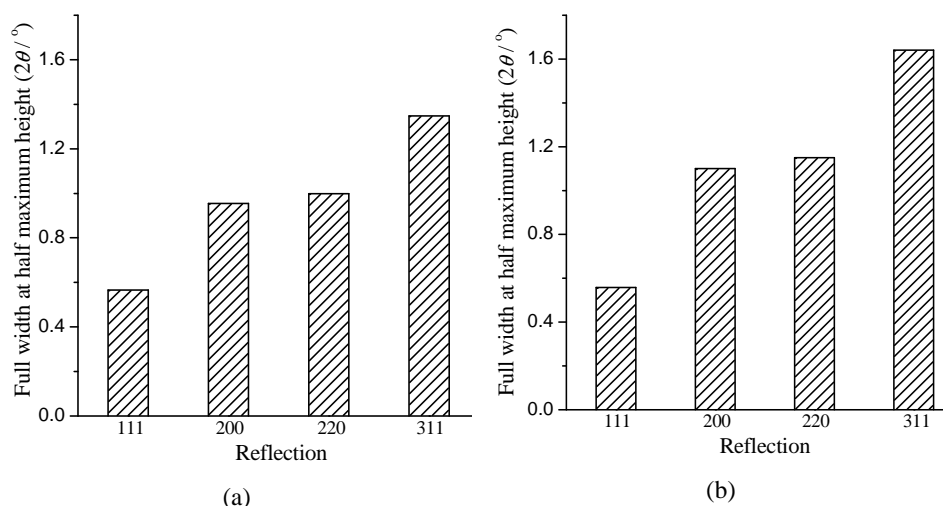


Fig. 3. Full width at half maximum (FWHM) height of: a) Cu–2Al and b) Cu–4 Al₂O₃ after 20 h of milling.

In view of these facts, the results presented in Figs. 3a and 3b and Fig. 4 should not be regarded as contradicting. Namely, the slightly higher values of the FWHM of the Cu*–4Al₂O₃ powders compared to those of Cu–2Al may be considered from the view that the influence of grain refinement on the FWHM surmounts not only the effect of the Al₂O₃ particle size, but also the decreasing influence of the elastic strain energy on the lattice distortion of Cu*–4Al₂O₃ powders.

The size of the grains, *i.e.*, the crystallites, formed inside the powder particles during milling abruptly decreased with milling time (Fig. 5). This decrease

was the highest up to 5 h of milling, when the grain size was between 30 and 40 nm. After 20 h of milling, the grain size was slightly changed, ranging between 20 and 30 nm, except for the grain size of Cu*–4Al₂O₃ powders, for which the grain size was somewhat smaller, *i.e.*, 15 nm. This result is in accordance with the FWHM results (see Figs. 3a and 3b). Generally, the smallest grain size found in the Cu*–4Al₂O₃ mixture may be ascribed to the fact that smaller powder particles are more easily subjected to higher deformation during milling than coarser particles.

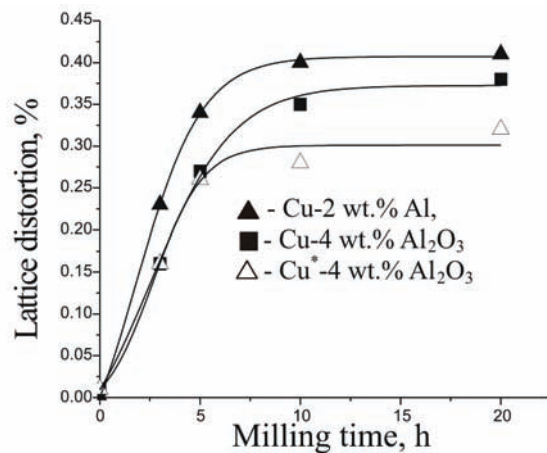


Fig. 4. Effect of milling time on the lattice distortion.

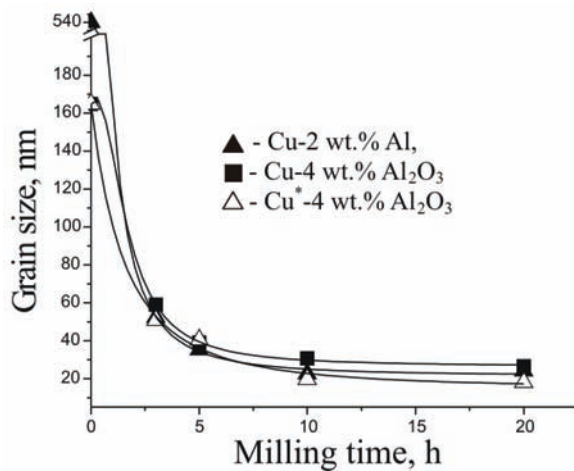


Fig. 5. Effect of milling time on the grain size.

Size, morphology and microstructure of the composite powders

The composite powder particles formed from the starting powders change their morphology, size and microstructure during high-energy milling as a consequence of repeated deformation, fracture and welding processes. Generally, at the beginning of milling, the average particle size of composite powders in-

creases until welding of the particles powders dominates the milling process, but the size of particles starts to decrease when the fracture process prevails. In the case of balance of fracture and welding processes, the particles are rather uniform in size and similar in shape.

SEM microphotographs showing the morphology of the composite powder particles after 5 and 20 h of milling are presented in Figs. 6a–6c and Figs. 6d–6f, respectively. Detailed observations of the morphology and particle size showed that the composite powders based on pre-alloyed powders and mixtures had a different size and morphology after 5 h of milling, Figs. 6a–6c. The composite

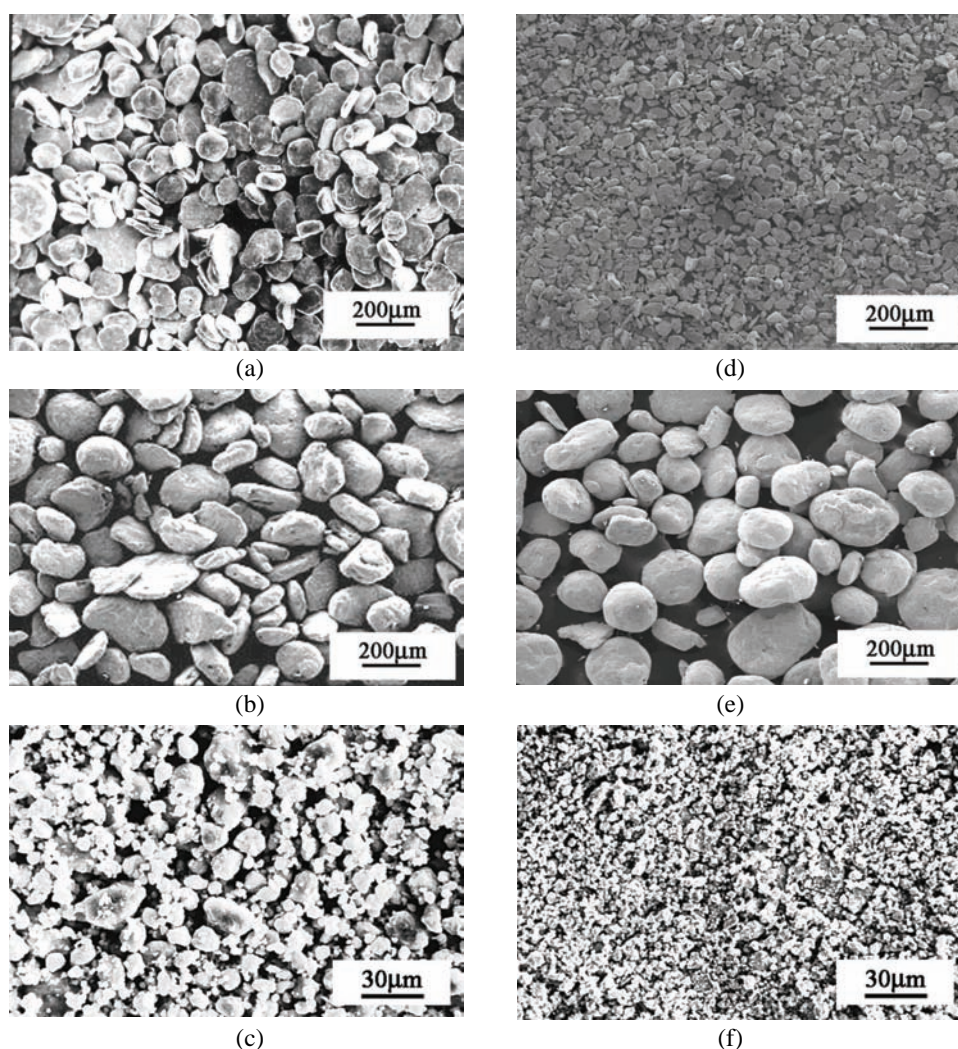


Fig. 6. SEM microphotographs. Morphology of Cu-2Al, Cu-4Al₂O₃ and Cu*-4Al₂O₃ composite powder particles after 5 (a–c) and 20 h (d–f) of milling.

Cu-2Al particles (Fig. 6a) are flattened, whereas the Cu-4Al₂O₃ and Cu*-4Al₂O₃ composite particles are more rounded (Figs. 6b and 6c, respectively). The flattened shape of the Cu-2Al composite particles is a consequence of the fact that the nano-sized Al₂O₃ particles formed by internal oxidation generate a higher resistance to the strong plastic deformation occurring at the beginning of the milling than the micro-sized commercial Al₂O₃ particles. During prolonged milling (20 h), the size of Cu-2Al particles (Fig. 6d) significantly decreased, becoming more rounded in shape. On the other hand, the size of Cu-4Al₂O₃ particles (Fig. 6e) increased to some extent and they had a completely rounded shape. No significant change in the size and morphology could be detected in the Cu*-4Al₂O₃ particles (Fig. 6f). The results presented in Fig. 6 suggest that the size of the starting copper particles, as well as the Al₂O₃ particle size, has an influence on the different morphologies and particle sizes of the composite powders during milling.

Since the particles of the milled composite powders Cu-2Al and Cu-4Al₂O₃ were neither similar nor uniform in size, it is obvious that the balance of the fracture and welding processes of the powder particles has not been attained during 20 h of milling. Concerning this aspect, the situation with the Cu*-4Al₂O₃ composite powders is not quite clear.

The microstructure of the composite powder particles after 5 h of milling are illustrated in Fig. 7. Thereby, it was confirmed that the milled composite powder

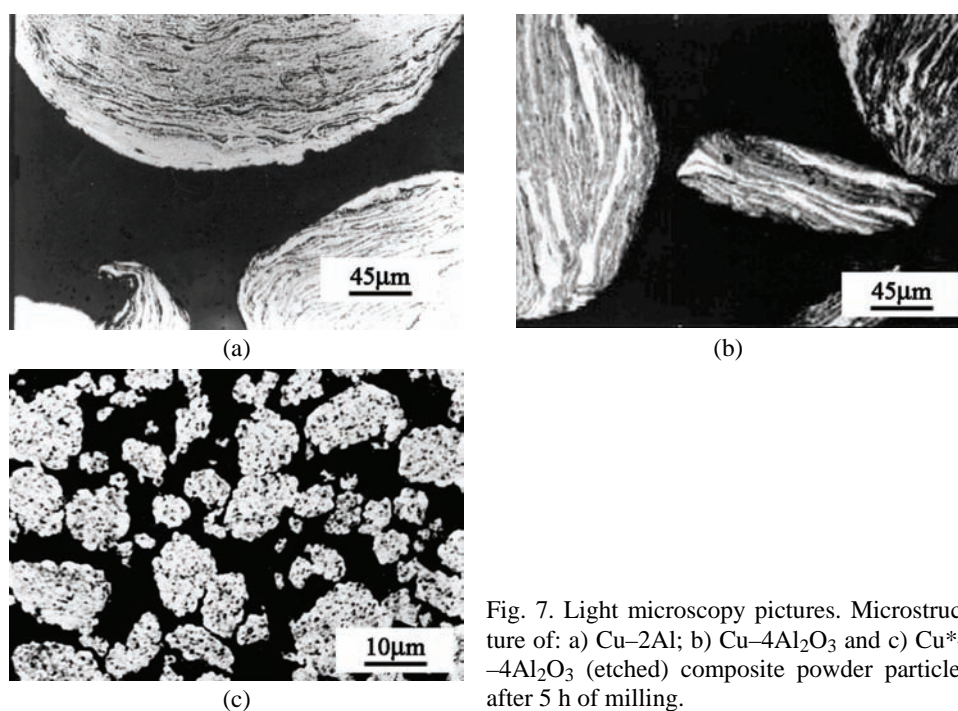


Fig. 7. Light microscopy pictures. Microstructure of: a) Cu-2Al; b) Cu-4Al₂O₃ and c) Cu*-4Al₂O₃ (etched) composite powder particles after 5 h of milling.

particles, except the Cu*–4Al₂O₃ particles, exhibit a lamellar structure (Figs. 7a and 7b), typical for high-energy milled powders. The lamellae represent individual plastically deformed starting pre-alloyed copper (Fig. 7a) and copper powder particles (Fig. 7b). Applying higher magnification, the uniform distribution of the commercial Al₂O₃ particles embedded in a matrix of agglomerated copper particles may be seen in the microstructure of the Cu*–4Al₂O₃ composite powder particle (Fig. 7c). In these milled powder particles, lamellae are not visible, probably due to very small powder particle size.

The structural observations showed that a very homogenous distribution of Al₂O₃ was achieved after 5 h of milling in the majority of the mechanically alloyed copper particles and that this distribution improved with increasing milling time. The distribution of Al₂O₃ particles in the Cu–4Al₂O₃ particles after 5 and 20 h of milling is illustrated in Figs. 8 a and 8b, respectively. In this case, when the size of the starting copper and Al₂O₃ particles were higher, the uniform distribution of Al₂O₃ particles between deformed copper particles, typical for composites obtained by high-energy milling, may be clearly seen.

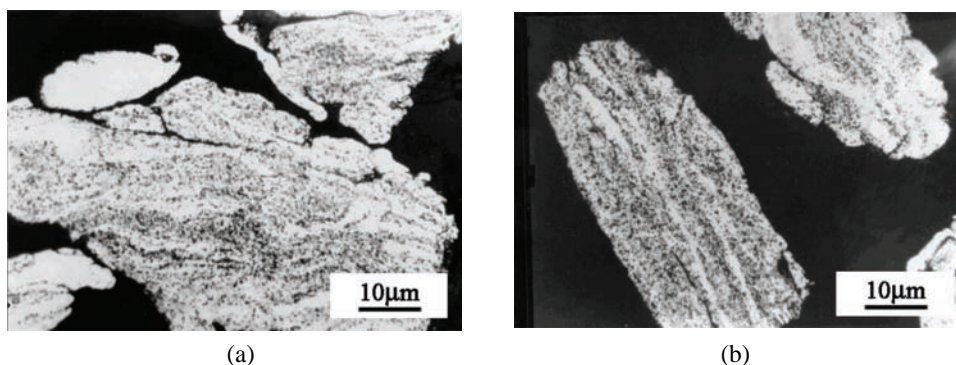


Fig. 8. Light microscopy pictures of Cu–4Al₂O₃ after: a) 5 and b) 20 h of milling (polished).

CONCLUSIONS

Powders composites of Cu–Al₂O₃ were obtained using high-energy milling in air. Inert gas-atomized pre-alloyed copper powder containing 2 mass % Al and mixtures of various combinations of particle size with an approximately constant content of Al₂O₃ were used as the starting materials. Depending on the characteristics of the starting powders, the milled powders possessed different properties.

The decrease of the Cu–2Al lattice parameter with milling time was the result of oxidation of aluminum, which precipitated from the pre-alloyed copper forming a fine dispersion of Al₂O₃ particles. Assuming that the all the aluminum was oxidized, it was calculated that 3.7 mass % of Al₂O₃ was produced in the copper matrix by internal oxidation of 2 mass % Al.

The full width at half maximum (FWHM) height of the peaks in the X-ray diffraction patterns of the examined powders showed a progressive line broadening with milling time. The effect of the smaller copper particles had a more pronounced effect on the FWHM than the larger Al_2O_3 particles.

The lattice distortion was found to increase with increasing milling time. The lattice distortion was highest in the Cu–2Al sample strengthened with very small Al_2O_3 particles, *i.e.*, nano-sized (0.01 μm) Al_2O_3 particles caused a higher lattice distortion than the coarser micro-sized (0.75 μm) particles. The crystal lattice of the smaller (15 μm) starting copper powder was distorted to a lesser extent than the lattice of the coarser (30 μm) particles.

The Cu– Al_2O_3 composite powder showed high grain size refinement. The most intensive grain refinement occurred in the early stage (up to about 5 h) of milling. In the period from 5 to 20 h of milling, the grain size of the powders remained practically constant (between 20 and 30 nm), except for the powders with 15 μm copper powder particles, in which case the grain size was 15 nm.

The starting copper particles size and size of the Al_2O_3 particles affected the morphology, size and microstructure of the composite powders formed during milling.

The Cu*–4 Al_2O_3 composite powder particles did not exhibit a characteristic lamellar structure, due to the small starting copper powder particles (15 μm).

Acknowledgement. Authors are indebted to the Ministry of Science and Technological Development of the Republic of Serbia for financial support of this investigation realized through the Project No. 142027.

ИЗВОД

КАРАКТЕРИСТИКЕ КОМПОЗИТА Cu– Al_2O_3 СА РАЗЛИЧИТИМ ПОЧЕТНИМ ЧЕСТИЦАМА ПРАХА ДОБИЈЕНОГ МЛЕВЕЊЕМ У ВИСОКО-ЕНЕРГЕТСКОМ МЛИНУ

ВИШЕСЛАВА РАЈКОВИЋ, ДУШАН БОЖИЋ и МИЛАН Т. ЈОВАНОВИЋ

Институт за нуклеарне науке "Винча", бр. 522, 11001 Београд

Прахови композита на бази Cu– Al_2O_3 добијени су млевењем у високо-енергетском млину. Почетни материјал представљале су комбинације прахова различитих величина као и смеше различитог састава. Прахови су одвојено млевени у планетарном млину са куглама и то на ваздуху при чему је време млевења било 20 h. За ојачавање основе бакра примењени су унутрашња оксидација и механичко легирање. За време млевења под утицајем унутрашње оксидације у предлегираном праху Cu–2 мас %–Al настало је 3,7 мас % фино диспергованих нано-честица Al_2O_3 . Испитиван је утицај почетне величине честица бакра и честица Al_2O_3 на параметар кристалне решетке и њену дисторзију, као и на величину кристалног зрна. Такође су испитивани величина честица праха, морфологија и микроструктура композита Cu– Al_2O_3 .

(Примљено 9. децембра 2008)

REFERENCES

1. C. Jianyi, W. Mingpu L. Zhou, W. Yanhui, in *China-EU Forum on Nano-sized Technology*, Beijing, 2002, <http://www.863.org.cn/english/Forum/17.doc> (accessed 2002)
2. L. Shuhua, F. Liang, X. Lei, F. Zhikang, *J. Comp. Mat.* **38** (2004) 1495
3. B. Tian, P. Liu, K. Song, Y. Li, Y. Liu, F. Ren, J. Su, *Mat. Sci. Eng. A* **435–436** (2006) 705
4. D. L. Zhang, S. Rayanova, C. C. Koch, R. O. Scattergodd, K. M. Youssef, *Mat. Sci. Eng. A* **410–411** (2005) 375
5. G. Ziegler, *Powder Met. Int.* **10** (1978) 70
6. K. G. Williams, H. W. Hall, *Acta Met.* **1** (1953) 22
7. R. H Palma, A. O. Sepulveda, *Mat. Sci. Forum* **416–418** (2003) 162
8. V. Rajković, D. Božić, M. T. Jovanović, *J. Alloys Compd.* **459** (2008) 177
9. B. Lonnberg, *J. Mat. Sci.* **29** (1994) 3224
10. Y. Kanno, *Powder Met.* **44** (1985) 93.